UNIV RSI
OF MICHIGAN
SEP 18 1951
ENGINEERING
LIBRARY

JOURNAL OF THE
AERONAUTICAL
SCIENCES

VOLUME 18 SEPTEMBER, 1951 NUMBER 9

CONTENTS

Aerodynamic Stability and Automatic Control (Wright Brothers Lecture)..... WILLIAM BOLLAY 569

A Limiting Case for Missile Rolling Moments..... ERNEST W. GRAHAM 624

Interference Between Wing and Body at Supersonic Speeds—Theoretical and Experimental Determination of Pressures on the Body..... R. H. CRAMER 629

Readers' Forum: "Lateral Elastic Instability of Hat-Section Stringers," by C. M. Tyler, Jr., and T. J. Walker; "Reflection of Strong Shock at Nearly Glancing Incidence," by Donald R. White; "Ring Shape Source Distribution in Axially Symmetrical Supersonic Flow," by S. I. Pai; "The Effect of Surface Cooling on Laminar Boundary-Layer Stability," by Martin Bloom; "Astroballistic Heat Transfer," by R. N. Thomas and F. L. Whipple; "On an Extension of Glauert's Theory of Thin Airfoils to Profiles in Cascade," by N. Scholz; "The Flow Around a Rotating Disc in a Uniform Stream," by H. Schlichting and E. Truckenbrodt..... 633–640

Published by the

INSTITUTE OF THE AERONAUTICAL SCIENCES, INC.

JOURNAL OF THE AERONAUTICAL SCIENCES

Editor: HUGH L. DRYDEN, *Director, N.A.C.A.*

Associate Editor: ROBERT R. DEXTER *Managing Editor:* BERNEICE H. JARCK

Editorial Committee

Aerodynamics

Francis Clauser
Howard Emmons
Alexander Flax
R. Paul Harrington
R. T. Jones
Carl Kaplan
H. W. Liepmann
C. C. Lin
H. F. Ludloff
Harold Luskin
John R. Markham
Clark B. Millikan
Shatswell Ober
W. Bailey Oswald
Allen E. Puckett
Elliott G. Reid
H. J. F. Reid
Russell Robinson
G. B. Schubauer
W. R. Sears
John Stack
Theodore von Kármán
Richard von Mises

Flight Testing

W. K. Ebel
R. R. Gilruth
Melvin N. Gough
E. G. Stout

Meteorology

C. F. Brooks
D. M. Little
E. J. Minser
F. W. Reichelderfer
H. C. Willett

Structures and Materials

W. B. Bleakney
E. W. Conlon
L. H. Donnell
E. C. Hartmann
N. J. Hoff
Samuel Levy
E. E. Lundquist
J. S. Newell
Alfred S. Niles
W. Ramberg
E. Reissner
F. R. Shanley
H. W. Sibert
C. R. Strang
S. Timoshenko
H. S. Tsien
Chi-Teh Wang

Rotating Wing Aircraft

F. B. Gustafson
K. H. Hohenemser
Bartram Kelley
R. B. Maloy
Ralph McClarren
R. H. Miller
R. H. Prewitt
Igor I. Sikorsky

Physiologic Problems

H. G. Armstrong
Louis H. Bauer
Eugene Du Bois
W. Randolph Lovelace, II
Ross A. MacFarland
A. D. Tuttle

Flight Propulsion

George W. Brady
Frank W. Caldwell
L. S. Hobbs
E. E. Johnson
Joseph Keenan
R. P. Kroon
Hans Reissner
Abe Silverstein
C. Fayette Taylor
E. S. Taylor
P. Taylor
E. S. Thompson
H. S. Tsien

Aircraft Design

W. E. Beall
W. K. Ebel
Hall L. Hibbard
Richard Hutton
C. L. Johnson
A. A. Kartveli
C. J. McCarthy
Fred E. Weick
Robert J. Woods

Air Transport

Charles Froesch
J. A. Herlihy
R. D. Kelly
Otto E. Kirchner
Jerome Lederer
John C. Leslie
R. Dixon Speas

Instruments

Allan G. Binnie
W. G. Brombacher
Charles H. Colvin
B. M. Craig
C. S. Draper
S. G. Eskin
O. E. Esval
W. L. Howland
George H. Purcell
C. F. Savage
O. Hugo Schuck
L. N. Schwien
C. L. Seward, Jr.
L. D. Statham
R. C. Sylvander
D. K. Warner
P. F. Weber
Elmer P. Wheaton

Vibration and Flutter

Lee Arnold
M. A. Biot
R. L. Bisplinghoff
William Bollay
Chieh-Chien Chang
I. E. Garrick
Martin Goland
J. P. Den Hartog

Fuels and Oils

D. P. Barnard
J. H. Doolittle
Graham Edgar
R. T. Goodwin
S. D. Heron
A. M. Rothrock

SUBSCRIPTION RATES

JOURNAL OF THE AERONAUTICAL SCIENCES, Published Monthly.—United States and Possessions: 1 Year, $12.00; Single Copies, $1.50. Foreign Countries Including Canada (American Currency Rates): 1 Year, $13.00; Single Copies, $1.50.

AERONAUTICAL ENGINEERING REVIEW, Published Monthly.—United States and Possessions: 1 Year, $3.00; Single Copies, $0.50. Foreign Countries Including Canada (American Currency Rates): 1 Year, $3.50; Single Copies, $0.50.

Notices of change of address should be sent to the Institute at least 30 days prior to actual change of address.

Manuscripts for publication, proofs, and all correspondence should be addressed to the Editorial Office of the JOURNAL.

Correspondence regarding subscriptions may be addressed to Publication Office, 20th and Northampton Sts., Easton, Pa., or to the Editorial Office of the JOURNAL OF THE AERONAUTICAL SCIENCES, 2 East 64th Street, New York 21, New York.

Copyright, 1951, by the Institute of the Aeronautical Sciences, Inc.

Entered as Second Class Matter at the Post Office, Easton, Pa., May 1, 1937. Acceptance for mailing at a special rate of Postage provided for in the Act of August 24, 1912. Authorized April 29, 1937.

JOURNAL OF THE AERONAUTICAL SCIENCES

VOLUME 18 SEPTEMBER, 1951 NUMBER 9

Aerodynamic Stability and Automatic Control

The Fourteenth Wright Brothers Lecture*

WILLIAM BOLLAY†

University of California at Los Angeles

SUMMARY

This paper summarizes the more recent developments in the field of aerodynamic stability and automatic control with particular reference to the analytical and experimental methods that are used in the design of aircraft control systems. It traces the historical development of automatic control systems from the Watt Steam Engine Governor (1784) to the Sperry Gyroscopic Stabilizer (1910) and the modern automatic interceptor. It indicates that the analytical methods for studying automatic control systems are essentially the same as those presented by Routh in his Adams Prize Essay of 1877 and that the principal new step has been the reduction of these analytical methods to graphical techniques. The most useful of these are the "root-locus" method of Evans, the amplitude and phase plots of Bode, and the vector response plots of Nyquist. These methods are illustrated by simple examples. The general methods of design, including the use of analog computers (simulators) and the analysis of flight-test data, are discussed. Some of the future potentialities of automatic controls in the application to aircraft are discussed: (1) automatic cruise control of propulsion systems, (2) stabilization of an aircraft in the stall, (3) automatic stabilization of helicopters, (4) gust alleviation, and (5) automatic stabilization of seaplanes and hydroplanes. It is concluded that, while the past 25 years have brought revolutionary developments in aerodynamics and aircraft propulsion, the next 25 years will see comparably important advances in aeronautics by the application of automatic controls culminating not only in guided missiles, but also in transport aircraft that will be on automatic control from initial take-off to their landing at the destination.

(I) INTRODUCTION

(A) *Wright Brothers' Experiments on Stability and Control in 1900*

THE PRACTICAL ACHIEVEMENT of satisfactory stability and control is probably the greatest contribution of the Wright Brothers in the development of the airplane.* Their predecessors, Lilienthal, Mouillard, and Chanute, had carried out short soaring and gliding flights with primitive control systems; however, the Wright Brothers were the first to introduce effective aerodynamic control surfaces. Their first gliders and aircraft incorporated a tail-first configuration with a controllable elevator for longitudinal control, and they employed differential torsion of the wing tips to achieve lateral control (see Fig. I-1). Their first tests with these control systems were made during the summer of 1900 on an unpowered aircraft, which they tested both as a glider and as a kite. These early flights in 1900 were the basis of their first airplane design. The topic of stability and control is therefore a particularly appropriate subject at the 1950 Wright Brothers Lecture—a half century since the Wrights first verified their theories on stability and control.

Received May 8, 1951.

* Presented before the Institute of the Aeronautical Sciences in the U.S. Chamber of Commerce Auditorium, Washington, D.C., December 16, 1950.

† Visiting Professor of Engineering; formerly Technical Director, Aerophysics Laboratory, North American Aviation, Inc.

* Wilbur Wright in 1901 outlined the problems of the airplane very well when he stated,[2] "The difficulties which obstruct the pathway to success in flying-machine construction are of three general classes: (1) those which relate to the construction of the sustaining wings; (2) those which relate to the generation and application of the power required to drive the machine through the air; (3) those relating to the balancing and steering of the machine after it is actually in flight. Of these, two are already to a certain extent solved. Men already know how to construct wings of aeroplanes, which, when driven through the air at sufficient speed, will not only sustain the weight of the wings themselves, but also that of the engine and the engineer as well. Men also know how to build engines and screws of sufficient lightness and power to drive these planes at sustaining speed. Inability to balance and steer still confronts students of the flying problem, although nearly ten years (since Lilienthal's success) have passed. When this one feature has been worked out, the age of flying machines will have arrived, for all other difficulties are of minor importance."

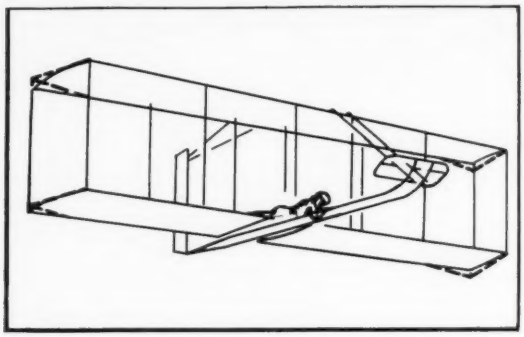

FIG. I-1. Wright's gliding apparatus.

(B) *The Present—A Period of Transition—Subsonic to Supersonic Speed—Manual to Automatic Control*

At present, the airplane is going through another period of transition similar to that of a half century ago. The power plants now available are powerful enough and light enough to permit airplanes to fly at speeds equal to, and greater than, the velocity of sound. The major problems that are encountered in flying in this regime are again stability and control problems. The transonic flow regime behaves in many respects like a stall regime. Below the so-called critical Mach Number, as long as the angle of attack is below the stall angle, the airflow follows the contour of the wings. In the transonic regime, even though the free-stream velocity is subsonic, the local velocities of flow over portions of the wing are supersonic, and thus it is possible for shock waves to form. These shock waves have two important effects: (1) They change the pressure distribution over the wing and thus change the center of pressure of the wing. (2) Where they intersect the wing surface, they give rise to a steep pressure gradient that often leads to flow separation and thus buffeting. When the airplane speed is well up into the supersonic regime, the airflow again follows the wing contours; the principal shock waves are ahead and behind the wing, and the flow is smooth again. These phenomena are illustrated in Fig. I-2. The variation of the aerodynamic characteristics in the subsonic, transonic, and supersonic regime is illustrated in Fig. I-3 for the German V-2 rocket. It will be noted that these coefficients vary smoothly in the subsonic and supersonic regime, although at different levels. In the transonic regime, the coefficients vary rapidly and, in some cases, relatively erratically as a function of Mach Number M, angle of attack α, and control surface deflection δ. The center of pressure on aerodynamic surfaces changes from the vicinity of the 25 per cent chord point at subsonic speeds toward the 50 per cent chord point at supersonic speeds. This is the principal reason for the large shift in the aerodynamic center. The hinge moments vary correspondingly because the center of pressure moves aft at supersonic speeds. An elevator that is balanced at subsonic speeds requires a large hinge moment to move it at supersonic speeds. In sizing up the magnitudes of these moments, it must be remembered that hinge moment = $C_H.(1/2)\rho V^2.c.S$; thus, the absolute magnitude of the hinge moment is proportional to the product of C_H and $(1/2)\rho V^2$. Using Fig. I-3, we compute, for example, that if the stick force per degree elevator deflection is +1 lb. at $M = 0.2$, it is −94 lbs. at $M = 0.8$ and +210 lbs. at $M = 1.2$.* Such stick forces are too high for manual control of an airplane. Thus, it is essential to use either power boost or, preferably, full power control. The latter is the present trend.

The increase in aircraft speeds brings with it another requirement—the necessity for decreasing the time of response of the pilot and the necessity for increasing the precision of his maneuvers. Consider, for example, the problem of shooting down a 600-m.p.h. bomber with an interceptor plane capable of a speed of 1,000 m.p.h. The time available for interception is likely to be so short that the interceptor must be vectored by ground control into the approximate attack position. If the attack proceeds from the front, the relative speed between the two aircraft is 1,600 m.p.h. If the intercep-

* Such changes in trim could, for example, be produced by opening flaps or dive brakes.

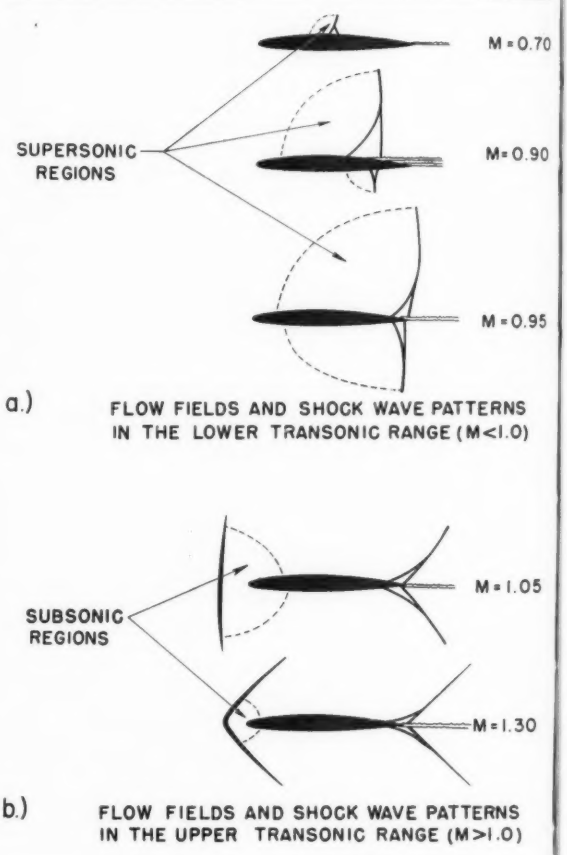

FIG. I-2. Flow separation on airfoil surface.[52]

tor pilot first sees the bomber 5 miles away, he has 11 sec. to identify his target, to line up his airplane, to fire his guns, and to get out of the way. The likelihood of scoring a hit under conditions of such a high closing rate is extremely low. If he decides to go around to make an approach from the rear, even if he turns at 4g normal acceleration, it will require a 6-mile diameter circle to turn around and a time of 72 sec. During this time the bomber has traveled 12 miles and has therefore a good possibility of being under cloud cover.

It is because of such considerations that the "automatic fighter" and, eventually, the guided missile will be required to intercept high-performance bombers. In reference 7 a typical interceptor mission, illustrated in Fig. I-4, is described as follows:

"The automatic control system of the future will navigate an interceptor into proximity of the target, track and attack the target, and navigate the interceptor back to its base. . .the target will originally be located by ground-based, long-range radar. The information obtained as to bearing of the target will be manually set into the system by the pilot, and the aircraft will then take off, climb to cruise altitude, and navigate to the vicinity of the target area. At this point, airborne radar in the interceptor will take over, search for the target, identify it, and begin to track it. While tracking, the system will automatically maneuver the airplane into the attack position. At the proper instant, calculated to yield the best 'kill' probability, guided missiles or rockets will be automatically released. After sufficient time has elapsed for the system to determine the results of the attack on the target, automatic evasive action will begin. The system then will return to automatic navigation, either to another target area or to the home base. At the home base, an instrument landing pattern will be automatically entered, and the plane brought to touchdown. The action in any phase of this sequence will be completely automatic; the pilot's job will be to determine when to switch from one phase to the next."

The development of such automatic control systems involves two important types of technical problems:

(1) The combination of the many different elements into a single, well-integrated system. The airplane with its autopilot are only two of the elements of this system. These two elements must be capable of responding to the directions of (a) the ground radar, which vectors the airplane into the vicinity of the bomber; (b) the airplane's target seeker, which steers the airplane into firing position and fires the guns or rockets; and (c) the automatic-ground-approach system (Fig. I-4). The overall system must be stable over the wide range of speeds and altitudes involved. The system must reject the spurious "noise" input signals that behave like turbulent fluctuations about a mean velocity. The system must be precise enough to provide accurate fire control during the attack. The landing approach has to be precise enough so that the airplane does not exceed its design landing-load factors upon touch-down.

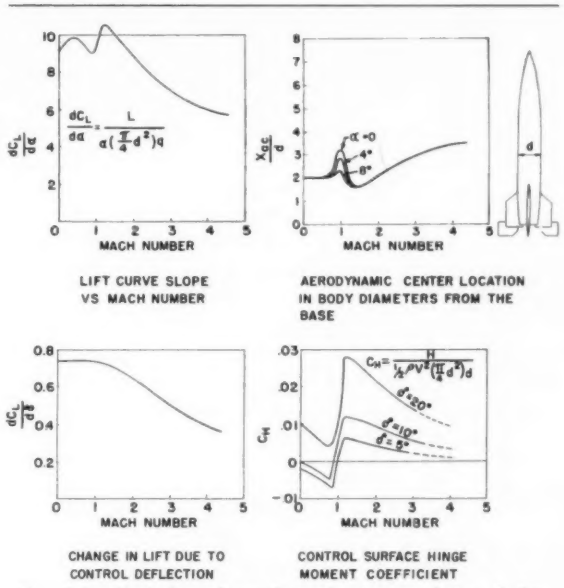
MACH NUMBER
LIFT CURVE SLOPE VS MACH NUMBER
AERODYNAMIC CENTER LOCATION IN BODY DIAMETERS FROM THE BASE
CHANGE IN LIFT DUE TO CONTROL DEFLECTION
CONTROL SURFACE HINGE MOMENT COEFFICIENT

FIG. I-3. Variation of aerodynamic characteristics of the V-2 with Mach Number.

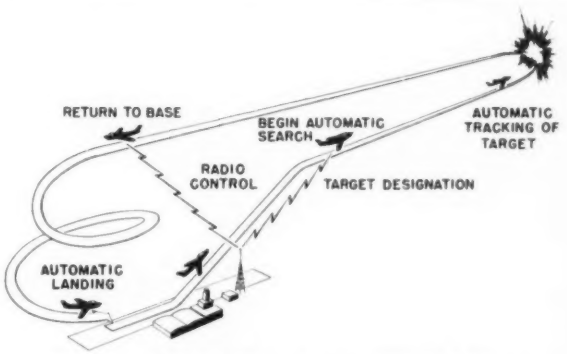

FIG. I-4. A typical mission for an automatic fighter.

The requirement for rapid automatic control systems with reasonable control forces will require much closer teamwork between aerodynamicists and autopilot designers than ever existed in the past. There are good possibilities for new types of aerodynamic controls which were not necessary previously. Spoilers may be used for rapid control, leaving the trimming to the more conventional surfaces.[72] New types of aerodynamic balances must still be invented which will be effective over a wide range of Mach Numbers, angles of attack, and angles of yaw. The dynamic analysis of these systems must be carried out as a joint enterprise by the aerodynamicist and the autopilot designer.

(2) The achievement of a high degree of reliability in this complicated system.* This can be achieved par-

* An excellent review of the problems involved in achieving a reliable powered control system for aircraft is given by Lyons.[54]

tially by careful initial design, such as the use of duplicate components for critical elements and the use of miniaturized "plug-in" boxes that can be easily checked and replaced. The high degree of reliability will be finally achieved only as the result of an intensive ground and flight-test program in much the same way as the current aircraft engines have evolved.

After this has been achieved, the automatically controlled airplane will also have important peacetime potentialities. The transport aircraft of the future may well be on automatic control from the moment of take-off to the automatic landing at its destination. Such a system would free the air transport of its most serious handicap—the weather. The human pilot would serve mainly to oversee the flight instruments and to take over in case of an emergency.

(II) Stability and Control Problems of the Past Decade

During the past decade, airplanes have moved into the transonic regime. They have thus pierced what used to be called the sonic wall. This was a wall not only from the standpoint of requiring tremendous powers to penetrate, but even more, it was a region of great ignorance regarding the stability and control problems that it involved.

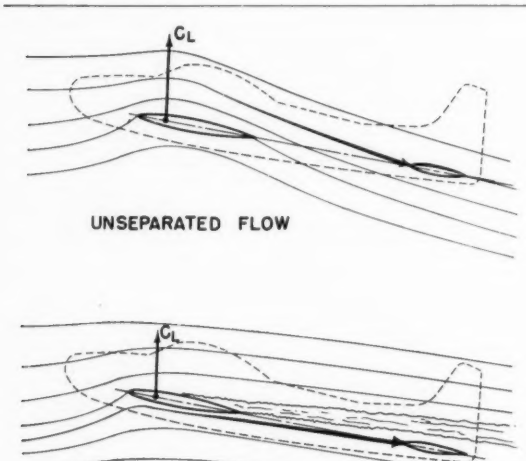

Fig. II-1. Typical effect of flow separation on downwash angle.

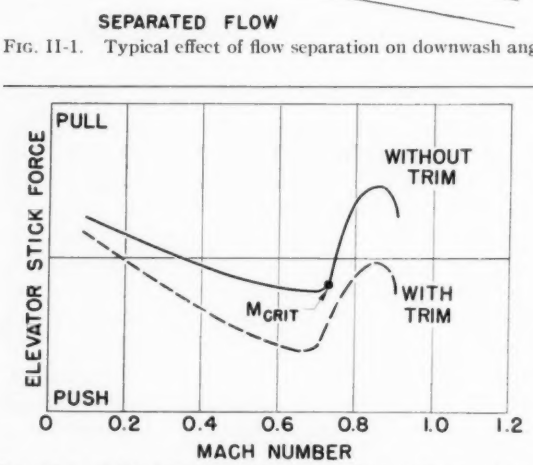

Fig. II-2. Stick force variation with Mach Number. [Lower curve with trim tabs at $\delta = +10°$ (nose up).]

The fighter airplanes developed during the early 1940's were the first airplanes operating at speeds high enough to encounter these "compressibility effects." During steep dives these airplanes reached Mach Numbers of the order of 0.70 and experienced many severe stability and control difficulties. Buffeting occurred at these high speeds. This was associated with a flow separation from the wing when a shock wave was formed on the upper surface (see Fig. I-2). In addition, the airplane experienced a severe change in trim, which was associated with the unsymmetrical flow separation from the wing and a reduction in downwash over the tail (Fig. II-1). The resulting change in pressure distribution gave a variation in elevator stick force, as shown in Fig. II-2. It is noted that, at $M = 0.72$, a reversal in stick force occurs, followed by a severe diving or "tucking" moment as Mach Number increased. The pilot, realizing that the pull forces were exceeding his strength capabilities, normally used the elevator trim tab to trim the airplane nose up. This displaced the stick force curve as shown in the dotted portion of Fig. II-2. As the airplane continued its dive to lower altitudes, the speed of sound increased because of the higher ambient temperatures. Consequently, the airplane rather rapidly decreased Mach Number, and, if the pilot had used too much nose-up trim tab, the airplane rapidly pulled out of the dive, often with disastrous results. This was alleviated in the P-38 and P-47 airplanes by the addition of dive-recovery flaps. These flaps tended to increase the downwash over the tail and to induce separation on the lower surface to balance the separation on the upper surface of the wing. The effect of these flaps is shown in Fig. II-3. In the design of the newer jet fighters, these troubles are first of all minimized by design changes—the use of sweepback of wings, the use of extremely thin wings, or the use of low aspect ratio. Fig. II-4 shows the effect of reducing wing thickness. Fig. II-5 shows the effect of sweepback. It will be noted that the effect of these design changes is to postpone the "transonic bump."

At supersonic speeds the effectiveness of trailing-edge elevators is much reduced (Fig. II-6), and thus it has become desirable to use an all-movable stabilizer.[66] The control moments on such a movable stabilizer become so high at high speeds that either power boost or power controls are essential. With power controls the surface is actuated directly by a hydraulic actuator or motor-driven screw jack. This has the additional advantage that the undesirable reversals in hinge moments are not transmitted back to the pilot. The pilot's stick merely controls the hydraulic actuator. In order to provide a simulated feel in the stick, it is connected to a

spring for centering. In addition, the aerodynamic loads are simulated by a "q" actuator, a device that is sensitive to free-stream dynamic pressure; it increases the effective spring stiffness by shifting the spring bungee connected to the stick.

In order to limit the accelerations that the pilot will apply to the aircraft, bob-weights may be connected to the control system. When the airplane experiences a normal acceleration, these bob-weights exert a moment on the stick in a direction tending to reduce the control-surface deflection. The effect of such bob-weights is shown in Fig. II-7 on a P-51 airplane. This airplane was overloaded by the addition of a fuel tank behind the pilot to increase its range. This made the airplane unstable longitudinally, so that when the pilot applied a normal acceleration to the airplane by pulling back on the stick, an increase in acceleration required less stick force or even a push force. The addition of the bob-weights gave the airplane a more nearly normal feel.

Another family of stability and control problems which showed up during the past 10 years was associated with aeroelasticity—i.e., the deformation of the aircraft structure due to the air forces. Some of these can be cured only by a stiffening of the structure. For example, during high-speed dives, the elevator contour would tend to bulge outward and, in some cases, would rupture completely. The bulged surfaces resulted in a decreased stability or stick-force gradient. Vented surfaces and strengthened structures usually eliminated this problem.

A typical problem of control-force reversal occurs when an aileron deflection, say, up, tends to twist the nose of the wing in the same direction—i.e., up. As the dynamic pressure is increased, the rolling effectiveness of the aileron is continuously decreased until, at a certain speed, the aileron effectiveness becomes zero. This is shown in Fig. II-8. A solution to this problem is the use of spoiler ailerons that produce a given rolling moment with less twisting moment on the wing. Thus, they are effective in increasing the speed at which aileron effectiveness is reduced to zero.

Another aileron-control problem encountered at high Mach Numbers under high normal accelerations on a sweptback wing is "upfloating"—i.e., a deflection of the control cables permitting both ailerons to deflect upward. If the ailerons are far behind the c.g. (as for swept-wing aircraft), this acts like an additional elevator deflection and therefore results in a still greater acceleration on the airplane. One cure for this problem is a mechanical restraint of the aileron.

A dynamic instability that has been encountered on high-speed aircraft is "snaking." This is a rapid directional oscillation at the short period lateral frequency apparently caused by a wide variety of elements—flow separation in the vicinity of the vertical tail, fuel sloshing, and low lateral damping associated with aeroelasticity or high-altitude flight. This builds up a vibration involving bending of the fuselage. Two methods of fixing this vibration have been employed. The first adds trailing-edge strips to the rudder to increase its effectiveness at low deflection angles. However, this "fix" also increases rudder forces rapidly. Another means of eliminating this vibration has been by an automatic control system—a yaw damper that is actuated by a rate-sensitive gyro and which damps the vibration by deflecting the rudder in a direction opposing the motion. This method, described in reference 82 and shown in Fig. II-9, has been found effective.

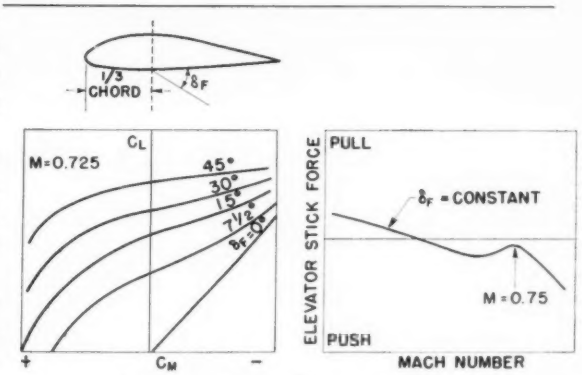

FIG. II-3. Effect of dive recovery flaps.

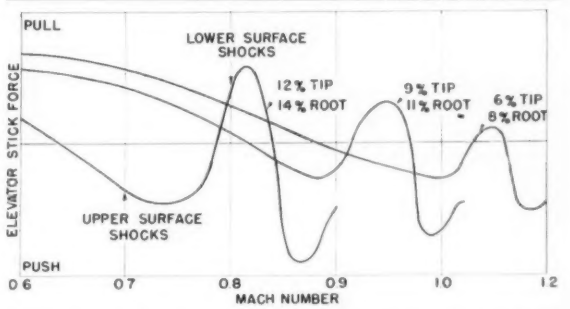

FIG. II-4. Effect of reducing wing thickness on stick force straight wing airplane with NACA 64, 65, 66 series airfoil.

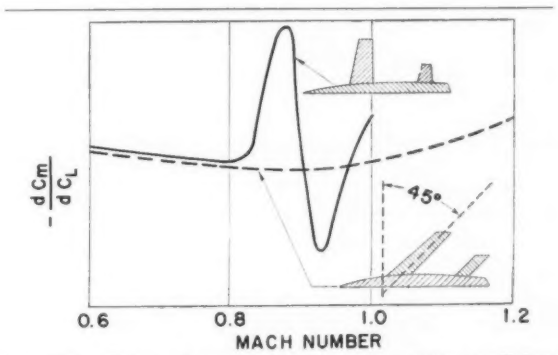

FIG. II-5. Effect of sweepback on static stability coefficient (dC_m/dC_L).

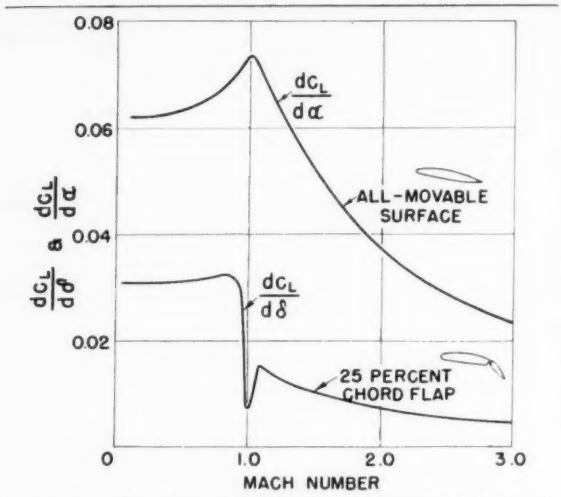

FIG. II-6. Effectiveness of trailing-edge elevators (A.R. = 4).

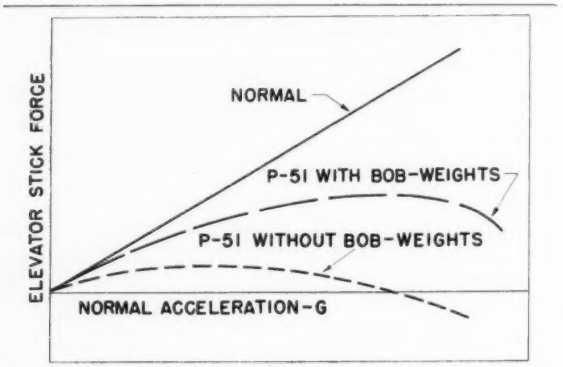

FIG. II-7. Effect of bob-weights on stick force P-51 airplane.

(III) DEVELOPMENT OF AUTOMATIC CONTROL SYSTEMS

The theory of dynamic stability of aircraft has until recently been considered largely as an academic subject. The basic reason for the low practical importance of the earlier dynamic stability calculation was the artificial boundary conditions that were ordinarily assumed for the control system—i.e., either that the controls were locked in a trimmed position or that the controls were completely free. Both of these assumptions are unrealistic, since actually the pilot sits at the controls and, if a disturbance increases the airplane attitude and thus reduces its speed, he counteracts this disturbance through his controls. The difficulty with the mathematical analysis was that it was impractical to include the human pilot as a part of the dynamical system.

With the development of automatic control systems this situation changed. The autopilot system and its input information (no matter whether it comes from a radar signal or a gyroscope system) is susceptible to a dynamic analysis. This dynamic analysis is ordinarily based partially on theory and partially on performance tests of the actual equipment. The overall system, consisting of the aerodynamic, inertial, and elastic elements of the airplane combined with the electrical, mechanical, and hydraulic elements of the autopilot, forms a closed-loop network. The analysis of such feedback networks forms the next subject of our discussion [Section (IV)]. This entire system must be carefully engineered as a unit in order to combine these many elements into an overall precision device. This process is called the synthesis of the airplane-autopilot system.

The development of automatic control systems has progressed far, particularly during the past 10 years. Automatic controls have, however, been known for a long time. One of the first was the flyball governor for the Watt Steam Engine (about 1784). Routh (1884)

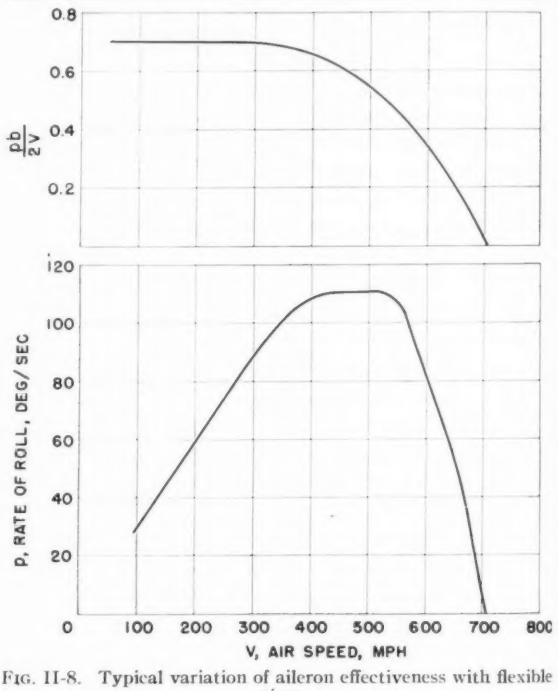

FIG. II-8. Typical variation of aileron effectiveness with flexible wing.

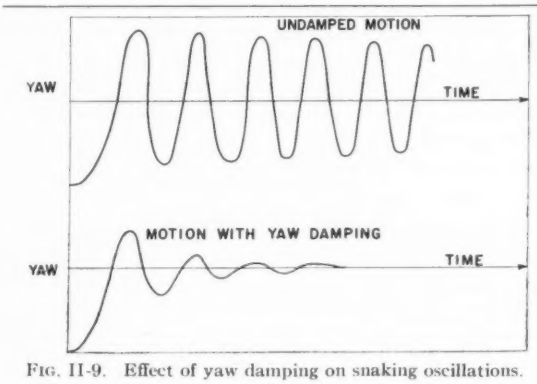

FIG. II-9. Effect of yaw damping on snaking oscillations.

analyzed the stability of this system[22] and noted that, unless damping was introduced in the spindle on which the flyballs move up and down, the system would hunt. A great improvement in the achievement of uniform rotation was the invention (1843) by Siemens[24] of a governor that controlled the steam valve of an engine by the error signal between a uniform angular velocity and the actual angular velocity. This instrument, the chronometric governor (Fig. III-1), was applied by Sir G. B. Airy, the Astronomer Royal, for regulating astronomical and chronographical instruments. This governor operated on the principle of what is now called a simple feedback servo network (Fig. III-3).

The invention and description of the hydraulic servomotor occurred almost simultaneously in England by Brown[4] in 1871 and in France by Farcot[10] in 1873. Lincke[16] in Germany (1879) presented an excellent survey of many mechanical feedback servosystems. He showed, among other things, the analogy of these systems to the human nervous and muscular system and indicated the future potentialities of servosystems for the automatic control of machines and factories. He was thus an early exponent of what Wiener[91] now calls "cybernetics." The application of servos to the regulation of steam turbines was studied experimentally and theoretically by Stodola[25] in 1893 with particular reference to the conditions of stability. Later summaries of regulators were given by Tolle[26] in 1921, by Wünsch[27] in 1930, by Engel[8] in 1944, and by Hänny[13] in 1946.

A new element involved in servo-control was the combination of the mechanical feedback and power amplification. The application of such servomechanisms to the directional control and stabilization of vehicles started with the control of torpedoes by Whitehead (1862). It is interesting to note that Sir Hiram Maxim* considered the use of a gyro-controlled servosystem for the stabilization of his first airplane in 1891. The practical application of a gyro for the stabilization of an airplane was started in April, 1910, when Elmer A. Sperry† and H. C. Ford installed a gyro in a monoplane belonging to Mr. Stanley Y. Beach. This device was known as the "Gyroscopic Stabilizer." These experiments were continued by Lawrence Sperry in cooperation with the U.S. Navy on a confidential basis. In 1914 a public exhibition was given in Paris of a Curtis flying boat under the control of an automatic pilot (see Fig. III-2). For this exhibition, L. B. Sperry received the Grand Prize; he had demonstrated to the world, for the first time, the practicability of automatic flight. The analysis of servo-control systems for the steering of ships was made by Minorsky[17] in 1922. This study led to the application of autopilots for the control of ships.

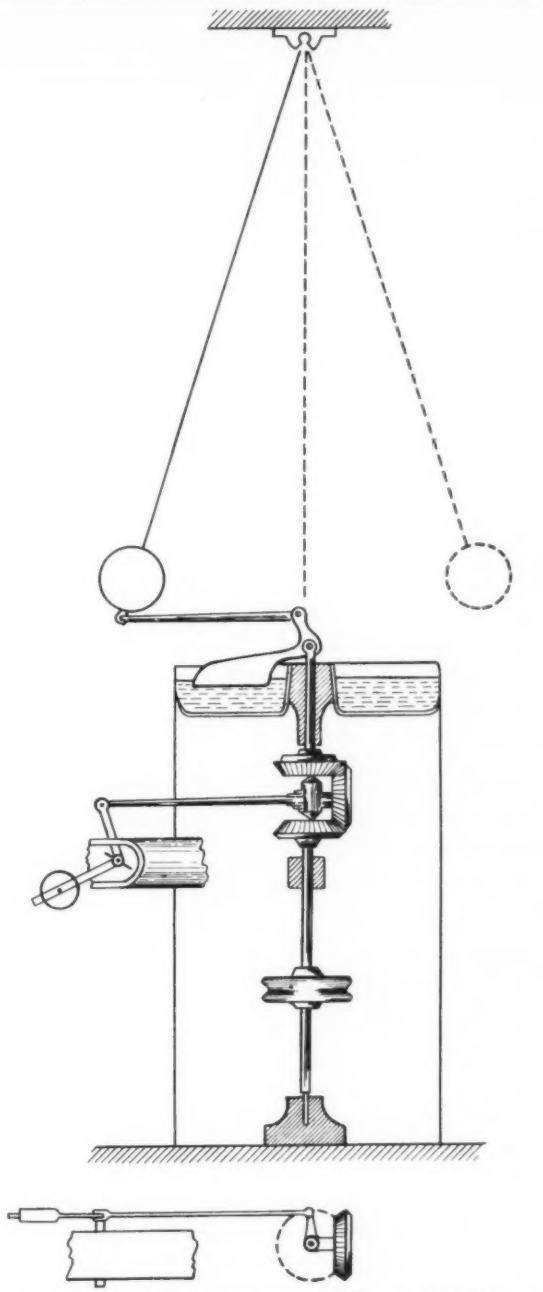

FIG. III-1. Chronometric governor (Siemens,[24] 1843).

Feedback control systems were also applied to electrical networks, and the theory of feedback systems was expanded particularly in connection with the design of electrical feedback amplifiers. Nyquist[19] (1932) in a

* According to Lanchester[1] (*Aerodonetics*, p. 424, 1908): "In 1891 Sir Hiram Maxim proposed to secure the longitudinal stability of his flying machine by means of a gyroscope arranged to actuate horizontal bow and stern rudder, through the medium of a steam or pneumatic relay, in a manner similar to the maintenance of course in the Whitehead torpedo. As this machine never got beyond the captive stage, it may be presumed that the arrangement in question was not carried into effect."

† This information was kindly made available by Mr. P. R. Bassett, President of the Sperry Gyroscope Company, from his company's private files.

FIG. III-2. Prize-winning flight with Sperry gyro stabilizer in Curtiss F-boat, Paris, 1914. L. B. Sperry, pilot, standing in cockpit with hands off controls while mechanic walks out on wing.

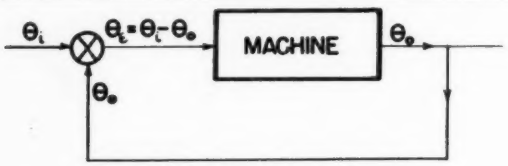

FIG. III-3. Simple feedback loop.

noteworthy paper applied the techniques developed by Cauchy and Routh to the feedback amplifier. Bode[3] extended these techniques and developed a simple graphical analysis. Hazen[14] presented a summary of the theory of servomechanisms (1934). The most widespread application of these techniques came during the early 1940's in connection with the development of antiaircraft gun directors. This work is well presented in a number of excellent books[5, 12, 15] by the M.I.T. staff. A simple, but effective, extension of these techniques was developed by Evans.[9] The application of these techniques for the study of the dynamic performance of an airplane-autopilot system is illustrated in Section (IV).

Probably the major development in aircraft stability during the past 10 years has been the evolution of analytical and experimental techniques that permit an engineering calculation of the motion of an airplane when under the control of an automatic pilot. None of these techniques appears particularly new or novel when viewed by itself. Routh in 1878 used the fundamentals of all of these theoretical techniques in his stability calculations. Thus, to the mathematician, there is little new represented here. The new element is largely that during the past 10 years the engineers have appropriated some of these powerful tools of the mathematical physicist, that they have learned to think in terms of them, and that they have learned thereby to conceive an overall control system that is able to perform not only stably, but accurately according to the input commands.

The principal techniques that have made this development possible are the following:

(*1*) *The Laplace transform method of solving differential equations.*—This technique, which is also called operational calculus, was popularized by Heaviside[33] (1893), who introduced it to electrical engineering. The mathematical fundamentals of this technique are more than 150 years old. Its great usefulness is not only its function as a shorthand method of *solving* differential equations, but even more, its aid in helping the engineer in *synthesizing* a suitable control system. The elements of this method, particularly as they apply to the design of automatic control systems, are summarized in Appendix (A).

(*2*) *The graphical methods of analyzing the dynamic performance of a system, particularly the diagrams often associated with the names of Nyquist, Bode, and Evans.*—These methods are summarized in Section (IV).

(*3*) *The experimental techniques of simulating the physical dynamical system by an equivalent electrical network.*

Last but not least in importance in the evolution of these techniques has been a series of excellent summary reports and textbooks[5, 12, 13, 15] that have introduced these new techniques to a wide circle of engineers.

(IV) Dynamic Analysis of Automatic Control Systems

(*A*) *Introduction*

The general approach in the development of automatic control systems is similar to that of the aerodynamicist in the development of an airplane configuration. It involves the following steps:

(1) Use of a simplified theory with empirical corrections in order to determine the general circuit design. This step is commonly referred to as the synthesis of the system.

(2) Use of models and application of the theory of similarity in order to obtain a better approximation of the performance of the system. Ordinarily, the aerodynamic and inertial elements of the airplane are replaced by a "simulator," an electrical network whose constants are adjusted so that it obeys the same differential equations as the airplane on a one-to-one time basis. In the early phases of the design, the servo-

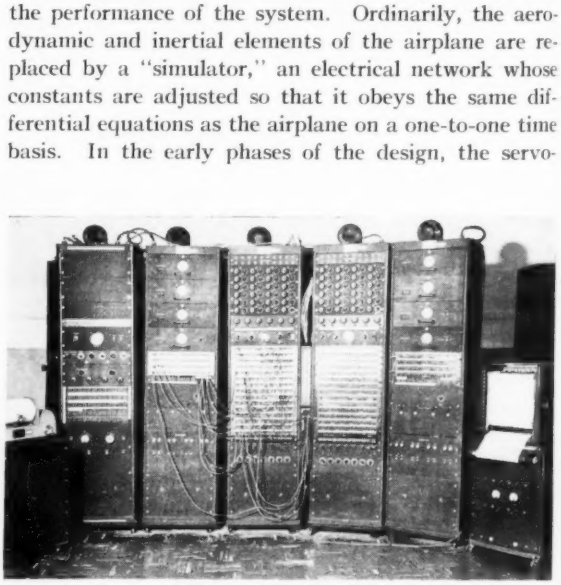

FIG. IV-1. Analog computer.

system elements may also be replaced by an equivalent electrical network. In the later phases of design, the actual servosystem elements are included in the circuit. Thus, the nonlinear characteristics of the hydraulic systems or the effects of mechanical backlash may be correctly introduced.*

(3) Flight tests to determine the actual performance, including the nonlinearities of the elastic and aerodynamic elements, interactions between longitudinal and lateral modes of motion, and the effects of environment (vibrations, pressure, and temperature).

Many of the research methods of aerodynamics also carry over into the analysis of automatic control systems. Thus, the theory of turbulence laid the foundation for the theory of "noise" in electrical circuits.

We shall discuss first of all the simplified theory in which the airplane and its control system are approximated by linear differential equations with constant coefficients. The actual airplane and its control elements are nonlinear systems. It is ordinarily, however, a good approximation to linearize the equations for small oscillations about an equilibrium position. When the nonlinearities become pronounced—for instance, when an airplane goes through a maneuver involving large changes in angle of attack—then the simple analytical methods no longer yield quantitatively correct answers, and they will only be used to obtain a qualitative idea of how to synthesize the system. Ordinarily a combination of analytical and experimental methods is then most conveniently employed in order to obtain the quantitative estimates of the stability and the response of the system.

The linear differential equations of the system are solved by the method of Laplace transforms [see Appendix (A)]. This technique converts the differential equations in terms of the time variable t into algebraic equations in terms of a complex frequency variable $p = \lambda + i\omega$. The solutions of the differential equations are of the type $Ce^{pt} = Ce^{\lambda t} \cdot e^{i\omega t}$. Thus, it is seen that λ, the real part of p, corresponds to the damping coefficient of the solution and that ω, the imaginary part of p, corresponds to the angular frequency.

In order to maintain a good physical insight into the behavior of the system, it is ordinarily desirable not to proceed with the solution in a purely formal manner.

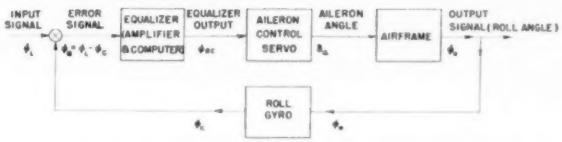

FIG. IV-2. Block diagram of simple roll-control system.

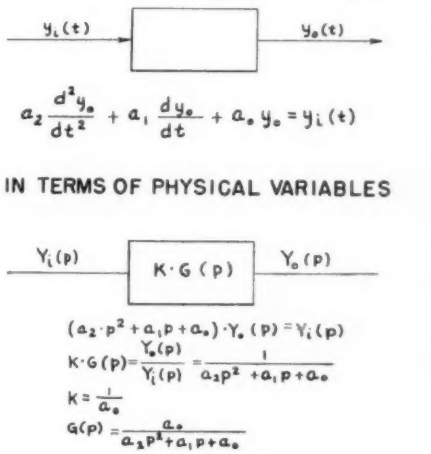

FIG. IV-3. Block diagram of a second-order system.

Ordinarily it is helpful to break down the system by means of a block diagram into its major components. Thus, a simple airplane roll control system consists of the major components shown in Fig. IV-2.

(1) An input signal directs the airplane to roll through an angle φ_i.

(2) The measured roll angle φ_c is compared with the input by a potentiometer and the error angle $\varphi_e = \varphi_i - \varphi_c$ is determined.

(3) This error angle φ_e is the input to an amplifier and computer. Its output is φ_{ec}.

(4) This signal φ_{ec} is introduced into a hydraulic aileron servo, resulting in an output aileron angle δ_a.

(5) This aileron angle δ_a is applied to the air frame, resulting in an actual roll angle φ_0.

(6) This roll angle φ_0 is measured by a roll gyro, resulting in an output signal φ_c (which may be slightly in error due to instrument imperfections).

(7) This gyro signal φ_c is compared with the input φ_i as in step (2).

Each of these block components may then have a further breakdown into its block elements.

The characteristics of any block are determined by the input $y_i(t)$, and the output $y_{0b}(t)$. A more convenient description is obtained in terms of their Laplace transforms (Fig. IV-3). Thus, we shall define

* The most commonly used simulators are of the analog computer type, in which amplification and integration are accomplished electronically. Such a computer is shown in Fig. IV-1. This type is particularly well adapted for tests at the true time scale in connection with autopilot elements for frequencies between 0.005 and 20 cycles per sec. The straightforward electrical analog computer, consisting of resistances, capacitances, and inductances, is suitable for calculation of autopilot responses but not for connection with the actual autopilot hardware. The reason is that inductances and capacitances must be constant and have low losses; thus, the magnitude of LC is limited to approximately 10^{-4}, and correspondingly, the frequency must be 20 cycles per sec. or greater. This type of computer operates therefore, at a much shorter time scale than the actual autopilot.

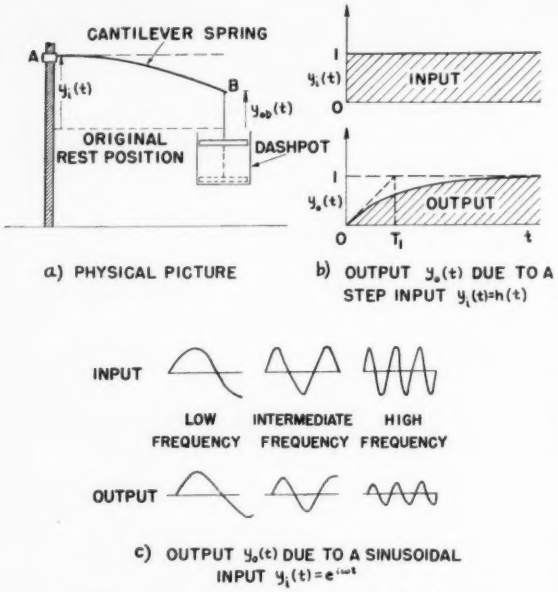

FIG. IV-4. First-order system: spring plus dashpot.

$$Y_i(p) = p \int_0^\infty e^{-pt} . y_i(t) . dt = \text{Laplace transform of input signal } y_i(t)$$

$$Y_{0b}(p) = p \int_0^\infty e^{-pt} . y_{0b}(t) . dt = \text{Laplace transform of output signal } y_{0b}(t)$$

The output $y_{0b}(t)$ and, correspondingly, its transform $Y_{0b}(p)$ would in general consist of two parts:

$$y_{0b}(t) = y_0(t) + y_b(t)$$

(a) The output $y_0(t)$ and its transform

$$Y_0(p) = p \int^\infty e^{-pt} . y_0(t) . dt$$

which are due to the input signal $y_i(t)$.

(*b*) The output $y_b(t)$ and its transform $Y_b(p)$, which are due to the boundary conditions at $t = 0 - \epsilon$—that is, to $y_b(0)$, $y_b'(0)$, $y_b''(0)$, etc.

We define

$$Y_0(p)/Y_i(p) = K . G(p) = \text{ratio of output to input} \tag{IV-1}$$

where

$$Y_0(0)/Y_i(0) = \lim_{p \to 0} Y_0(p)/Y_i(p) = K = \text{"gain"} \tag{IV-2}$$

and

$$G(p) = (1/K)\ Y_0(p)/Y_i(p) = \text{"transfer function"} \tag{IV-3}$$

Note that the input and output do not necessarily have the same dimensions. Thus, the input may be the transform of a linear velocity, $V_i(p) = p . Y_i(p)$, and the output may be the transform of a displacement, $Y_0(p)$. Then the ratio

$$\frac{Y_0(p)}{V_i(p)} = \frac{Y_0(p)}{p . Y_i(p)} = K . G(p)$$

and

$$\frac{Y_0(p)}{Y_i(p)} = K G_1(p)$$

where $G_1(p) = p . G(p)$.

Fig. IV-3 illustrates the definitions of the gain and the transfer function for a second-order system. It is seen from Fig. IV-19 that the gain of a series circuit is the product of the gains of the elements and that the overall transfer function is the product of the transfer functions of the elements.

The basic elements into which these blocks are resolved are first-order or second-order systems. In our simple analysis, we shall therefore study particularly the characteristics of the first-order and second-order systems and the methods for combining the solutions of these simple systems. The purpose of the analysis will be two-fold: (a) to determine the range of parameters for which the overall system is stable and (b) to determine the accuracy of control—i.e., to compute the overall output response for a given input.

(*B*) *Analysis of First-Order Systems*

Consider a cantilever spring (Fig. IV-4) which has a dashpot at its end B. The spring stiffness is k, the damping constant of the dashpot is c. The end A of the cantilever spring is moved upward; its position being given by $y_i(t)$. End B lags behind the input due to the damping; it experiences the displacement $y_{0b}(t)$. (This simple case approximates, for example, the motion of a recording pen having viscous friction.) Neglecting the mass-acceleration forces, the forces acting on the dashpot are

$$\text{Spring force—upward} = k(y_i - y_{0b})$$

$$\text{Damping force—upward} = -c . dy_{0b}/dt$$

Thus, the equation of motion is

$$c(dy_{0b}/dt) + k y_{0b} = k y_i \tag{IV-4}$$

or

$$T_1 . (dy_{0b}/dt) + y_{0b} = y_i$$

where $T_1 = c/k$. The boundary condition is $y_{0b} = y_b(0)$ at $t = 0 - \epsilon$ where $y_b(0)$ is a constant. The Laplace transform of this equation is

$$(T_1 . p + 1) . Y_{0b}(p) = Y_i(p) + T_1 . p . y_b(0)$$

and thus

$$Y_{0b}(p) = \underbrace{\frac{1}{T_1 p + 1} \cdot Y_i(p)}_{Y_0(p)} + \underbrace{\frac{T_1 p}{T_1 p + 1} \cdot y_b(0)}_{Y_b(p)} \quad \text{(IV-5)}$$

The term $Y_0(p)$ represents the Laplace transform of the output motion which is due to the input signal $y_i(t)$. The term $Y_b(p)$ represents the Laplace transform of the output motion which is due to the initial boundary condition $y_b(0)$.

The transfer function in this case is found from

$$KG(p) = Y_0(p)/Y_i(p) = 1/(T_1 p + 1) \quad \text{(IV-6)}$$

and thus

$$K = 1$$
$$G(p) = 1/(T_1 p + 1)$$

The poles and zeros* completely characterize the transfer function $G(p)$. We shall represent $G(p)$ in the p-plane by indicating each zero with a cross and each pole with a small circle. The transfer function $G(p) = 1/(T_1 p + 1)$ has no zeros, but it has a simple pole at $p = -1/T_1$, as shown in Fig. IV-5c.

Special case: $y_i(t) = h(t)$

For the special case of a unit step input in displacement, we have [from Eq. (B-9)]

$$y_i(t) = h(t)$$
$$Y_i(p) = 1$$

The corresponding solution for the first-order Eq. (IV-6) is [from Eq. (B-8)]

$$\left.\begin{aligned} Y_0(p) &= 1/(T_1 p + 1) \\ y_0(t) &= (1 - e^{-t/T_1}) \end{aligned}\right\} \quad \text{(IV-7)}$$

and from Eq. (B-1)

$$\left.\begin{aligned} Y_0(p) &= [T_1 . p . y_b(0)]/(T_1 p + 1) \\ y_b(t) &= y_b(0) . e^{-t/T_1} \end{aligned}\right\} \quad \text{(IV-8)}$$

and thus the complete solution is

$$y_{0b}(t) = \underbrace{(1 - e^{-t/T_1})}_{y_0(t)} + \underbrace{y_b(0) . e^{-t/T_1}}_{y_b(t)} \quad \text{(IV-9)}$$

The term $y_b(t) = y_b(0) . e^{-t/T_1}$ represents a damped subsidence due to the initial boundary condition $y_b(0)$. This term enters into the analysis of automatic control systems only when it is necessary to compute the response of a system that is not initially at rest and in equilibrium.

The term $y_0(t) = 1 - e^{-t/T_1}$ represents the output motion due to the step input $h(t)$. This term is shown in Fig. IV-4b. It is represented by an exponential approach to the input. It indicates that the output lags behind the input, that at a time $t = T_1$, the output has reached 63 per cent of its asymptotic deflection. The error signal is

$$y_e(t) = y_i(t) - y_0(t) = e^{-t/T_1}$$

We note that the error $y_e(t) \to 0$ as $t \to \infty$ and that the initial slope of the output is

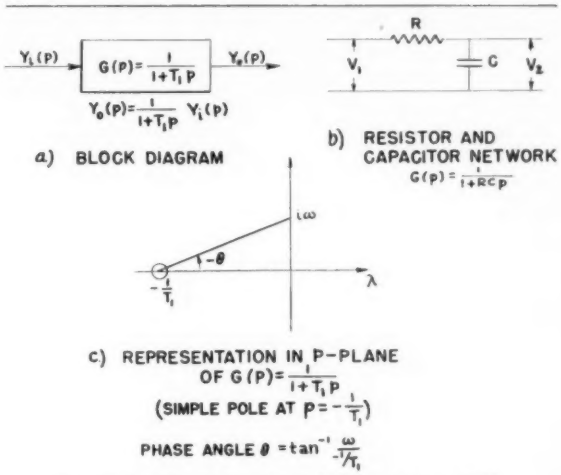

FIG. IV-5. Simple lag circuit $G(p) = 1/(1 + T_1 p)$.

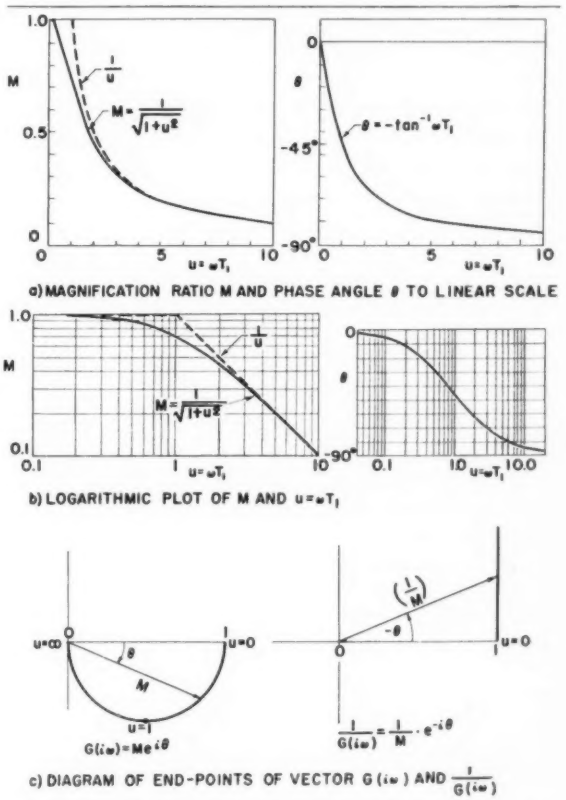
M
$\frac{1}{u}$
$M = \frac{1}{\sqrt{1+u^2}}$
$\theta = -\tan^{-1} \omega T_1$
$u = \omega T_1$
a) MAGNIFICATION RATIO M AND PHASE ANGLE θ TO LINEAR SCALE
b) LOGARITHMIC PLOT OF M AND $u = \omega T_1$
$u = \infty$
$u = 0$
$G(i\omega) = Me^{i\theta}$
$\frac{1}{G(i\omega)} = \frac{1}{M} \cdot e^{-i\theta}$
c) DIAGRAM OF END-POINTS OF VECTOR $G(i\omega)$ AND $\frac{1}{G(i\omega)}$

FIG. IV-6. Simple lag circuit: $G(i\omega) = Me^{i\theta} = 1/(1 + i\omega T_1)$; response to sinusoidal input.

* We define a *simple pole* of a function as a point at which the function becomes infinite, like $1/x$ as $x \to 0$. We define a *simple zero* of a function as a point at which the function becomes zero, like x as $x \to 0$. Thus, the function $Y(p) = p/(p - a)$ has a simple pole at $p = a$ and a simple zero at the origin $p = 0$.

$$\left.\frac{dy_0(t)}{dt}\right]_{t=0} = \left.\frac{1}{T_1}\cdot e^{-t/T_1}\right]_{t=0} = \frac{1}{T_1}$$

Special case: $y_i(t) = y_{im}\cdot e^{i\omega t}$

The special case of a sinusoidal input with frequency ω is most conveniently represented by writing the input $y_i(t) = y_{im}\cdot e^{i\omega t}$ where $e^{i\omega t} = \cos\omega t + i\sin\omega t$. Thus, the real part of the input is $y_{im}\cdot\cos\omega t$, the imaginary part is $y_{im}\cdot\sin\omega t$. The Laplace transform of the input is $Y_i(p) = y_{im}\cdot p/(p - i\omega)$ from Eq. (B-2). The corresponding solution for the first-order equation [Eq. (IV-6)] is

$$\left.\begin{aligned} Y_b(p) &= [T_1 p\cdot y_b(0)]/(T_1 p + 1) \\ y_b(t) &= y_b(0)\cdot e^{-t/T_1} \end{aligned}\right\} \quad \text{(IV-10)}$$

$$\left.\begin{aligned} Y_0(p) &= y_{im}\cdot\frac{p}{p - i\omega}\cdot\frac{1}{T_1 p + 1} \\ y_0(t) &= \underbrace{\frac{-y_{im}}{1 + i\omega T_1}\cdot e^{-t/T_1}}_{[y_0(t)]_{\text{transient}}} + \underbrace{\frac{y_{im}}{1 + i\omega T_1}\cdot e^{i\omega t}}_{[y_0(t)]_{\text{steady}}} \end{aligned}\right\} \quad \text{(IV-11)}$$

The terms $Y_b(p)$ and $y_b(t)$ are the same as obtained in the previous special case. The solution $y_0(t)$ may be obtained from Eq. (A-15) or by expressing $Y_0(p)$ in partial fractions of the form

$$Y_0(p) = Y_0(0) + A_1\cdot\frac{p}{p + (1/T_1)} + A_2\cdot\frac{p}{p - i\omega}$$

We then have from Eq. (A-9):

$$\begin{aligned} Y_0(0) &= 0 \\ A_1 &= -y_{im}/(1 + i\omega T_1) \\ A_2 &= y_{im}/(1 + i\omega T_1) \end{aligned}$$

We note that the solution $y_0(t)$ has as its first term $A_1\cdot e^{-t/T_1}$, a damped subsidence. This term represents a transient disturbance associated with the initial application of the force.

The second term of $y_0(t)$ is $y_{im}/(1 + i\omega T_1)e^{i\omega t}$. This term represents a steady sinusoidal vibration at the same frequency ω as the input.

The ratio

$$\frac{[y_0(t)]_{\text{steady}}}{y_i(t)} = \frac{1}{1 + i\omega T_1} \quad \text{(IV-12)}$$

It will be noted that this ratio is the same as would be obtained by writing $i\omega$ instead of p in $G(p)$—that is,

$$G(i\omega) = 1/(1 + i\omega T_1)$$

and thus for a sinusoidal input

$$[y_0(t)]_{\text{steady}} = G(i\omega)\cdot y_i(t)$$

This result follows as a special case of Eq. (A-15). It is convenient to express the complex vector $G(i\omega)$ in terms of its magnitude M and its phase angle θ—that is,

$$G(i\omega) = Me^{i\theta}$$

In the above example of a first-order system we then find

$$Me^{i\theta} = \frac{1}{1 + i\omega T_1} = \frac{1 - i\omega T_1}{1 + \omega^2 T_1^2}$$

that is,

$$M = 1/\sqrt{1 + \omega^2 T_1^2} \quad \text{(IV-13)}$$

$$\tan\theta = -\omega T_1 \quad \text{(IV-14)}$$

The above relations indicate how well the output is able to follow a sinusoidal variation in the input; corresponding experimental records are shown in Fig. IV-4c. We note that at very low frequencies the steady output $y_0(t)$ follows the input $y_i(t)$ in magnitude and phase, at higher frequencies the ratio M becomes less than one and the output lags the input, and at very high frequencies $M \to 0$ and the phase angle lags by 90°. The variation of M and θ with the dimensionless frequency $u = \omega T_1$ is shown in Fig. IV-6a. It will be noted that for large values of u, $M \approx 1/u$. It is convenient to plot the curves of M vs. u on log-log paper (Fig. IV-6b). This corresponds to plotting $\log_{10} M$ vs. $\log_{10} u$. Then we note that for large values of u, since $\log_{10} M \approx \log_{10} 1/u = -\log_{10} u$, the slope becomes -1; for small values of u, $\log_{10} M$ starts with a slope of 0. Thus, the first-order system can be approximated by the two dotted straight lines on this diagram.

In the acoustic and electrical literature it is customary to plot $20\log_{10} M$ in order to convert the amplitude units into decibels. A doubling in frequency is called an octave, and thus the region where our curve of $\log_{10} M$ vs. $\log_{10} u$ has a slope of -1 is denoted by a slope of $-20\log_{10} 2 = -6.03$ db. per octave. In order to read the electrical literature, it is necessary to know this definition; there appears to be little reason, however, to introduce this complication into the aerodynamics literature.

It will be noted that on this logarithmic plot the approximate curve $\log_{10} M$ goes through 0 at $u = 1$—that is, at $\omega = 1/T_1$. If we therefore measure the experimental response of a first-order system and plot it as indicated above, the delay time T_1 is easily estimated by noting the frequency at which a straight-line approximation for large values of ω crosses the axis. The above described methods of plotting the response curves to a logarithmic scale and the corresponding approximations were pointed out by Bode.[3]

Another convenient method of representing $G(i\omega) = Me^{i\theta}$ is directly as a complex vector of magnitude M and argument θ. Since both of these functions have already been plotted in Fig. IV-6b, it is simple to construct the vector diagram of $G(i\omega)$. This diagram for a first-order system is shown in Fig. IV-6c. We note that this diagram consists of a half circle, starting at $G(i\omega) = 1$ at $\omega = 0$, going through $G(i\omega) = 1/(1 + i) = (1/\sqrt{2})(1 - i)$ at $\omega T_1 = 1$, and ending at $G(i\omega) = 0$ at

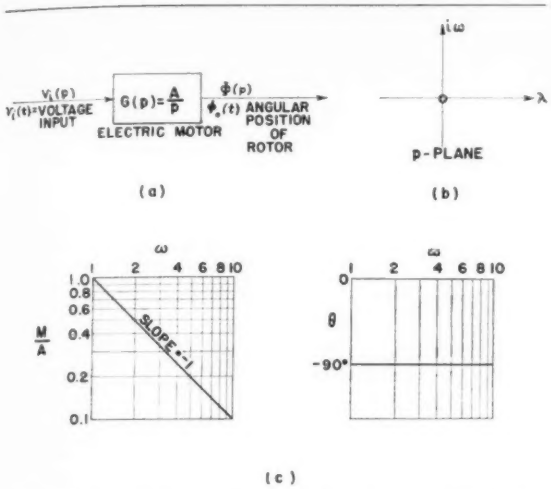

FIG. IV-7. Integrator circuit: $G(i\omega) = A/i\omega$. (a) Block diagram of $G(p) = A/p$. (b) Representation in p-plane (simple pole at $p = 0$). (c) Response to sinusoidal input: $G(i\omega) = Me^{i\theta}$. $M = A/\omega$ = magnification ratio (logarithmic scale), $\theta = -90°$ = phase angle, and ω = exciting frequency (logarithmic scale).

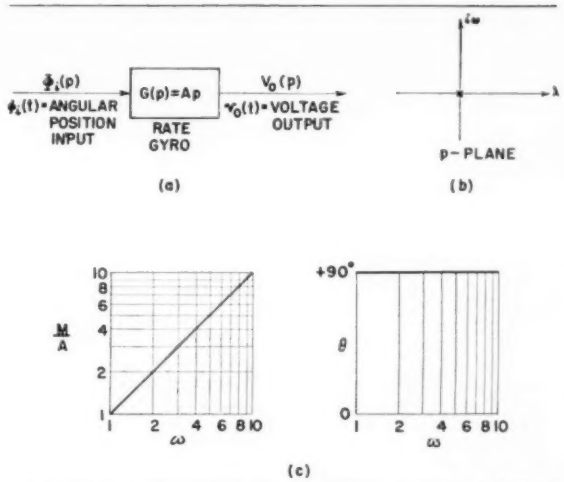

FIG. IV-8. Differentiator circuit: $G(i\omega) = i\omega A$. (a) Block diagram of $G(p) = Ap$. (b) Representation in p-plane (simple zero at $p = 0$). (c) Response to sinusoidal input: $G(i\omega) = Me^{i\theta}$. $M = A\omega$ = magnification ratio (logarithmic scale), $\theta = +90°$ = phase angle, and ω = exciting frequency (logarithmic scale).

$\omega T_1 = \infty$. This vector representation of the response curves was introduced by Nyquist. For many purposes it is more convenient to plot $1/G(i\omega)$. It will be noted that, in the case of a first-order system, this results in the straight line $1/G(i\omega) = 1 + i\omega T_1$ (Fig. IV-6c).

Summary.—Summarizing the important conclusions for a simple first-order system we note the following:

(1) Its transfer function is $G(p) = 1/(T_1 p + 1)$, which has a simple pole at $p = -1/T_1$.

(2) For a step input the output approaches the input exponentially with the time constant T_1.

(3) For a sinusoidal input there is a transient and a steady-state output. The ratio of steady-state output to sinusoidal input, which is most important for the stability analysis, may be written down directly from the transfer function

$$\frac{[y_0(t)]_{\text{steady}}}{y_i(t)} = Me^{i\theta} = G(i\omega) = \frac{1}{1 + i\omega T_1}$$

(4) The transient disturbance due to the initial boundary conditions at $t = 0 - \epsilon$ and the transient disturbance associated with the initial application of the force are damped out like e^{-t/T_1}. These terms are important for calculation of the response curve but not for the stability analysis.

Examples of Other First-Order Systems.—The following physical systems may be approximated by first-order differential equations, and they frequently occur in the synthesis of aircraft control systems:

(1) Integrator:

$$G(p) = A/p \qquad \text{(IV-15)}$$

An electric motor whose speed $d\varphi_0/dt$ is proportional to an input voltage v_i follows the equation $d\varphi_0/dt = Av_i$ where A is a scale factor. Thus, the angular rotation φ_0 of the motor is proportional to $\int_0^t v_i \, dt$. This relation is represented by the block diagram of Fig. IV-7a in terms of the Laplace transforms $\Phi_0(p)$ and $V_i(p)$. This transfer function represents a limiting case of $G(p) = 1/(T_1 p + 1)$ as $T_1 \to \infty$. Thus, the transfer function is represented by a pole at the origin. The output response to a sinusoidal input is obtained from

$$Me^{i\theta} = G(i\omega) = A/i\omega = (A/\omega)e^{-i\pi/2}$$

Thus

$$M = A/\omega \qquad \text{(IV-16)}$$

i.e., the output is attenuated at high frequencies proportional to $1/\omega$ and

$$\theta = -\pi/2 = -90° \qquad \text{(IV-17)}$$

i.e., the output *lags* the input by 90°. These relations are shown in Fig. IV-7c.

(2) Differentiator: A rate gyro gives a voltage output v_0 proportional to the angular velocity $d\varphi_i/dt$ of the precession axis—i.e., $v_0 = A(d\varphi_i/dt)$ where A is the scale factor. This case is, therefore, the inverse of the preceding one. The block diagram is shown in Fig. IV-8a. The transfer function $G(p) = Ap$ has a zero at the origin (Fig. IV-8b). The output response to a sinusoidal input is obtained from

$$Me^{i\theta} = G(i\omega) = Ai\omega = A\omega e^{i\pi/2} \qquad \text{(IV-18)}$$

Thus,

$$M = A\omega \qquad \text{(IV-19)}$$

i.e., the output is proportional to the input frequency ω and

$$\theta = \pi/2 = +90^\circ \qquad \text{(IV-20)}$$

i.e., the output *leads* the input by 90°. These relations are shown in Fig. IV-8c.

(3) Simple lag network:

$$G(p) = 1/(1 + T_1 p) \qquad \text{(IV-21)}$$

The resistor and capacitor network shown in Fig. IV-5b has the transfer function

$$V_2(p)/V_1(p) = G(p) = 1/(1 + RCp)$$

which is the same as that of the spring-damper system of Fig. IV-4a with $T_1 = RC$. This circuit is frequently used in order to introduce a phase lag into a system. If the input signal is sinusoidal with frequency ω, the phase angle θ may be read conveniently from Fig. IV-5c, since $\tan\theta = -\omega T_1$. The output response to a sinusoidal input is given in Fig. IV-6. It is generally more convenient to deal with the reciprocal of the delay time, and thus we define $\omega_1 = 1/T_1$ and correspondingly the transfer function for a simple lag network

$$G(p) = 1/[1 + (p/\omega_1)] = \omega_1/(\omega_1 + p)$$

(4) Lead network:

$$G(p) = \frac{1}{\epsilon}\cdot\frac{\epsilon\omega_1 + p}{\omega_1 + p}, \qquad K = \epsilon \qquad \text{(IV-22)}$$

The resistor and capacitor network shown in Fig. IV-9 obeys the following relations:

$$\frac{V_2(p)}{V_1(p)} = KG(p) = \frac{R_2 + R_1R_2Cp}{(R_1 + R_2) + R_1R_2Cp} \qquad \text{(IV-23)}$$

or

$$G(p) = \frac{1 + (p/\epsilon\omega_1)}{1 + (p/\omega_1)}, \qquad K = R_2/(R_1 + R_2) \qquad \text{(IV-24)}$$

where

$$\omega_1 = (R_1 + R_2)/R_1R_2C, \qquad \epsilon = R_2/(R_1 + R_2) \qquad \text{(IV-25)}$$

The transfer function $G(p)$ has a zero at $p = -\epsilon\omega_1$ and a pole at $p = -\omega_1$. The value of ϵ varies ordinarily between 0.1 and 1. The characteristics of this system are as follows for a sinusoidal input:

$$Me^{i\theta} = G(i\omega) = \frac{1}{\epsilon}\,\frac{\epsilon\omega_1 + i\omega}{\omega_1 + i\omega}$$

where

$$M = \sqrt{[1 + (\omega^2/\epsilon^2\omega_1^2)]/[1 + (\omega^2/\omega_1^2)]} \qquad \text{(IV-26)}$$

$$\theta = \underbrace{\tan^{-1}\omega/\epsilon\omega_1}_{\theta_1} - \underbrace{\tan^{-1}\omega/\omega_1}_{\theta_2} \qquad \text{(IV-27)}$$

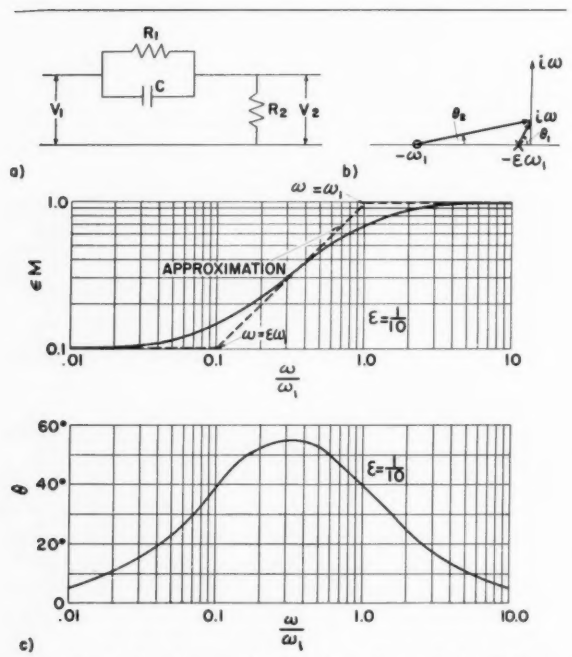

FIG. IV-9. Lead network $KG(i\omega) = [1 + i(\omega/\epsilon\omega_1)]/[1 + (i\omega/\omega_1)]$. (a) Block diagram, $V_2(p)/V_1(p) = KG(p) = (\epsilon\omega_1 + p)\div(\omega_1 + p)$. (b) Representation in p-plane. $G(p)$ has a simple zero at $p = -\epsilon\omega_1$ and a simple pole at $p = -\omega_1$. (c) Response to sinusoidal input $G(i\omega) = Me^{i\theta}$. M = magnification ratio (logarithmic scale), $\theta = \theta_1 - \theta_2$ = phase angle, ω = exciting frequency (logarithmic scale), and $\epsilon = K$ = gain.

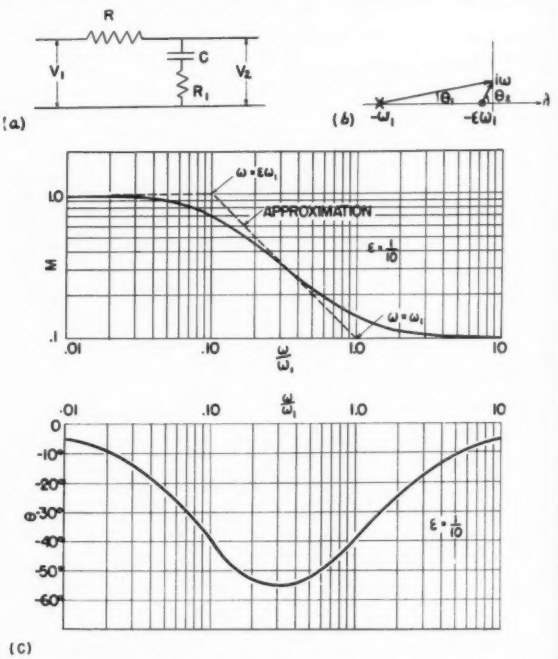

FIG. IV-10. Restricted lag network $G(i\omega) = [1 + i(\omega/\omega_1)]\div[1 + i(\omega/\epsilon\omega_1)]$. (a) Block diagram, $V_2(p)/V_1(p) = KG(p) = \epsilon(\omega_1 + p)/(\epsilon\omega_1 + p)$. (b) Representation in p-plane; $G(p)$ has a simple pole at $p = -\epsilon\omega_1$ and a simple zero at $p = -\omega_1$. (c) Response to sinusoidal input $G(i\omega) = Me^{i\theta}$. M = magnification factor (logarithmic scale), $\theta = \theta_1 - \theta_2$ phase angle, ω = exciting frequency (logarithmic scale), and $K = 1$ = gain.

The angles θ_1 and θ_2 are indicated in Fig. IV-9. We note that for very low frequencies ($\omega \to 0$) $\theta \approx 0$, $M \approx 1$, and $KM \approx \epsilon$; for very high frequencies ($\omega \to \infty$) $\theta \approx 0$, $M \approx 1/\epsilon$, and $KM \approx 1$; and for intermediate frequencies $0 < \theta < 90°$ and $\epsilon < KM < 1$. Thus, this circuit introduces a *phase lead* into the system over a limited band of frequencies. The values of M and θ are shown in Fig. IV-9c.

(5) Restricted lag network:

$$G(p) = \epsilon(\omega_1 + p)/(\epsilon\omega_1 + p), \qquad K = 1 \quad \text{(IV-28)}$$

The resistor and capacitor network shown in Fig. IV-10 has the transfer function

$$\frac{V_2(p)}{V_1(p)} = K.G(p) = \frac{1 + R_1Cp}{1 + (R_1 + R)Cp} \quad \text{(IV-29)}$$

$$G(p) = [1 + (p/\omega_1)]/[1 + (p/\epsilon\omega_1)]$$
$$K = 1$$

where

$$\omega_1 = 1/RC \quad \text{(IV-30)}$$

$$\epsilon = R_1/(R_1 + R) \quad \text{(IV-31)}$$

The transfer function $G(p)$ has a zero at $p = -\omega_1$ and a pole at $p = -\epsilon\omega_1$. The value of ϵ varies ordinarily between 0.1 and 1.

The characteristics of this system are as follows for a sinusoidal input:

$$Me^{i\theta} = G(i\omega) = \frac{1 + i(\omega/\omega_1)}{1 + i(\omega/\epsilon\omega_1)}$$

where

$$M = \sqrt{[1 + (\omega^2/\omega_1^2)]/[1 + (\omega^2/\epsilon^2\omega_1^2)]} \quad \text{(IV-32)}$$

$$\theta = \underbrace{\tan^{-1}\omega/\omega_1}_{\theta_1} - \underbrace{\tan^{-1}\omega/\epsilon\omega_1}_{\theta_2} \quad \text{(IV-33)}$$

The angles θ_1 and θ_2 are indicated in Fig. IV-10b. We note that this circuit introduces a *phase lag* over a limited band of frequencies. The values of M and θ are shown in Fig. IV-10c.

(6) Simplified aerodynamic stability equations: The simplified equations for the rolling motion of an airplane are

$$I\frac{d^2\varphi}{dt^2} + L_\varphi.\frac{d\varphi}{dt} = k.\delta \quad \text{(IV-34)}$$

where I is the moment of inertia about the roll axis, L_φ is the aerodynamic damping in roll, and $k\delta$ is the torque applied due to the aileron deflection δ. Writing $n = d\varphi/dt$, then

$$I(dn/dt) + L_\varphi.n = k\delta$$

In terms of Laplace transforms we find, if $n(0) = 0$

$$(Ip + L_\varphi).N(p) = k.D(p)$$

Thus

$$KG(p) = N(p)/D(p) = k/(Ip + L_\varphi)$$

or

$$G(p) = 1/[(I/L_\varphi).p + 1] \quad \text{(IV-35)}$$
$$K = k/L_\varphi$$

The analysis of these simplified equations follows that of the simple lag network, Figs. IV-5 and IV-6. Sometimes the aerodynamic damping L_φ is so small as to be negligible; then the analysis follows that of the simple integrator circuit, Fig. IV-7.

(C) *Analysis of Second-Order Systems*

Let us consider the cantilever spring of Fig. IV-4 which has a dashpot at its end B and include the finite mass m of this dashpot. Then, the additional force acting upward on the dashpot is $-m.(d^2y_{0b}/dt^2)$. The equation of motion then becomes

$$m\frac{d^2y_{0b}}{dt^2} + c\frac{dy_{0b}}{dt} + ky_{0b} = ky_i \quad \text{(IV-36)}$$

with boundary conditions

$$y_{0b}(t) = y_b(0) \text{ at } t = 0 - \epsilon$$
$$dy_{0b}(t)/dt = y_b'(0) \text{ at } t = 0 - \epsilon$$

We introduce the following ratios

$\omega_0 = \sqrt{k/m}$ = natural frequency of undamped mass-spring system

$\zeta = (c/m)/2\omega_0$ = ratio of actual damping coefficient to critical damping coefficient

Then the equation of motion becomes

$$\frac{d^2y_{0b}}{dt^2} + 2\zeta\omega_0.\frac{dy_{0b}}{dt} + \omega_0^2.y_{0b} = \omega_0^2.y_i$$

and its Laplace transform is

$$(p^2 + 2\zeta\omega_0.p + \omega_0^2).Y_{0b}(p) = \omega_0^2.Y_i(p)$$

Thus

$$Y_{0b}(p) = \underbrace{\frac{\omega_0^2}{p^2 + 2\zeta\omega_0 p + \omega_0^2}.Y_i(p)}_{Y_0(p)} + \underbrace{\frac{p.y_b'(0) + (p^2 + 2\zeta\omega_0 p).y_b(0)}{p^2 + 2\zeta\omega_0 p + \omega_0^2}}_{Y_b(p)} \quad \text{(IV-37)}$$

The term $Y_0(p)$ represents the Laplace transform of the output motion which is due to the input signal $y_i(t)$. The term $Y_b(p)$ represents the Laplace transform of the output motion which is due to the initial boundary conditions $y_b(0)$ and $y_b'(0)$. The transfer function in this case is

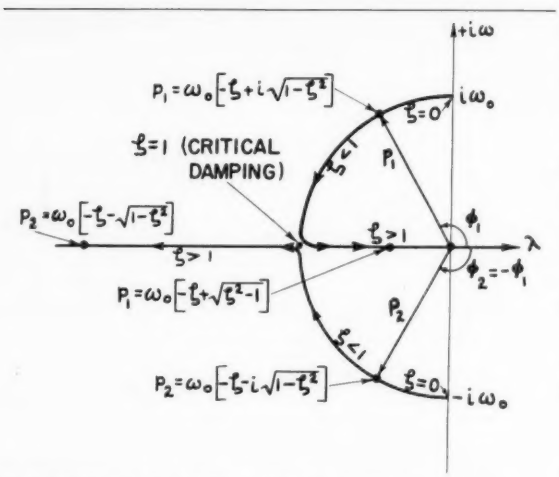

a) VARIATION OF ROOTS WITH DAMPING RATIO ζ

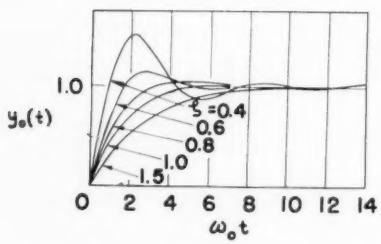

b) RESPONSE TO A STEP-INPUT: $y_i(t)=h(t)$

FIG. IV-11. Second-order system characteristics.

$$K.G(p) = \frac{Y_0(p)}{Y_i(p)} = \frac{\omega_0^2}{p^2 + 2\zeta\omega_0 p + \omega_0^2}$$

and thus

$$K = 1$$

$$G(p) = \omega_0^2/(p^2 + 2\zeta\omega_0 p + \omega_0^2) \qquad \text{(IV-38)}$$

This transfer function $G(p)$ has no zeros, but it has two poles at p_1 and p_2, respectively, where p_1 and p_2 are the roots of the denominator $D(p) = p^2 + 2\zeta\omega_0 p + \omega_0^2 = 0$. These are

$$\left.\begin{aligned} p_1 &= \omega_0(-\zeta + \sqrt{\zeta^2 - 1}) \\ p_2 &= \omega_0(-\zeta - \sqrt{\zeta^2 - 1}) \end{aligned}\right\} \text{ if } \zeta > 1$$

$$\left.\begin{aligned} p_1 &= \omega_0(-\zeta + i\sqrt{1 - \zeta^2}) = \\ &\quad \lambda + i\nu = \omega_0 e^{i\varphi_1} \\ p_2 &= \omega_0(-\zeta - i\sqrt{1 - \zeta^2}) = \\ &\quad \lambda - i\nu = \omega_0 e^{-i\varphi_1} \end{aligned}\right\} \text{ if } \zeta < 1 \qquad \text{(IV-39)}$$

We shall find that $\lambda = -\omega_0\zeta$ is the damping factor and $\nu = \sqrt{1 - \zeta^2}.\omega_0$ is the natural frequency of this second-order system. The roots p_1 and p_2 are complex conjugates if $\zeta < 1$. For a fixed value of ω_0, the locus of these roots as the damping coefficient c is varied is on a circle of radius ω_0 about the origin, Fig. IV-11. This is easily seen, since $\lambda^2 + \nu^2 = \omega_0^2$, which is the equation of a circle in the p-plane. For $\zeta = 0$, the roots are $p_1 = i\omega_0$ and $p_2 = -i\omega_0$. For $\zeta = 1$, the roots are $p_1 = p_2 = -\omega_0$. This point corresponds to critical damping of the system. For intermediate values $0 < \zeta < 1$, the roots lie at intermediate points on the upper and lower half of the circle, respectively. As ζ increases above $\zeta = 1$, the root p_1 moves along the negative real axis toward the origin, and the root p_2 moves along the negative real axis toward $\lambda = -\infty$.

The solution $y_b(t)$ due to the initial boundary conditions is found as follows for the case $\zeta < 1$. We introduce $\lambda = -\zeta\omega_0$ and $\nu = \sqrt{1 - \zeta^2}.\omega_0$ into $Y_b(p)$. Since

$$D(p) = p^2 + 2\zeta\omega_0 p + \omega_0^2 = (p - \lambda)^2 + \nu^2$$

we have

$$\begin{aligned} Y_b(p) &= \frac{p.y_b'(0)}{(p - \lambda)^2 + \nu^2} + \frac{p.(p - 2\lambda).y_b(0)}{(p - \lambda)^2 + \nu^2} \\ &= \frac{p.\nu}{(p - \lambda)^2 + \nu^2}.\frac{y_b'(0)}{\nu} + \frac{p(p - \lambda)}{(p - \lambda)^2 + \nu^2}. \\ &\quad y_b(0) + \frac{p.\nu}{(p - \lambda)^2 + \nu^2}.\left(\frac{-\lambda}{\nu}\right).y_b(0) \end{aligned}$$

and thus from Eqs. (B-6) and (B-7),

$$y_b(t) = \frac{y_b'(0)}{\nu}.e^{\lambda t}.\sin \nu t + y_b(0).e^{\lambda t}.\cos \nu t + \left(\frac{-\lambda}{\nu}\right).y_b(0).e^{\lambda t}.\sin \nu t \qquad \text{(IV-40)}$$

Since λ is a negative number, it is seen that the initial motion due to the boundary conditions is a damped sine wave with damping factor $\lambda = -\zeta\omega_0$ and with the natural frequency $\nu = \sqrt{1 - \zeta^2}\omega_0$. The solution for $\zeta > 1$ is obtained similarly.

Let us examine more carefully the forced motion due to the input $y_i(t)$.

(1) *Special case:* $y_i(t) = h(t)$.—For the special case of a unit step input in displacement, $y_i(t) = h(t)$ and $Y_i(p) = 1$. The corresponding solution for the second-order equation is then

$$Y_0(p) = \frac{\omega_0^2}{p^2 + 2\zeta\omega_0 p + \omega_0^2} = \frac{\omega_0^2}{(p - \lambda)^2 + \nu^2} \qquad \text{(IV-41)}$$

and thus from Eqs. (B-6) and (B-7) we find

$$y_0(t) = 1 - [\cos \nu t - (\lambda/\nu).\sin \nu t].e^{\lambda t} \qquad \text{(IV-42)}$$

This solution is plotted in Fig. IV-11b. We note that the output $y_0(t)$ approaches the input $y_i(t)$ for large values of t. After the initial application of the force, the output overshoots the equilibrium position if $\zeta < 1$; it approaches the equilibrium exponentially if $\zeta > 1$. The region $0.4 < \zeta < 1$ is ordinarily considered a good compromise between quick approach to the input and excessive overshooting.

(2) Special case: $y_i(t) = y_{im} \cdot e^{i\omega t}$.—The special case of sinusoidal input $y_i(t) = y_{im} \cdot e^{i\omega t}$ is solved most conveniently by applying Eq. (A-15). We have

$$Y_i(p) = y_{im} \cdot [p/(p - i\omega)]$$

and

$$\left.\begin{aligned} G(p) &= \frac{N(p)}{D(p)} = \frac{\omega_0^2}{p^2 + 2\zeta\omega_0 p + \omega_0^2} \\ G(p) &= \omega_0^2/[(p - p_1)(p - p_2)] \end{aligned}\right\} \quad \text{(IV-43)}$$

$$\begin{aligned} N(p) &= \omega_0^2 \\ D'(p) &= 2p + 2\zeta\omega_0 = 2(p - \lambda) \\ p_1 &= \lambda + i\nu, \qquad D'(p_1) = 2i\nu \\ p_2 &= \lambda - i\nu, \qquad D'(p_2) = -2i\nu \end{aligned}$$

Thus,

$$Y_0(p) = y_{im} \{[p/(p - i\omega)] \cdot G(p)\} \quad \text{(IV-44)}$$

and

$$\begin{aligned} y_0(t) &= y_{im}\left[G(i\omega) \cdot e^{i\omega t} + \frac{N(p_1)}{(p_1 - i\omega) \cdot D'(p_1)} e^{p_1 t} + \frac{N(p_2)}{(p_2 - i\omega) \cdot D'(p_2)} e^{p_2 t}\right] \\ &= y_{im}\left[G(i\omega) \cdot e^{i\omega t}\right] + y_{im} \cdot \underbrace{\left[\frac{\omega_0^2}{\lambda + i(\nu - \omega)} \cdot \frac{1}{2i\nu}\right]}_{A} e^{(\lambda + i\nu)t} + y_{im} \underbrace{\left[\frac{\omega_0^2}{\lambda - i(\nu + \omega)} \cdot \frac{1}{-2i\nu}\right]}_{B} e^{(\lambda - i\nu)t} \end{aligned}$$

and simplifying, we find

$$y_0(t) = \underbrace{y_{im} \cdot \left[\frac{\omega^2}{(\omega_0^2 - \omega^2) + 2i\zeta\omega_0\omega} e^{i\omega t}\right]}_{[y_0(t)]_{\text{steady}}} + \underbrace{y_{im} \cdot \left[Ae^{\lambda t}e^{i\nu t} + Be^{\lambda t} \cdot e^{-i\nu t}\right]}_{[y_0(t)]_{\text{transient}}} \quad \text{(IV-45)}$$

The second part of this solution, $[y_0(t)]_{\text{transient}}$, is the transient disturbance associated with the initial application of the force. It is damped out, since $\lambda = -\zeta\omega_0$ is a negative number. The first term, $[y_0(t)]_{\text{steady}}$, represents the steady-state vibration, at the same frequency ω as the input, which results after the starting transient has damped out. We again have the relation

$$[y_0(t)]_{\text{steady}}/y_i(t) = Me^{i\theta} = G(i\omega)$$

where

$$Me^{i\theta} = \omega_0^2/[(\omega_0^2 - \omega^2) + 2i\zeta\omega_0\omega]$$

Thus, for the second-order system

$$M = |G(i\omega)| = \frac{1}{\sqrt{[1 - (\omega^2/\omega_0^2)]^2 + [2\zeta(\omega/\omega_0)]^2}} \quad \text{(IV-46)}$$

and

$$\tan\theta = -2\zeta(\omega/\omega_0)/[1 - (\omega/\omega_0)^2] \quad \text{(IV-47)}$$

At $\omega = \omega_0$, we find $M = 1/[2\zeta \cdot (\omega/\omega_0)]$. The maximum value of M occurs for a slightly lower value of ω, as noted in Fig. IV-12. Also we notice that again there is a *phase lag*. The magnification ratio and phase angle are shown in Figs. IV-12 and IV-13 to linear and logarithmic scales, respectively. We note that at $\omega = \omega_0$ the phase angle is $-90°$, and, as $\omega/\omega_0 \to \infty$, the phase angle approaches $-180°$.

The logarithmic plot of M indicates that for large values of ω/ω_0, we have $M \approx 1/(\omega/\omega_0)^2$, and thus $\log_{10} M \approx -2 \log_{10} (\omega/\omega_0)$; i.e., the curves approach a slope of -2. The acoustic engineer would call this a slope of -12 db. per octave.

The transfer function $G(i\omega) = Me^{i\theta}$ is easily plotted on the basis of the previous calculations. The resulting curves are shown in Fig. IV-14 for various values of ζ. The vector $G(i\omega)$ starts from $M = +1$, $\theta = 0$ when $\omega = 0$; the vector increases to a maximum at resonance and then decreases in magnitude again as $M \to 0$ and $\theta = -180°$ as $\omega \to \infty$.

(3) Other Second-Order Systems.—The following physical systems that occur in the automatic control of aircraft may be approximated by second-order systems.

(a) Mechanical spring-mass-damping systems

(1) Hydraulic servo system.—A measured response curve for such a system is shown in Fig. IV-15.

(2) Rate gyro.—A better approximation than our previously used equation $KG(p) = Ap$ is

$$KG(p) = \frac{A \cdot p}{(p/\omega_0)^2 + 2\zeta(p/\omega_0) + 1} \quad \text{(IV-48)}$$

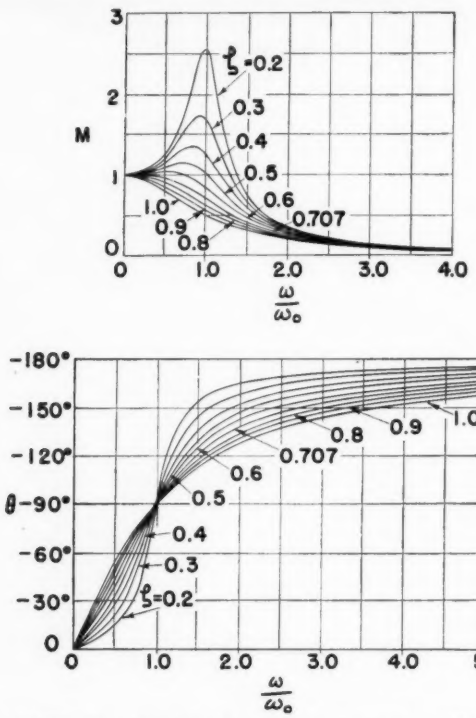

FIG. IV-12. Second-order system: Response to sinusoidal input $G(i\omega) = Me^{i\theta}$ (linear scales).

(3) Accelerometer

$$KG(p) = \frac{Ap^2}{(p/\omega_0)^2 + 2\zeta(p/\omega_0) + 1} \qquad \text{(IV-49)}$$

(4) Electric motor

$$KG(p) = A/\{p.[p + (1/T)]\} \qquad \text{(IV-50)}$$

(b) Electrical networks

Inductance, capacitance, and resistance networks

(c) Aerodynamic systems

(1) The short pitching oscillation of an airplane

(2) The phugoid pitching oscillation

(3) The yawing oscillation

The above-mentioned aerodynamic systems can only approximately be represented by second-order systems; the actual motions are described by the equations of Appendix (C). The solution of these equations is well known to the aerodynamicist. A typical solution of these equations for a modern plane is given in Fig. IV-16 which shows the dynamic longitudinal response for an F-80 airplane as computed by Walkowicz.[81] This calculation, incidentally, also illustrates the great importance of aeroelastic deformations.

(4) *Analogy Between Transfer Functions and Hydrodynamic Potential Functions.*—There is a relation between the elementary transfer functions $G(p)$ and corresponding complex potential functions $w = \varphi + i\psi$ expressible by $w = \log G(p)$. This analogy is summarized in Figs. IV-17 and IV-18 for some simple examples.

We write $p = re^{i\theta}$ and $G(p) = R.e^{i\Theta}$. We note that a hydrodynamic source corresponds to a zero of $G(p)$ (Fig. IV-17a), a hydrodynamic sink to a pole of $G(p)$ (Fig. IV-17b), and that the stream lines ψ = constant correspond to lines of equal phase angle Θ for the vector $G(p)$. A simple lead or lag network corresponds to a source and a sink of equal strength on the x-axis (Fig. IV-18a). A simple second-order system corresponds to a pair of sources at conjugate complex points (Fig. IV-18b).

(D) *Composition of Elements*

(1) *Series Circuit.*—Consider a series arrangement of n elements. The rth element has a gain K_r and a transfer function $G_r(p) = M_r.e^{i\theta_r}$. This series array is equivalent to a single block having a transfer function $K.G(p)$ where

$$\left.\begin{aligned} K &= K_1.K_2 \ldots K_r \ldots K_n \\ G(p) &= (M_1e^{i\theta_1}).(M_2e^{i\theta_2}) \ldots (M_re^{i\theta_r}) \ldots . (M_ne^{i\theta_n}) \\ &= (M_1.M_2 \ldots M_r \ldots M_n).e^{i(\theta_1+\theta_2+\ldots+\theta_r+\ldots\theta_n)} \end{aligned}\right\} \qquad \text{(IV-51)}$$

Such an arrangement is illustrated in Fig. IV-19a for three elements in series. The Laplace transform of the input to this system is $Y_1(p)$, the Laplace transform of the output due to the input signal is $Y_4(p)$, and thus,

$$Y_4(p)/Y_1(p) = K.G(p)$$

where

$$K = K_1.K_2.K_3$$

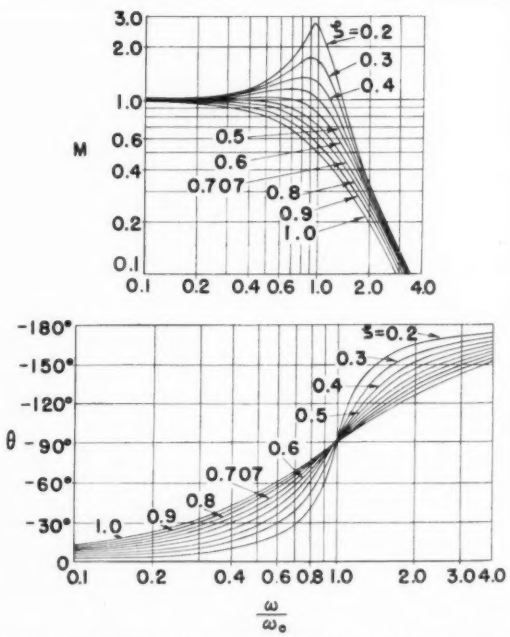

FIG. IV-13. Second-order system: Response to sinusoidal input $G(i\omega) = Me^{i\theta}$ (M and ω to logarithmic scales).

The overall transfer function $G(p) = Me^{i\theta}$ may be obtained graphically by adding the logarithmic response curves, since

$$\log_{10} Me^{i\theta} = \log_{10} [(M_1e^{i\theta_1}).(M_2e^{i\theta_2}).(M_3e^{i\theta_3})]$$

and thus,

$$\log_{10} M = \log_{10} M_1 + \log_{10} M_2 + \log_{10} M_3 \quad \text{(IV-52)}$$

and

$$\theta = \theta_1 + \theta_2 + \theta_3 \quad \text{(IV-53)}$$

This is illustrated in Fig. IV-19b for the series arrangement of linear networks. It will be noted that it is possible to approximate the product by adding the straight-line approximations for each of the elements.

(2) *Parallel Circuit.*—A parallel connection is shown in a similar manner in Fig. IV-20a. The outputs add following the same law as electric currents.

(3) *Simple Feedback Servo.*—A simple feedback servo is shown schematically in Fig. IV-20b. The equations that apply are

$$E(p) = Y_i(p) - Y_0(p) \quad \text{(IV-54)}$$
$$Y_0(p) = K.G(p).E(p) \quad \text{(IV-55)}$$

and thus,

$$E(p)/Y_i(p) = 1/[1 + KG(p)] \quad \text{(IV-56)}$$

and

$$Y_0(p)/Y_i(p) = KG(p)/[1 + KG(p)] \quad \text{(IV-57)}$$

This overall ratio $Y_0(p)/Y_i(p)$ could be represented by a system transfer function $K_s.G_s(p)$.

The feedback servo is the most important element for automatic control systems. The input $Y_i(p)$ is compared with the actual output $Y_0(p)$, and only the difference $E(p) = Y_i(p) - Y_0(p)$ is passed on to the airplane as a control signal. This trick permits the output to be controlled by an error signal rather than by direct input, and, as a result, the accuracy and speed of response are much increased. It will be remembered that this technique is the same as that used by Siemens in 1843 in his "chronometric governor" (Fig. III-1).

(4) *General Feedback Servo.*—The general feedback servo is shown in Fig. IV-20. Its arrangement is similar to the simple servo, except that the signal that is fed back is modified in amplitude and phase by a corrective network with the transfer function $K_2.G_2(p)$. We have the relations

$$E(p) = Y_i(p) - Y_f(p) \quad \text{(IV-58)}$$
$$Y_f(p) = K_2G_2(p).Y_0(p) \quad \text{(IV-59)}$$
$$Y_0(p) = K_1G_1(p).E(p) \quad \text{(IV-60)}$$

and thus,

$$\frac{Y_0(p)}{Y_i(p)} = \frac{K_1G_1(p)}{1 + [K_1G_1(p)].[K_2G_2(p)]} \quad \text{(IV-61)}$$

(E) *Stability of Feedback Networks*

(1) *Routh Criterion for Coefficients of the Frequency Equation.*—We have seen that for the simple feedback network the overall system transfer function is defined by

$$\frac{Y_0(p)}{Y_i(p)} = K_s.G_s(p) = \frac{N_s(p)}{D_s(p)} = \frac{KG(p)}{1 + KG(p)} \quad \text{(IV-62)}$$

The function $G(p)$ will ordinarily be expressible as the ratio of two polynomials, each of which is given in factored form. Thus, for example, the roll-control system shown in Fig. IV-2 has the gain and transfer function:

$$KG(p) = \frac{N(p)}{D(p)} = \underbrace{\left\{\frac{k_1/L_\phi}{p.(1 + pT_1)}\right\}}_{\text{due to airplane}} \cdot \underbrace{\left\{\frac{1 + \epsilon_2T_2p}{1 + T_2p}\,\frac{\epsilon_3 + T_3p}{1 + T_3p}\,\frac{\epsilon_4 + T_4p}{1 + T_4p}\right\}}_{\text{due to amplifier and computer}} \cdot \underbrace{\left\{\frac{\mu\omega_0^2}{p^2 + 2\zeta\omega_0p + \omega_0^2}\right\}}_{\text{due to aileron control servo}} \quad \text{(IV-63)}$$

The numerator $N(p)$ of this function is of the third degree in p, the denominator $D(p)$ is of the seventh degree in p. Each is given in factored form so that we know the three zeros and seven poles of $G(p)$. We note that

$$K_sG_s(p) = \frac{N_s(p)}{D_s(p)} = \frac{N(p)}{D(p) + N(p)} \quad \text{(IV-64)}$$

Thus, the zeros of $G_s(p)$ are the same as those of $G(p)$. The poles of $G_s(p)$ are, however, changed. The degree of $D_s(p)$ is the same as that of $D(p)$, since ordinarily $D(p)$ is of equal or higher degree than $N(p)$. Let us write, in general,

$$K_s.G_s(p) = \frac{N_s(p)}{D_s(p)} = A\,\frac{(p - z_1).(p - z_2)...(p - z_m)}{(p - p_1).(p - p_2)...(p - p_n)} \quad \text{(IV-65)}$$

where $z_1, z_2, \ldots z_m$ are the zeros of $G_s(p)$, $p_1, p_2, \ldots p_n$ are the poles of $G_s(p)$, and A is a constant.

The principal mathematical problem of the servo analysis is ordinarily to go from the function $G(p)$ to

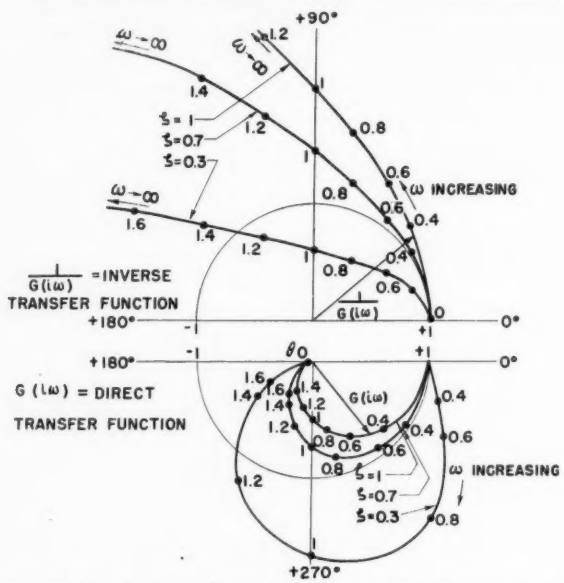

FIG. IV-14. Second-order system: Vector plot of response to sinusoidal input $G(i\omega) = Me^{i\theta}$.

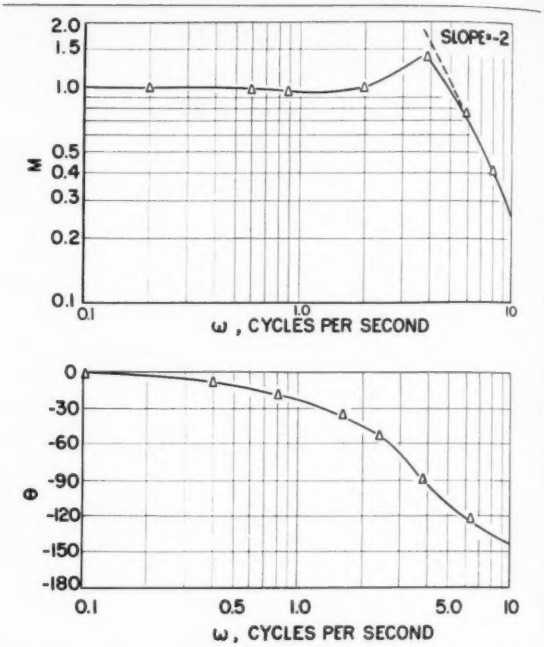

FIG. IV-15. Frequency response of a hydraulic servo: $G(i\omega) = Me^{i\theta}$ (experimentally determined).

the function $G_s(p)$ in factored form. For after the latter has been written in factored form, the solution of the problem is immediately available. If, for example, the input is a sinusoidal force $F_i = F_{max.} \cdot e^{i\omega t}$, then

$$Y_i(p) = F_{max.} \cdot p/(p - i\omega)$$

and the solution from Eq. (A-15) is

$$y_0(t) = F_{max.} \cdot \underbrace{\left[K_s G_s(i\omega) e^{i\omega t} \right.}_{\text{steady-state vibration}} + \underbrace{\left. \sum_{r=1}^{n} \frac{N_s(p_r)}{(p_r - i\omega) \cdot D_s'(p_r)} e^{p_r t} \right]}_{\text{initial transient}} \tag{IV-66}$$

where the p_r's are the roots of the so-called frequency equation $D_s(p) = 0$. It is obvious, therefore, that in order for the terms $e^{p_r t}$ to vanish as $t \to \infty$, it is necessary that the real part of each of the p_r's be negative. *This means then that all of the roots p_r must lie in the negative half of the p-plane.* The determination of the roots p_r is ordinarily not simple if the equation $D_s(p)$ is a high-order polynomial. In the above example of the roll-control system, it would be necessary to solve a seventh-order equation. This problem is generally analogous to the problem of determining the dynamic stability characteristics of an airplane. In the past, the aerodynamicist studied this problem, say, for a fourth-degree equation, by expanding $D_s(p)$ in the form

$$D_s(p) = p^4 + Bp^3 + Cp^2 + Dp + E$$

and then applied Routh's criterion[24] that for stability the coefficients B, C, D, and E and X should be all positive where $X = BCD - D^2 - EB^2$. This technique has the disadvantage that one loses all insight into the physical behavior as the various parameters are changed. The following techniques are superior in this respect.

(2) *Root Locus Method (Evans's Method).*—Let us examine the problem of finding the poles of $G_s(p)$ according to a method recently introduced by Evans.[9]

He considers the function

$$K_s G_s(p) = \frac{KG(p)}{1 + KG(p)} = \frac{N_s(p)}{D_s(p)}$$

and studies the variation of the poles of $G_s(p)$—i.e., the

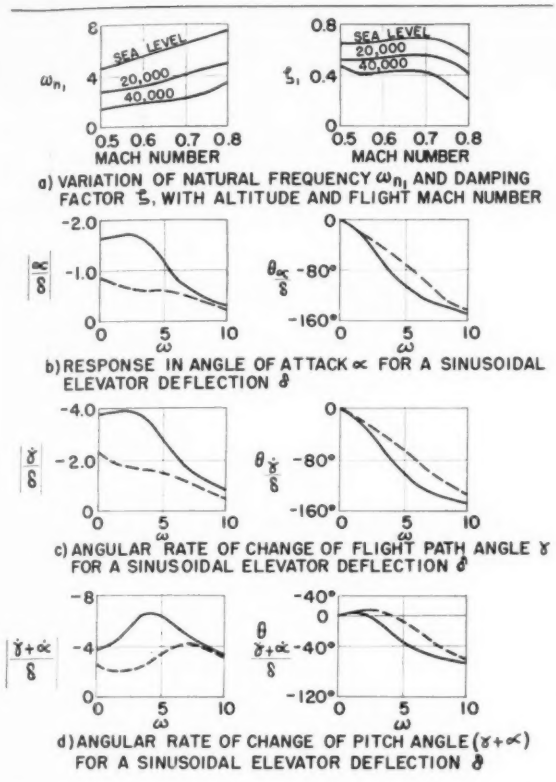
SEA LEVEL
20,000
40,000
MACH NUMBER
a) VARIATION OF NATURAL FREQUENCY ω_{n_1} AND DAMPING FACTOR ζ_1 WITH ALTITUDE AND FLIGHT MACH NUMBER
b) RESPONSE IN ANGLE OF ATTACK α FOR A SINUSOIDAL ELEVATOR DEFLECTION δ
c) ANGULAR RATE OF CHANGE OF FLIGHT PATH ANGLE γ FOR A SINUSOIDAL ELEVATOR DEFLECTION δ
d) ANGULAR RATE OF CHANGE OF PITCH ANGLE $(\gamma+\alpha)$ FOR A SINUSOIDAL ELEVATOR DEFLECTION δ

FIG. IV-16. Dynamic longitudinal response of an F-80 airplane.[81] $M = 0.6$, $h = 10{,}000$ ft. for (b), (c), and (d). ——— = rigid airplane, - - - - = elastic airplane.

roots of the frequency equation $D_s(p) = 0$ as the parameter K is varied from $K = 0$ to $K = \infty$. Let us assume that $G(p)$ is given in factored form

$$G(p) = A \frac{(p - s_1)(p - s_2) \ldots (p - s_m)}{(p - q_1)(p - q_2) \ldots (p - q_n)} \quad \text{(IV-67)}$$

where

$$A = (q_1 . q_2 \ldots q_n)/(s_1 . s_2 \ldots s_m)$$

Ordinarily the denominator of $G(p)$ is of equal or higher order than the numerator—i.e., $n \geq m$. Let us express each of the factors in vector form.

$$\left.\begin{aligned} p - s_1 &= S_1 . e^{i\varphi_1} \\ p - s_2 &= S_2 . e^{i\varphi_2} \\ &\vdots \\ p - s_m &= S_m . e^{i\varphi_m} \\ p - q_1 &= Q_1 . e^{i\theta_1} \\ p - q_2 &= Q_2 . e^{i\theta_2} \\ &\vdots \\ p - q_n &= Q_n . e^{i\theta_n} \end{aligned}\right\} \quad \text{(IV-68)}$$

Fig. IV-21*a* shows that the vector $p - s_r = S_r e^{i\varphi_r}$ starts from the end point of the vector s_r and goes to the end point of the vector p. The length of the vector $p - s_r$ is S_r; its angle with respect to the positive axis is φ_r. Similarly, the vector $Q_r . e^{i\theta_r}$ goes from the end point of the vector q_r to the end point of the vector p. The points s_r and q_r are, of course, the zeros and poles of $G(p)$. The point p is a variable point in the p-plane. Thus,

$$G(p) = A \frac{(S_1 e^{i\varphi_1}) . (S_2 e^{i\varphi_2}) \ldots (S_m e^{i\varphi_m})}{(Q_1 . e^{i\theta_1}) . (Q_2 e^{i\theta_2}) \ldots (Q_n e^{i\theta_n})} =$$

$$A \frac{S_1 S_2 \ldots S_m}{Q_1 . Q_2 \ldots Q_n} . e^{i[(\varphi_1 + \varphi_2 + \ldots + \varphi_m) - (\theta_1 + \theta_2 + \ldots + \theta_n)]} \quad \text{(IV-69)}$$

The function $G(p)$ may therefore be interpreted as another vector of magnitude R and phase angle Θ where

$$G(p) = Re^{i\Theta}$$

and

$$\left.\begin{aligned} R &= A(S_1 S_2 \ldots S_m)/(Q_1 Q_2 \ldots Q_n) \\ \Theta &= (\varphi_1 + \varphi_2 + \ldots + \varphi_m) - (\theta_1 + \theta_2 + \ldots + \theta_n) \end{aligned}\right\} \quad \text{(IV-70)}$$

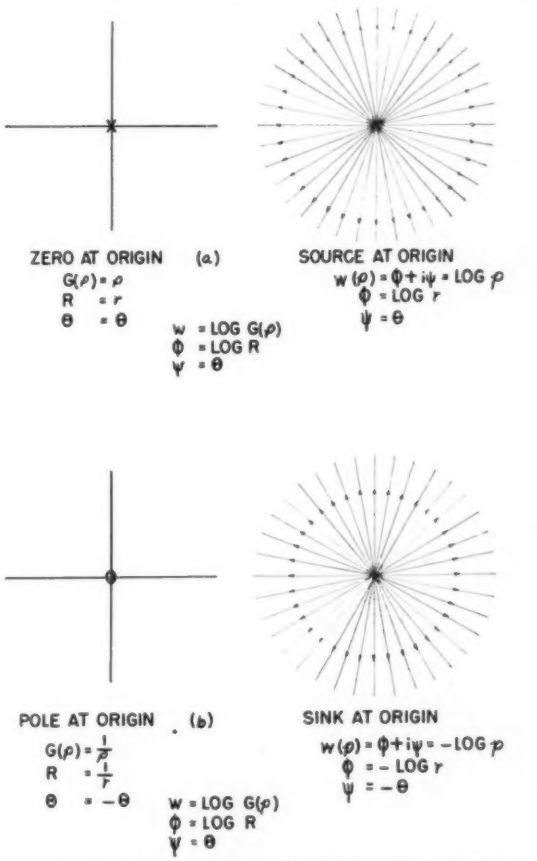
ZERO AT ORIGIN (a)
G(ρ) = ρ
R = r
Θ = θ
SOURCE AT ORIGIN
w (ρ) = Φ + iψ = LOG ρ
Φ = LOG r
ψ = θ
w = LOG G(ρ)
Φ = LOG R
ψ = θ
POLE AT ORIGIN (b)
G(ρ) = 1/ρ
R = 1/r
Θ = −θ
SINK AT ORIGIN
w (ρ) = Φ + iψ = −LOG ρ
Φ = − LOG r
ψ = −θ
w = LOG G(ρ)
Φ = LOG R
ψ = θ

FIG. IV-17. Analogy between transfer functions $G(p)$ and hydrodynamic potential functions.

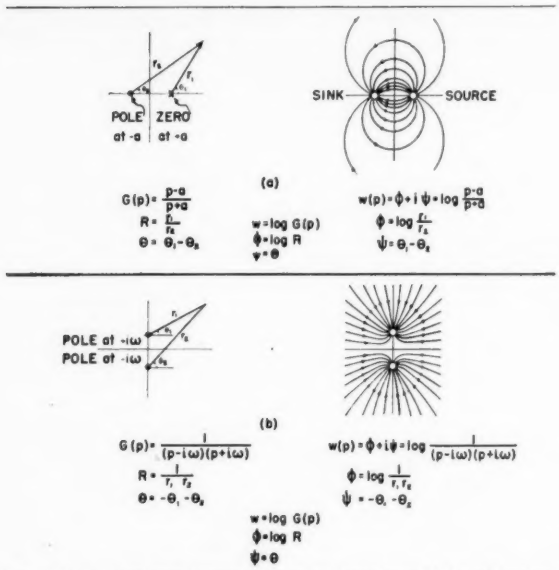

FIG. IV-18. Analogy between transfer functions $G(p)$ and hydrodynamic potential functions.

The poles of $G_s(p)$ are found from the condition $D_s(p) = 0$—that is,

$$1 + KG(p) = 0$$

or

$$1 + KRe^{i\Theta} = 0$$

which may be written

$$KRe^{i\Theta} = -1$$

or

$$KRe^{i\Theta} = 1 . e^{i\pi}$$

This vector equation may be resolved into two scalar conditions:

(1) Magnitude condition:

$$KR = 1 \text{ or } K = 1/R \qquad \text{(IV-71a)}$$

Thus, the vector $KG(p)$ will have a magnitude of one.

(2) Angle condition:

$$\Theta = \pi \text{ or } \Theta = 180° \qquad \text{(IV-71b)}$$

Thus, the vector $KG(p)$ will have an angle of 180°. Both of these conditions must be satisfied if the point p is a pole of $G_s(p)$. (The angle condition is also satisfied by $\Theta = \pi \pm \text{integer} \times 2\pi$.)

Evans studies this problem in two steps. He determines first of all the locus of all points which satisfy the angle condition (2). Then he computes the values of K for various points along this locus by measuring the lengths $S_1, S_2, \ldots S_m$ and $Q_1, Q_2, \ldots Q_n$ and computing the ratio R. For a given value of K, the points $p_1, p_2, \ldots p_n$ along these loci are then the roots of $D_s(p) = 0$—i.e., the poles of $G_s(p)$.

TABLE IV-1

$n - m$	Asymptote
1	180°
2	+90°, −90°
3	+60°, −60°, 180°
4	+45°, −45°, +135°, −135°

Evans has developed a number of simple rules that determine the locus of points satisfying the angle condition (2). These may be verified by simple examples:

Rule 1.—For a gain $K = 0$, the poles of $G_s(p)$ coincide with the poles of $G(p)$. Thus, the root locus *starts* from the poles of $G(p)$. This can be easily verified.

Consider, for example,

$$G(p) = [(p - s_1)/(p - q_1)] . q_1/s_1$$

where s_1 and q_1 are on the real axis. Then,

$$D_s(p) = 1 + K[(p - s_1)/(p - q_1)] . q_1/s_1 = 0$$

This is only possible if $[(p/q_1 - 1)/(p/s_1 - 1)] = -K$. As $K \to 0$ it is necessary that $p - q_1 \to 0$—i.e., that $p \to q_1$, which is the pole of $G(p)$.

Rule 2.—For a gain $K = \infty$, the poles of $G_s(p)$ coincide with the zeros of $G(p)$ or they are at $p = \infty$. If the number of poles n exceeds the number of zeros m, the direction of the infinite asymptotes of the loci are shown in Table IV-1. Thus, the root locus *ends* on the zeros of $G(p)$ or on the above-mentioned infinite asymp-

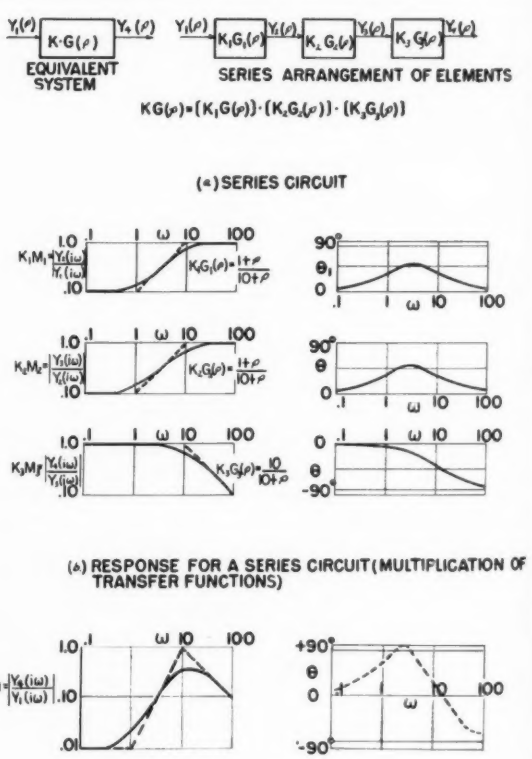
EQUIVALENT SYSTEM
SERIES ARRANGEMENT OF ELEMENTS
KG(p)=[K1G1(p)]·[K2G2(p)]·[K3G3(p)]
(a) SERIES CIRCUIT
(b) RESPONSE FOR A SERIES CIRCUIT (MULTIPLICATION OF TRANSFER FUNCTIONS)

FIG. IV-19. Series circuit.

totes. This can be verified, for example, if $G(p) = [(p - s_1)/(p - q_1)].(q_1/s_1)$. Then

$$D_s(p) = 1 + K[(p - s_1)/(p - q_1)].(q_1/s_1) = 0$$

only if

$$(q_1/s_1)[(p - s_1)/(p - q_1)] = -(1/K)$$

Thus, as $K \to \infty$ or $1/K \to 0$, it is necessary that $p - s_1 \to 0$, or $p \to s_1$, which is the zero of $G(p)$. If the function

$$G(p) = (1/p)[(p - s_1)/(p - q_1)].(q_1/s_1)$$

then

$$D_s(p) = 1 + K(p - s_1)/[p.(p - q_1)].(q_1/s_1) = 0$$

if

$$(q_1/s_1)(1/p)[(p - s_1)/(p - q_1)] = -(1/K)$$

As $K \to \infty$, we find that either $p \to s_1$ or $p \to \infty$ are possible solutions.

Rule 3.—The root locus along the real axis is along alternate segments connecting the zeros and poles located on the real axis, starting with the one farthest to the right.

This rule may be easily verified by considering any point on the real axis. The angle to this point from a pair of conjugate complex poles is $+\theta$ and $-\theta$, respectively, and thus their sum is zero. The angle to this point from the poles or zeros on the axis is $\theta = 0$ for all poles or zeros to the left of p, and it is $\theta = 180°$ for all poles or zeros to the right of p. Thus, the sum is 180° if there is an odd number of poles and zeros to the right of p.

Rule 4.—If there is a breakaway of the root locus from the real axis, the point of breakaway may be estimated from the conditions that, for a small displacement $\Delta\omega$ from the axis, the increase in angle due to the poles and zeros on the axis to the left must be just balanced by the effect of those to the right.

Example:

$$G(p) = 1/[p.(p - q_1)(p - q_2)]$$

We note from Fig. IV-24 that the point of breakaway V, is given by

$$\Delta\omega/x_0 = (\Delta\omega/x_1) + (\Delta\omega/x_2)$$

or

$$1/x_0 = (1/x_1) + (1/x_2)$$

Rule 5.—The point U at which the root locus crosses the imaginary axis into the positive half plane can often be estimated by taking advantage of the properties of the right angle.

Example:

$$G(p) = 1/[p.(p - q_1)(p - q_2)]$$

At the point u the angle θ_1 from $p = 0$ is 90°, the angles θ_2 and θ_3 must therefore also add to 90°. Take a trial point U and draw a 45° line. Then for u to be on the root locus, it would be necessary that $\alpha = \beta$ in Fig. IV-24.

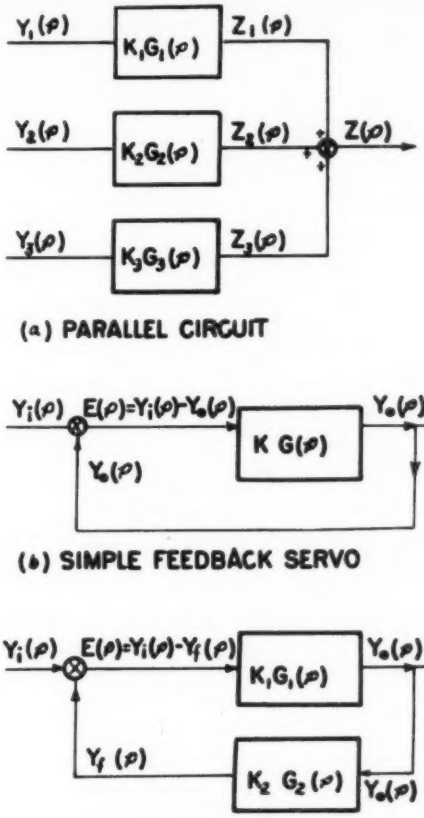

FIG. IV-20. Block diagrams of various circuits.

Rule 6.—The direction of locus departure from a pole (or locus approach to a zero) may be easily estimated by computing the angle at the pole under consideration from all of the other poles and zeros in the field.

For example, in Fig. IV-26 we wish to determine the angle at which the locus departs from the pole q_4. At the pole q_4, we have

$\theta_1 = 150°$	$\varphi_1 = 120°$
$\theta_2 = 90°$	$\varphi_2 = 45°$
$\theta_3 = 90°$	
$\theta_1 + \theta_2 + \theta_3 = 330°$	$\varphi_1 + \varphi_2 = 165°$

Now let us consider a point P on the locus a small distance away from the point q_4. This point P must be at an angle θ_4 from q_4 such that

$$\underbrace{(\varphi_1 + \varphi_2)}_{165°} - [\underbrace{(\theta_1 + \theta_2 + \theta_3)}_{330°} + \theta_4] = 180°$$

or

$$\theta_4 = -345° = +15°$$

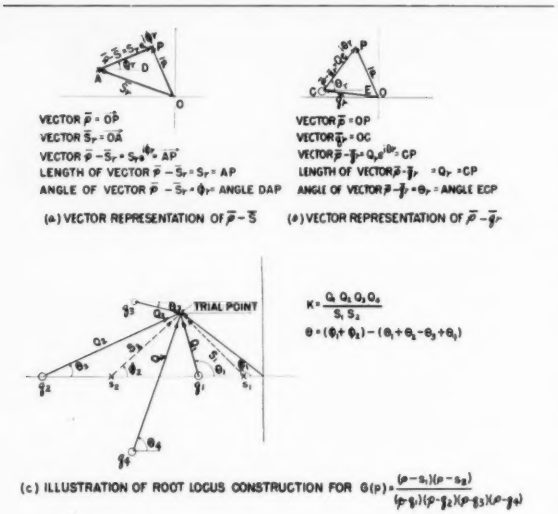
VECTOR $\bar{p}$ = OP
VECTOR $\bar{s}_r$ = OA
VECTOR $\bar{p}-\bar{s}_r$ = $S_r e^{i\varphi_r}$ = AP
LENGTH OF VECTOR $\bar{p}-\bar{s}_r$ = S_r = AP
ANGLE OF VECTOR $\bar{p}-\bar{s}_r$ = φ_r = ANGLE DAP
(a) VECTOR REPRESENTATION OF $\bar{p}-\bar{s}$
VECTOR $\bar{p}$ = OP
VECTOR $\bar{q}_r$ = OC
VECTOR $\bar{p}-\bar{q}_r$ = $Q_r e^{i\theta_r}$ = CP
LENGTH OF VECTOR $\bar{p}-\bar{q}_r$ = Q_r = CP
ANGLE OF VECTOR $\bar{p}-\bar{q}_r$ = θ_r = ANGLE ECP
(b) VECTOR REPRESENTATION OF $\bar{p}-\bar{q}_r$
TRIAL POINT
$K=\frac{Q_1 Q_2 Q_3 Q_4}{S_1 S_2}$
$\theta=(\phi_1+\phi_2)-(\theta_1+\theta_2+\theta_3+\theta_4)$
(c) ILLUSTRATION OF ROOT LOCUS CONSTRUCTION FOR $G(p)=\frac{(p-s_1)(p-s_2)}{(p-q_1)(p-q_2)(p-q_3)(p-q_4)}$

FIG. IV-21. Elements of root-locus construction.

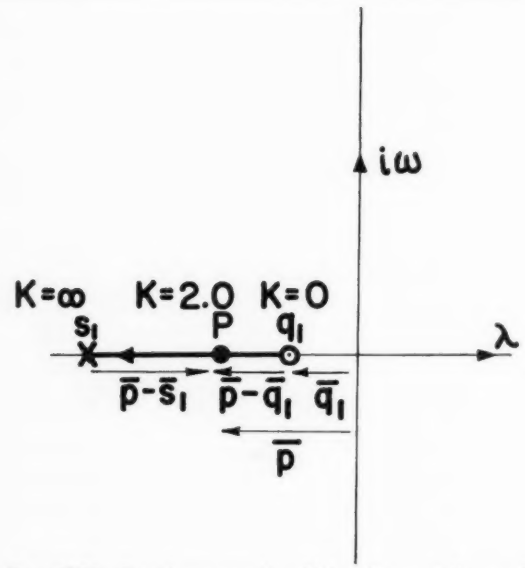

FIG. IV-22. Root locus on axis: $G(p) = [(p - s_1)/(p - q_1)] \cdot q_1/s_1$. Locus moves from a pole (for $K = 0$) to a zero (for $K = \infty$). Example: $q_1 = -1$, $s_1 = -4$, $p = -2$; $|\bar{p} - \bar{q}_1| = Q_1 = 1$; $|\bar{p} - \bar{s}_1| = S_1 = 2$; therefore, $K = s_1/q_1 \cdot |(p - q_1)/(p - s_1)| = 2$.

i.e., the point p is at an angle $\theta_4 = +15°$ with respect to q_4.

For intermediate locations, the root locus is found by taking a number of trial points, measuring the angles θ_r and φ_r, and taking the algebraic sum $\alpha = \Sigma\varphi_r - \Sigma\theta_r$. This addition can be conveniently performed by a special plastic device called the "spirule" (Fig. IV-27). A spiral curve on the device gives the logarithm of a length in the form of an angle so that addition of angles gives the logarithm of the product

$$K = A(Q_1 . Q_2 \ldots Q_m)/(S_1 . S_2 \ldots S_n)$$

Fig. IV-28 shows the root locus for the roll stabilization system of Fig. IV-2. A gain $K = 670$ would give satisfactory stabilization in this case with the roots indicated in the figure. The values of the gain corresponding to various points along the locus are shown on Fig. IV-28.

The above described technique is instructive in that it suggests methods for correcting adverse trends in the directions of the loci. For example, Fig. IV-29a shows the root locus for a simple system. Fig. IV-29b shows the effect of a lead network in stabilizing this system up to larger values of the gain.

The above technique also has a great advantage in visualizing clearly the trend of the roots in conditionally stable systems. For example, Fig. IV-30a illustrates the problem of an autopilot stabilizing an airplane that is statically unstable (without the autopilot). The locus starts at low values of gain in the right half plane. It crosses the axis at a gain K_1, and the system becomes stable. At a still higher value of gain K_2, another branch of the locus moves into the right half plane, and the system becomes unstable again. Fig. IV-30b shows the root locus for an autopilot controlling a statically stable air frame. It will be noted that both of these cases lead to a stable airplane-plus-autopilot combination. This example, taken from a systematic investigation of a large number of systems by Martin, illustrates his conclusion that the autopilot designer would most prefer to have an airplane possess small inherent "static stability" or even a small degree of instability.

Another interesting proposal suggested by Evans is to use an electric analogy to determine the root locus. This method is still under development; thus far, the graphical technique has proved to be the most convenient and rapid procedure.

(3) *Routh's Criterion for Stability of High-Order Systems.*—Routh deduced his famous criterion for stability of linear vibrating systems by using a theorem from the theory of complex variables (due to Cauchy). This theorem states that if $f(p)$ is the vector representing the function of a complex variable p, this function $f(p)$ having s poles and r zeros* within a closed contour C of the p-plane, and as the point p moves around the closed contour C encircling it once in the clockwise direction, the vector $f(p)$ carries out r-s clockwise revolutions about the origin. Routh applied this theorem to find the number of roots of the frequency equation $D_s(p) = 0$ in the right half of the p-plane. He took as boundaries for the contour C: (a) the imaginary axis, $p = i\omega$ [along this axis $D_s(p) = D_s(i\omega)$]; and (b) the infinite half circle to the right, $p = Re^{i\Phi}$, where $R \to \infty$. Nyquist carried over the application of these criteria to the simple feedback network for which

$$K_s G_s(p) = \frac{N_s(p)}{D_s(p)} = \frac{KG(p)}{1 + KG(p)}$$

* A pole or zero of order m is counted m-fold.

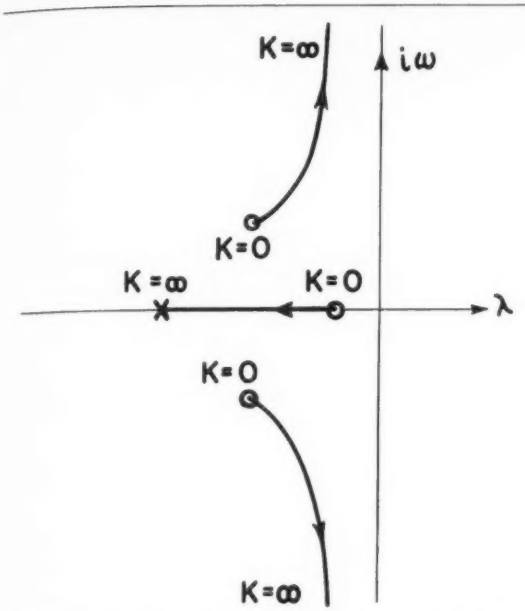

FIG. IV-23. Root locus moves from poles to zeros, or to infinity

$$G(p) = \frac{p+5}{p+1} \cdot \frac{(13/5)}{[p+(3+2i)][p+(3-2i)]}$$

Locus moves from poles (for $K = 0$) to zeros or to $p = \infty$ (for $K = \infty$). Infinite asymptotes at $+90°$, and $-90°$, since for large p, $G(p) \approx 1/p^2$.

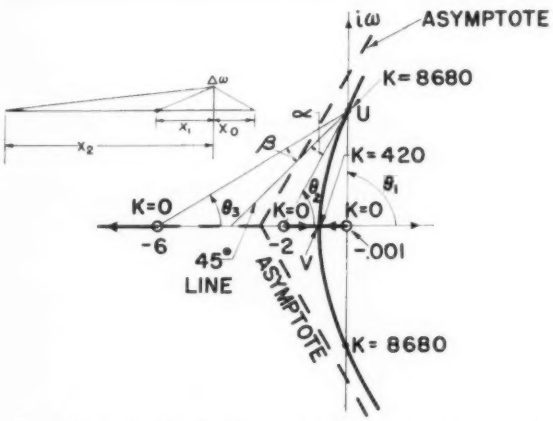

FIG. IV-24. Breakaway from axis and crossover to unstable region

$$G(p) = \frac{(0.001)(2)(6)}{(p+0.001)(p+2)(p+6)}$$

At $K = 0$, locus starts from -6, -2, and -0.001. Infinite asymptotes at $\pm 60°$ and $180°$, since for large p, $G(p) \approx 1/p^3$. Note breakaway from λ-axis (point V) at $\lambda_1 = -0.9$, where

$$\frac{\Delta\omega}{\lambda_1+6} + \frac{\Delta\omega}{\lambda_1+2} + \frac{\Delta\omega}{\lambda_1+0.001} = 0$$

Note crossing of ω-axis (point U) where $\alpha = \beta$.

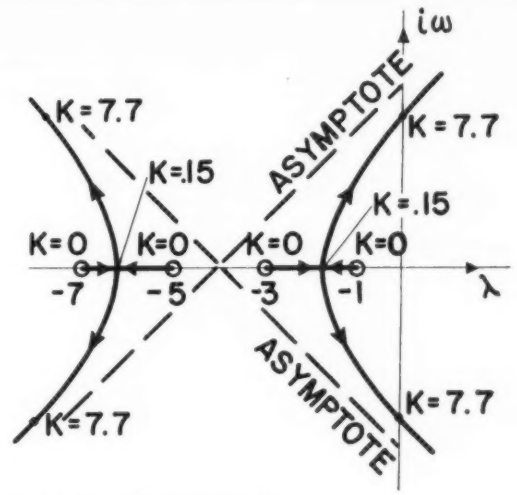

FIG. IV-25. Infinite asymptotes:

$$G(p) = \frac{(1)\cdot(3)\cdot(5)\cdot(7)}{(p+1)\cdot(p+3)\cdot(p+5)\cdot(p+7)}$$

At $K = 0$, locus starts from poles at -1, -3, -5, and -7. Infinite asymptotes at $\pm 45°$ and $\pm 135°$, since for large p, $G(p) \approx 1/p^4$. Note breakaway from λ-axis at $\lambda_1 = -1.75$, where

$$\frac{\Delta\omega}{\lambda_1+7} + \frac{\Delta\omega}{\lambda_1+5} + \frac{\Delta\omega}{\lambda_1+3} + \frac{\Delta\omega}{\lambda_1+1} = 0$$

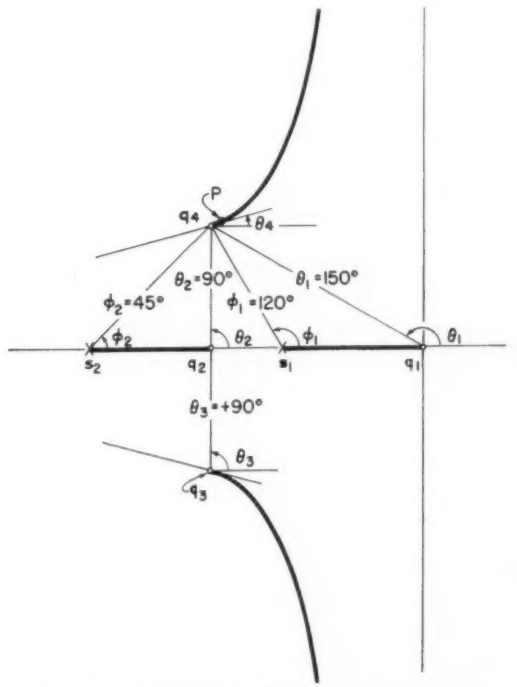

FIG. IV-26. Direction of locus departure from pole.

or

$$\frac{1}{K_s \cdot G_s(p)} = \frac{D_s(p)}{N_s(p)} = \frac{1}{KG(p)} + 1$$

The point $[D_s(p)]/[N_s(p)] = 0$ corresponds to $1 \div [K \cdot G(p)] = -1$ or $1/[G(p)] = -K$. Thus, if the vector $[D_s(p)]/[N_s(p)]$ encircles the origin as the point p moves clockwise around the contour C of the right half

p-plane, then the vector $1/[KG(p)]$ encircles the point -1, or the vector $1/[G(p)]$ encircles the point $-K$.

Let us illustrate the application of this method for the simple transfer function

$$G(p) = 1/[p.(1 + pT_1)(1 + pT_2)]$$

and thus

$$1/G(p) = p.(1 + pT_1).(1 + pT_2)$$

and

$$\frac{1}{K_s.G_s(p)} = \frac{D_s(p)}{N_s(p)} = \frac{p.(1 + pT_1).(1 + pT_2)}{K} + 1$$

(a) Along the imaginary axis: $p = i\omega$

$$\frac{1}{G(i\omega)} = i\omega.\underbrace{(1 + i\omega T_1)}_{M_1e^{i\theta_1}}.\underbrace{(1 + i\omega T_2)}_{M_2e^{i\theta_2}}$$

At $\omega = 0$

$$1/[G(i\omega)] = +0.i$$

At $\omega = +\infty$

$$\frac{1}{G(i\omega)} = \lim_{L\to\infty}(iL).(1 + iLT_1).(1 + iLT_2) \to -i\infty$$

The vector $M_1e^{i\theta_1}$ and $M_2e^{i\theta_2}$ which multiply $i\omega$ turn this vector progressively through $+180°$—i.e., from $+90°$ through $+180°$ to $+270°$. The end points of the vector $1/[G(i\omega)]$ are represented by the curve OAB. As p traverses the portion of the imaginary axis from $\omega = 0$ to $\omega = -\infty$, the end points of the vector $1/[G(i\omega)]$ follow the curve OA′B′, which is the mirror image of OAB in the real axis.

(b) Along the infinite contour: $p = Re^{i\Phi}$ as $R \to \infty$

$$\frac{1}{G(p)} = (Re^{i\Phi}).(1 + Re^{i\Phi}T_1).(1 + Re^{i\Phi}T_2) \to R^3.e^{3i\Phi}.T_1T_2$$

As the vector p rotates $180°$ clockwise along the infinite circle from B to C to B', the vector $1/[G(p)]$ rotates $3 \times 180° = 540°$ clockwise along the infinite circle.

Let us examine now whether the vector $1/[G(p)]$ encircles the point $-K$ as p describes the contour C. Imagine a string connected to a pin through the point $-K_1$. As the end of the string traverses the contour C' in the plane of $1/[G(p)]$, we note that the string has carried out no net rotation during this process—i.e., the positive and negative rotations are canceled out. We thus deduce that the system is stable for the gain K_1—i.e., it has no roots with a positive real part in the right half of the p-plane.

Let us now examine similarly whether the system is stable for the gain K_2—i.e., assume the pin anchored at the point $-K_2$ and trace the number of revolutions carried out by the string. We find that the string carries out two clockwise revolutions about the point $-K_2$. We thus deduce that the gain K_2 makes the system unstable and that there are two roots with a positive real part in the right half of the p-plane.

It is obvious by inspection that the system becomes unstable as the point $-K$ passes through the point A. This criterion for stability is called Nyquist's criterion; the diagram (Fig. IV-31d) is called Nyquist's diagram for the direct transfer function $G(p)$; and the diagram (Fig. IV-31c) is called Nyquist's diagram for the inverse transfer function $1/[G(p)]$. We do not, however, obtain any quantitative estimate from this diagram to indicate *how* unstable the system is. The root locus diagram (Fig. IV-29a) gives the solution of this same problem

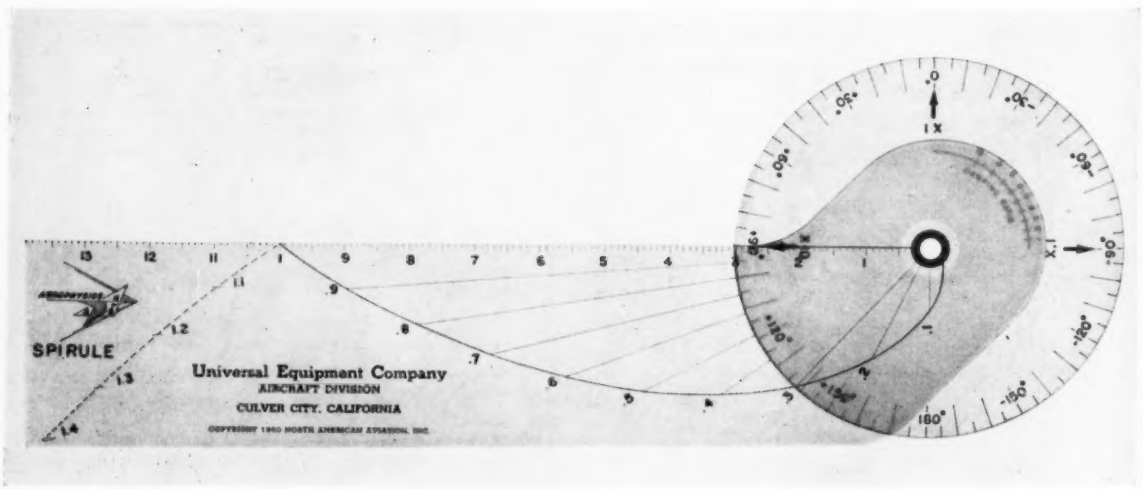

FIG. IV-27. "Spirule."

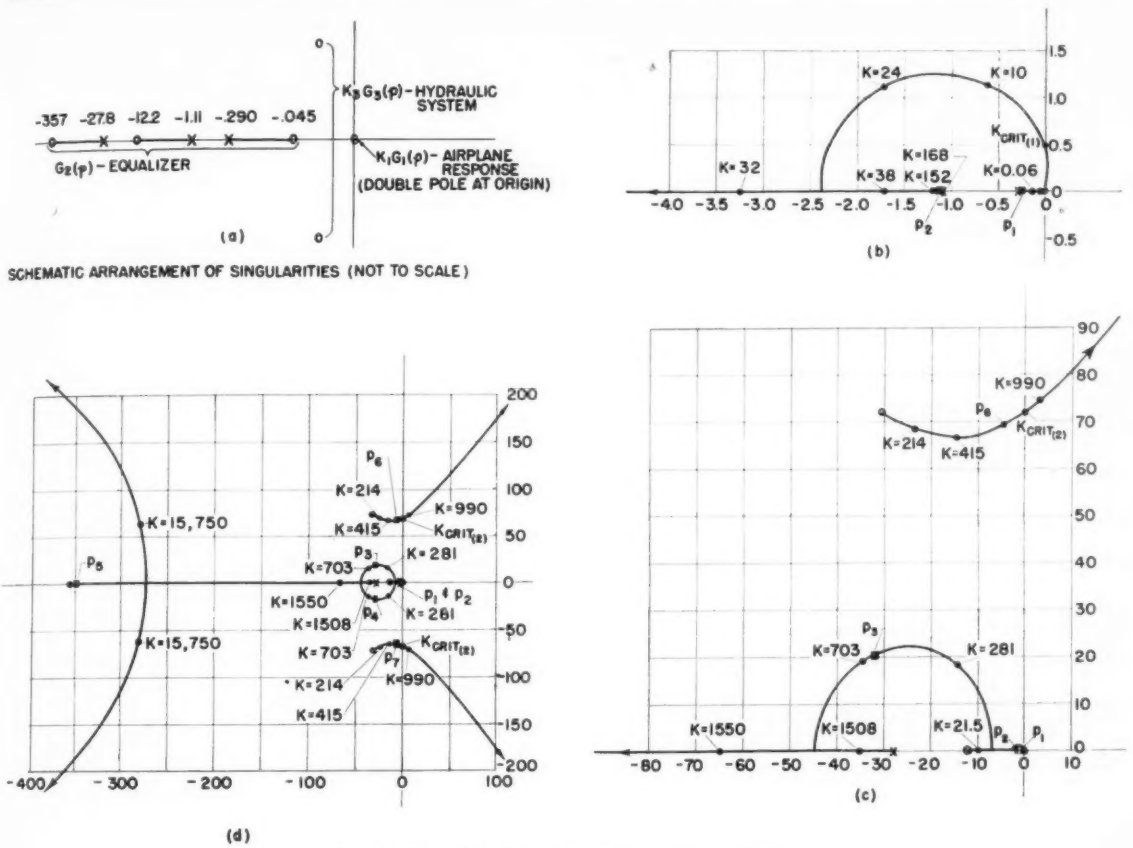

FIG. IV-28. Root locus plots of roll-control system.

including a quantitative measure of the negative damping coefficient as a function of the gain K.

In order to obtain a quantitative measure of the damping coefficient, positive or negative, it is in principle possible to carry out the conformal mapping not only of the line $p = i\omega$, but also of neighboring lines of constant damping $p = \lambda + i\omega$, keeping λ = constant, and of lines of constant frequency, keeping ω = constant. Such a map reproduced from Hänny[13] is shown in Fig. IV-32. This process is ordinarily too tedious for practical application. Osborne[20] showed that for typical control systems an approximate measure of the damping coefficient ζ for the most critical root is given by

$$\zeta = (1/60)(\alpha/m) \qquad \text{(IV-72)}$$

where α = "phase margin" in degrees at the cutoff frequency where $|KG(i\omega)| = 1$ and m = slope of the curve of $\log_{10}|KG(i\omega)|$ vs. $\log_{10}\omega$ at the point $|K.G(i\omega)| = 1$.

Thus if $\alpha = 30°$ and $m = 1.7$, then $\zeta \approx (1/60) \times (30/1.7) \approx 0.3$.

Another word of caution is necessary when the function $G(p)$ has *r zeros in the right half of the p-plane*. Then the vector $1/[G(p)]$ will carry out r counterclockwise rotations as p carries out one clockwise rotation around the contour C due to these r zeros. If the string whose end is anchored at the point $-K$ carries out r counterclockwise rotations in traversing the contour C, the system is stable. If it carries out $r-s$ counterclockwise rotations, then the system is unstable and has s roots within the right half of the p-plane.

It is seen from Fig. IV-31b that the function $K \div [K_sG(p)] = \{1/[G(p)]\} + K$ and thus the system transfer function $1/[G_s(p)]$ is obtained simply from $1/[G(p)]$ by a shift of the origin. This is the principal advantage of plotting $1/[G(p)]$ instead of the direct function $G(p)$.

Bode presents the function $KG(i\omega) = KMe^{i\theta}$ from $\omega = 0$ to $\omega = \infty$ by plotting its magnitude KM and phase θ separately vs. ω(KM and ω on a logarithmic scale). This is generally a more convenient method of presenting the data than Nyquist's vector diagram. The transition from stability to instability is again indicated when $G(i\omega) = -1/K$—i.e., when $KM = 1$ (i.e., $\log_{10} KM = 0$) and $\theta = 180°$. Fig. IV-33 presents the Bode curves for the same examples as Fig. IV-29a. In this example $\theta = 180°$ at $\omega = 3.4$. At this frequency $M = 0.074$. Thus, the transition from stability to instability occurs at $1/K = 0.074$ or $K = 13.5$. A desirable design condition in terms of the Bode diagram is

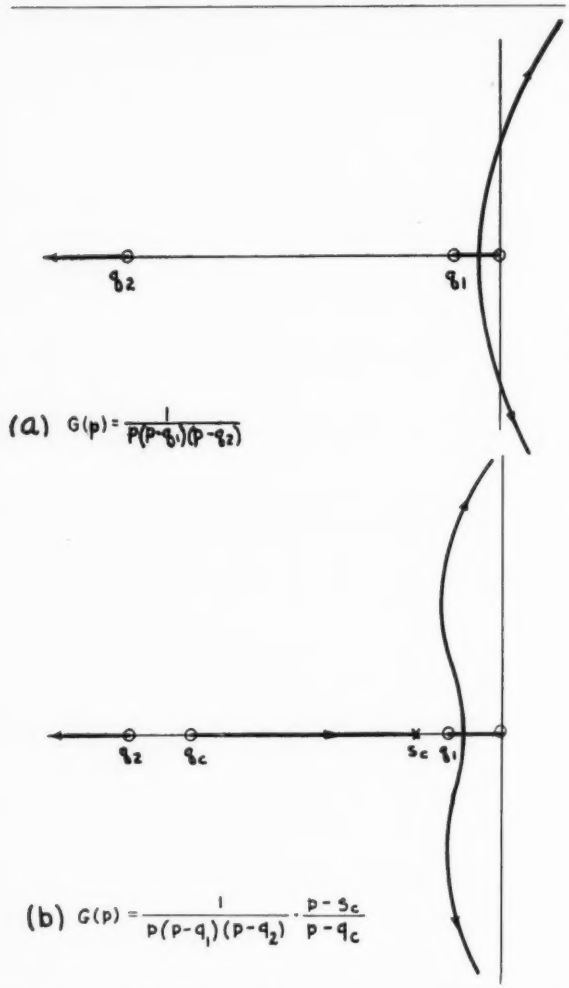

FIG. IV-29. (a) Root locus of simple system. (b) Root locus of system with lead network.

frequently stated to be a "phase margin" of about 30° to 50° at "gain cross over"—i.e., $\theta = 150°$ to 130° at the frequency where $KM = 1$. In the example of Fig. IV-33, $\theta = 150°$ at $\omega = 1.35$ where $M = 0.45$. In order to have $KM = 1$ at this frequency, the gain would be $K = 2.22$.

In comparing (a), the Bode or Nyquist presentation, with (b), the Evans root-locus method, we note that the Bode or Nyquist diagrams permit the direct use of experimental data; thus they do not require the approximation of the frequency-response curves of Fig. IV-15 by those of a second-order system.

On the other hand, the Evans root-locus method presents directly a complete picture of the stability and transient response characteristics that are most important for aircraft control; for airplanes are rarely subject to purely sinusoidal inputs. Its merits are as follows:

(1) The root locus gives the roots of the closed-loop system directly and, by a simple calculation, the transient response.

(2) The degree of stability can be read from the root locus directly.

(3) Complicated systems can be set up in such a fashion that the effect on transient response and stability of changing any parameter in the problem can easily be visualized.

(4) There is no ambiguity or confusion concerning interpretation of the plots even for complex systems having any number of roots and poles in either the right or left half of the complex plane.

For comparison, Fig. IV-34 presents the Bode diagram for the roll-control system of Figs. IV-2 and IV-28.

(*F*) *Illustrations of Simple Feedback Systems*

(*1*) *Roll Stabilization.*—The roll control of an aircraft or missile may be approximated by the differential equation

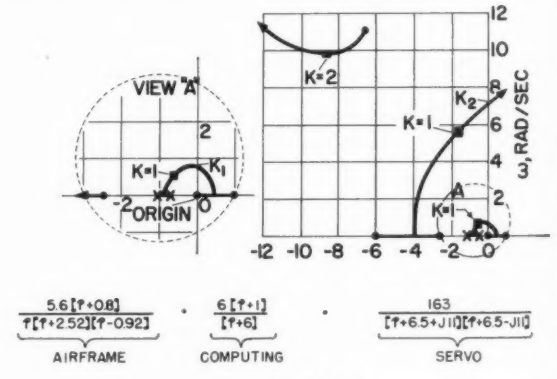

(a)

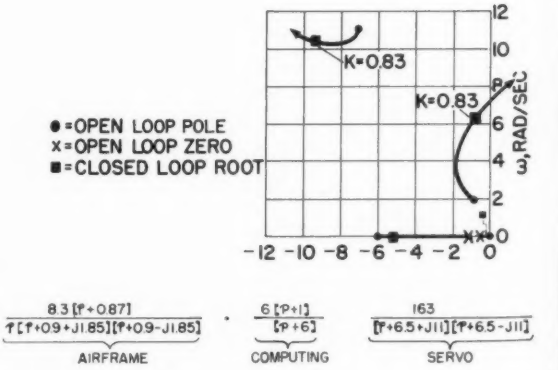

(b)

FIG. IV-30. (a) Autopilot control of a statically unstable air frame. (b) Autopilot control of a statically stable air frame.

$$I_x.(d^2\varphi/dt^2) + L_\varphi.(d\varphi/dt) = k\delta \qquad \text{(IV-73)}$$

where

$\varphi(t)$ = roll angle
$\Phi(p)$ = Laplace transform of $\varphi(t)$
$\delta(t)$ = aileron angle
$D(p)$ = Laplace transform of $\delta(t)$
I_x = moment of inertia about the longitudinal axis
L_φ = coefficient of damping in roll (usually denoted by L_p; we shall not use the common aerodynamic definition of $p = d\varphi/dt$ to avoid confusion with the Laplace operator p)

In Laplace transforms, Eq. (IV-73) reduces to

$$(I_x.p^2 + L_\varphi.p).\Phi(p) = k.D(p) \qquad \text{(IV-74)}$$

assuming a system initially at rest. Thus, the airplane transfer function will be defined by

$$K_1.G_1(p) = \frac{\Phi(p)}{D(p)} = \frac{k}{I_x.p^2 + L_\varphi.p} = \frac{k/L_\varphi}{p.(1 + pT_1)} \qquad \text{(IV-75)}$$

In many practical cases, the aerodynamic damping L_φ is so small that it may be neglected; then

$$K_1G_1(p) = k/(I_x.p^2)$$

The simplest servo-control system would be one that measures the angle $\epsilon = \varphi_i - \varphi_0$ by means of a position gyro and gives aileron deflection δ proportional to ϵ. Then $\delta = \mu(\varphi_1 - \varphi_0)$, and the transfer function for the servo would be $K_2G_2(p) = \mu$. The transfer function for the two systems in series would be

$$KG(p) = (\mu k/L_\varphi).1/[p(1 + pT_1)]$$

while that for the feedback system would be

$$K\,G_c(p) = KG(p)/[1 + KG(p)]$$

The function $G(p)$ has a simple pole at $p = 0$ and $p = -(1/T_1)$. The root-locus diagram (Fig. IV-35a) indicates that, as the gain K is increased, the new roots move toward each other and then along the vertical line $p = -(1/2T_1)$ to $+i\infty$ and $-i\infty$ W. This system is therefore always stable as long as L_φ is positive. The damping is, however, extremely low; the damping ratio is

$$\zeta = 1/2\omega_0T_1 = L_\varphi/2\sqrt{\mu k I_x}$$

A better approximation to a servo would allow for a small time delay T_h between the input signal ϵ and the resultant aileron deflection δ. This relation could be represented in terms of a first-order system by the transfer function $K_h.G_h(p) = \mu/(1 + T_hp)$. This would give the open-loop transfer function

$$KG(p) = \{(k/L_\varphi)/[p.(1 + pT_1)]\}\ [\mu/(1 + T_hp)]$$

and for the feedback system

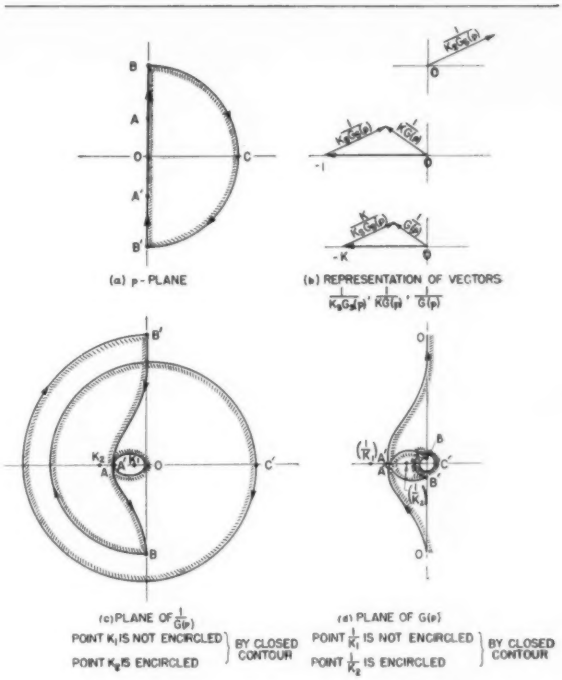
(a) p - PLANE
(b) REPRESENTATION OF VECTORS
(c) PLANE OF 1/G(p)
POINT K1 IS NOT ENCIRCLED
POINT K2 IS ENCIRCLED
BY CLOSED CONTOUR
(d) PLANE OF G(p)
POINT 1/K1 IS NOT ENCIRCLED
POINT 1/K2 IS ENCIRCLED
BY CLOSED CONTOUR

FIG. IV-31. Mapping of $G(p)$ and $1/G(p)$ for $G(p) = 1/[p(1 + pT_1)(1 + pT_2)]$. (Not drawn to scale.)

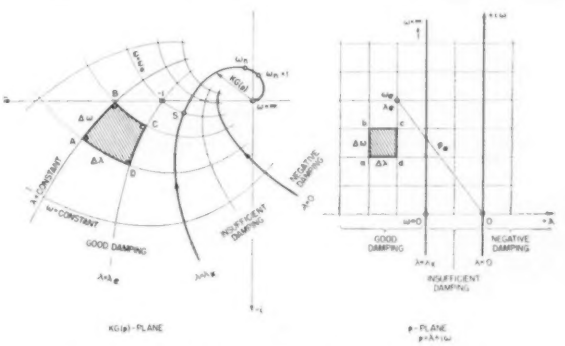

FIG. IV-32. Conformal map of transfer function.

$$K_sG_s(p) = [KG(p)]/[1 + KG(p)]$$

The root locus in this case starts from the poles at $p = 0$, $p = -(1/T_1)$, and $p = -1/T_h$. We have already seen this cubic system in Fig. IV-24, and we note that at a gain $K \geq K_c$ the system becomes unstable. In order to extend the regime of stable operation over a wider frequency regime, a lead and lag network is introduced, represented by the transfer function

$$K_2G_2(p) = \underbrace{\frac{1 + \epsilon_2T_2p}{1 + T_2p}}_{\text{Lag}}\ \underbrace{\frac{\epsilon_3 + T_3p}{1 + T_3p}}_{\text{Lead}}\ \underbrace{\frac{\epsilon_4 + T_4p}{1 + T_4p}}_{\text{Lead}}$$

The experimentally determined transfer function for the hydraulic system is approximated by

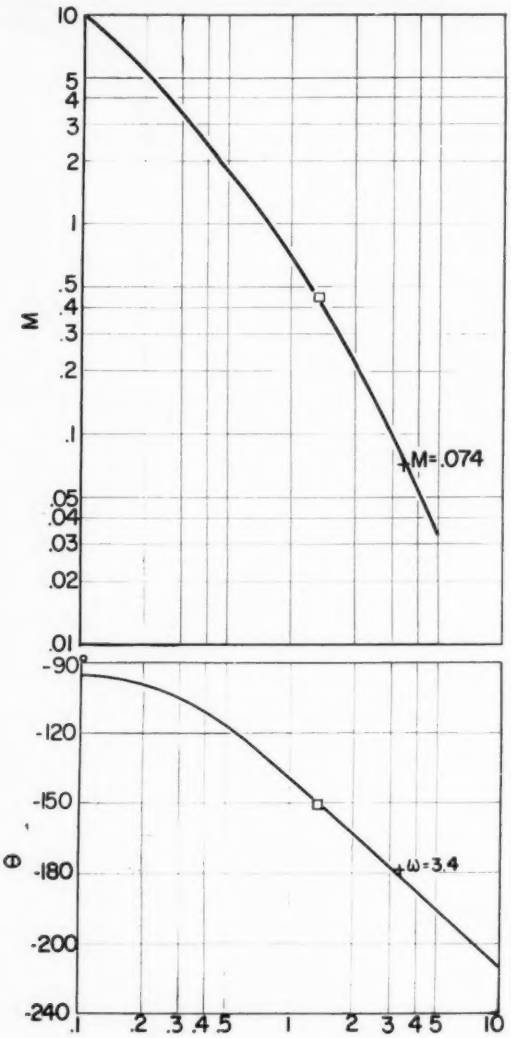

FIG. IV-33. Phase-amplitude diagram (Bode plot) for

$$G(i\omega) = \frac{1}{i\omega(1 + i\omega)[(1 + i\omega)/10]}.$$

$$K_3 G_3(p) = \frac{\mu}{(p^2/\omega_0^2) + 2\zeta(p/\omega_0) + 1}$$

and thus, the resultant transfer function $KG(p)$ shown in Eq. (IV-63) is obtained. The root locus for this system is shown in Fig. IV-28. It is seen that this system is stable above a gain of $K_{\text{crit.}(1)}$ and below a gain $K_{\text{crit.}(2)}$. The design range varies from a gain of $K = 9.75$ at low dynamic pressures up to a gain of $K = 670$ at high dynamic pressures. The roots corresponding to the latter case are shown as $p_1, p_2, \ldots p_7$.

(2) *Pitch Stabilization.*—The previous example showed how an airplane could be roll stabilized with a position gyro and a servo feedback network. Let us now study how a rate gyro could be used for pitch control. Let us assume that the speed of the airplane is kept constant by means of an automatic thrust control. This device would eliminate the slow phugoid oscillations. The remaining elements of the system and their transfer functions are shown in Fig. IV-36. The corresponding root-locus plot is shown for the conditions of high dynamic pressure (Fig. IV-37) and low dynamic pressure (Fig. IV-38), respectively. The servo gain selected for the high dynamic pressure condition is $K_1 = 0.40$; for the low dynamic pressure condition, $K_1 = 5.3$. The corresponding roots for the frequency equation are shown in Table IV-2.

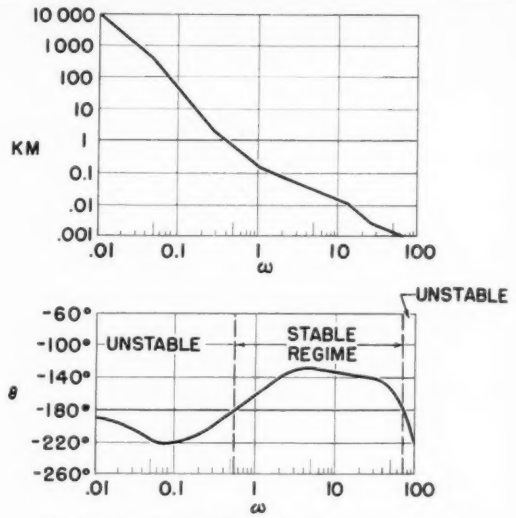

FIG. IV-34. Bode diagram for roll-control system.

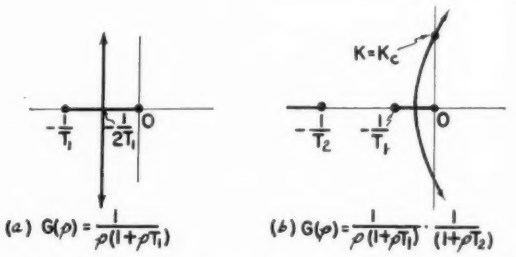

FIG. IV-35. Simple approximations for roll-control system.

(3) *Computation of System Response.*—Let us consider a simple feedback system whose open-loop transfer function is

TABLE IV-2

Condition	High Dynamic Pressure, $K = 0.40$	Low Dynamic Pressure, $K = 5.3$
p_1	$-28 + 50i$	$-16 + 43i$
p_2	$-28 - 50i$	$-16 - 43i$
p_3	$-27 + 22.5i$	$-27 + 22i$
p_4	$-27 - 22.5i$	$-27 - 22i$
p_5	-8	-2

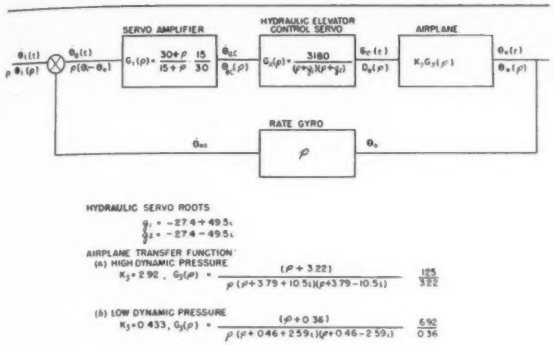

FIG. IV-36. Pitch stabilization system with rate gyro.

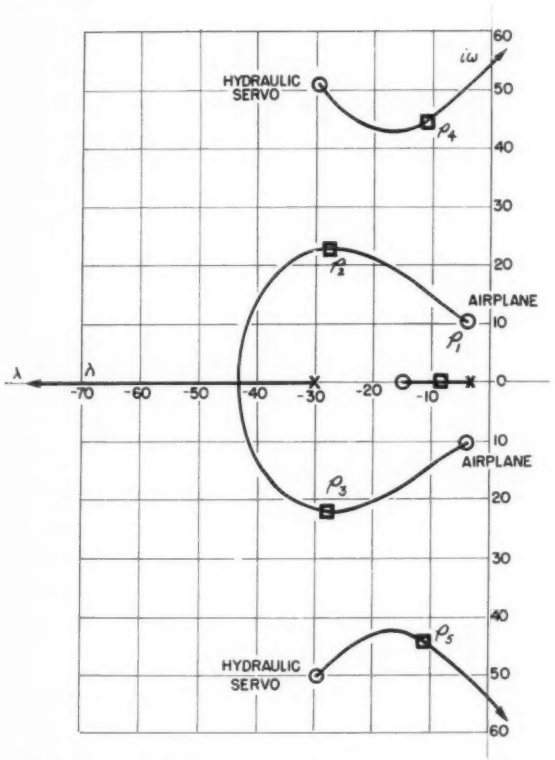

FIG. IV-37. Root locus for longitudinal dynamic stability analysis–high dynamic pressure. (Note: zero of origin due to rate gyro cancels pole due to airplane.)

$$G(p) = \frac{(p - s_1) \cdot (p - s_2) \cdots (p - s_m)}{(p - q_1) \cdot (p - q_2) \cdots (p - q_n)} \tag{IV-76}$$

and whose closed-loop transfer function is determined from the relation

$$K_s G_s(p) = \frac{KG(p)}{1 + KG(p)}$$

$$G_s(p) = \frac{N_s(p)}{D_s(p)} = \frac{(p - s_1) \cdot (p - s_2) \cdots (p - s_m)\ K}{(p - p_1) \cdot (p - p_2) \cdots (p - p_n)\ K_s} \tag{IV-77}$$

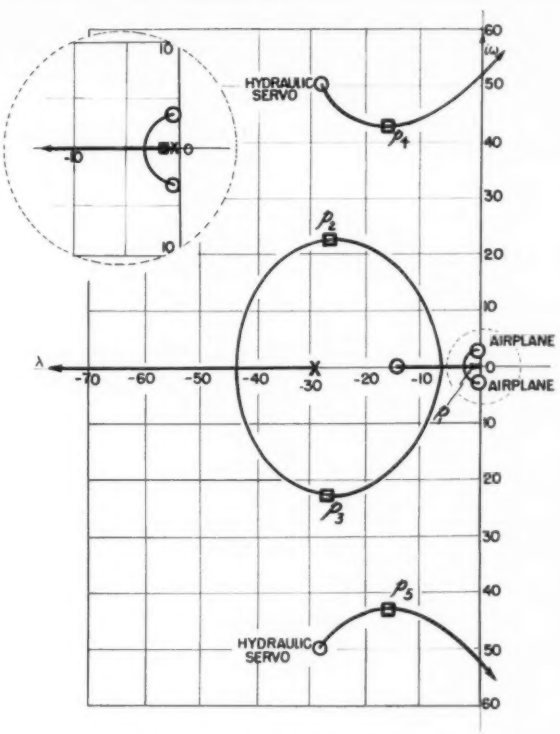

FIG. IV-38. Root locus for longitudinal dynamic stability analysis–low dynamic pressure. (Note: zero of origin due to rate gyro cancels pole due to airplane.)

It will be noted that the zeros of $G_s(p)$ are the same as the zeros of $G(p)$. The response due to a step-input $y_i(t) = h(t)$ is then

$$\left.\begin{aligned} y_0(t) &= K_s \cdot \left[G_s(0) + \sum_{r=1}^{n} \frac{N_s(p_r)}{p_r \cdot D_s'(p_r)}\ e^{p_r t} \right] \\ &= K_s \cdot [A_0 + \sum_{r=1}^{n} A_r e^{p_r t}] \end{aligned}\right\} \tag{IV-78}$$

These terms may be interpreted graphically from the positions of the poles and zeros in the p-plane. Consider, for example, a third-order system having the closed-loop transfer function

$$G_s(p) = 1/[(p - p_1)(p - p_2)(p - p_3)]$$

where $p_1 = -1 + i$, $p_2 = -1 - i$, $p_3 = -10$ and thus $(p_1 - p_2) = 2e^{i90°}$, $p_1 - p_3 = 9.05e^{i6.3°}$, $p_2 - p_3 = 9.05e^{-i6.3°}$. We find

$$A_0 = G_s(0) = \frac{-1}{p_1 \cdot p_2 \cdot p_3} = \frac{1}{20}$$

$$A_1 = \frac{N_s(p_1)}{p_1 \cdot D_s'(p_1)} = \frac{1}{p_1 \cdot (p_1 - p_2)(p_1 - p_3)} =$$

$$\frac{1}{25.6}\, e^{+i129°}$$

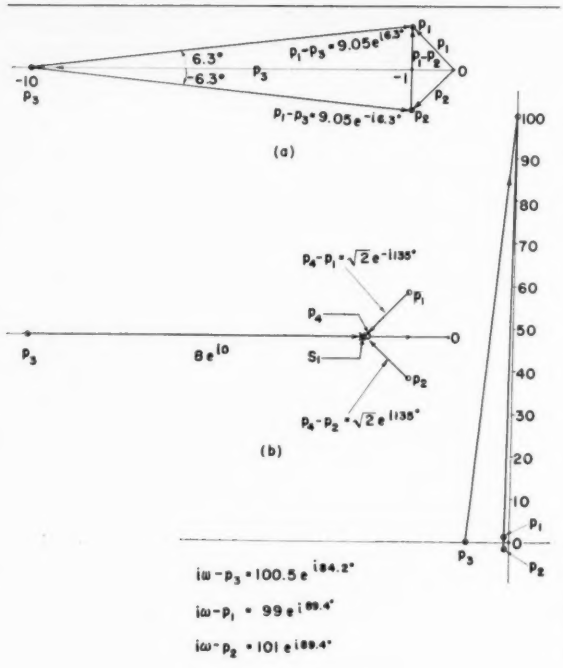

FIG. IV-39. Vectors representing terms of the response.

$$A_2 = \frac{N_s(p_2)}{p_2 . D_s'(p_2)} = \frac{1}{p_2 . (p_2 - p_1)(p_2 - p_3)} = \frac{1}{25.6} e^{-i129°}$$

$$A_3 = \frac{N_s(p_3)}{p_3 D_s'(p_3)} = \frac{1}{p_3 . (p_3 - p_1)(p_3 - p_2)} = \frac{1}{820}$$

The vector lengths p_1, $p_1 - p_2$, $p_1 - p_3$, etc., are easily measured in the p-plane (Fig. IV-39a). It is obvious by inspection that A_3 will be much smaller than A_1 and A_2 because the vector lengths to the point p_3 are much larger than the others. Thus, the term $A_3 e^{p_3 t}$ will be of small importance in the response compared to the first two terms.

If there is a zero in the p-plane, the effect is to reduce the effectiveness of a pole close to it. Thus, if to the above three poles we add a fourth $p_4 = -2.00$ and a zero $s_1 = -2.01$, then we would find

$$A_0' = \frac{s_1}{p_4} \cdot \frac{-1}{p_1 p_2 p_3} = 1.005 A_0$$

$$A_1' = \frac{s_1 - p_1}{p_4 - p_1} \cdot \frac{1}{p_1 . (p_1 - p_2)(p_1 - p_3)} = 1.007 e^{0.005i} \cdot A_1$$

$$A_2' = \frac{s_1 - p_2}{p_4 - p_2} \cdot \frac{1}{p_2 . (p_2 - p_1)(p_2 - p_3)} = 1.007 e^{-0.005i} A_2$$

$$A_3' = \frac{s_1 - p_3}{p_4 - p_3} \cdot \frac{1}{p_3 . (p_3 - p_1)(p_3 - p_2)} = 0.999 A_3$$

$$A_4' = \frac{s_1 - p_4}{p_4} \cdot \frac{1}{(p_4 - p_1)(p_4 - p_2)(p_4 - p_3)} = \frac{1}{3200}$$

The vector lengths are shown in Fig. IV-39b. This example illustrates that the coefficient A_4 is extremely small, and, if it were possible to have the zero s_1 and the pole p_4 coincide, they would completely cancel each other, and the coefficient A_4 would be zero and the motion $e^{p_4 t}$ would be completely eliminated.

If the exciting force is sinusoidal ($y_i = e^{i\omega t}$), then the response is

$$y_0(t) = K_s . \left[\underbrace{G_s(i\omega) . e^{i\omega t}}_{\text{steady-state vibration}} + \underbrace{\sum_{r=1}^{n} \frac{N_s(p_r)}{(p_r - i\omega) . D_s'(p_r)} e^{p_r t}}_{\text{transient vibration}} \right]$$

$$= K_s \left(A_\omega . e^{i\omega t} + \sum_{r=1}^{n} A_r e^{p_r t} \right)$$

It is clear from the preceding example that the coefficients A_ω, A_1, A_2 . . . A_n can again be determined graphically from the measured vector lengths and directions in the p-plane. If, for example, $\omega = 100$ rad. per sec. in the previous example, then

$$A_\omega = G_s(i\omega) = \frac{1}{(i\omega - p_1).(i\omega - p_2).(i\omega - p_3)}$$

$$A_1 = \frac{N_s(p_1)}{(p_1 - i\omega) D_s'(p_1)} = \frac{1}{(p_1 - i\omega) . (p_1 - p_2) . (p_1 - p_3)}$$

$$A_2 = \frac{N_s(p_2)}{(p_2 - i\omega) D_s'(p_2)} = \frac{1}{(p_2 - i\omega)(p_2 - p_1)(p_2 - p_3)}$$

$$A_3 = \frac{N_s(p_3)}{(p_3 - i\omega) D_s'(p_3)} = \frac{1}{(p_3 - i\omega)(p_3 - p_1)(p_3 - p_2)}$$

where

$$i\omega - p_1 = 99 e^{i89°}$$
$$i\omega - p_2 = 101 e^{i89°}$$
$$i\omega - p_3 = 100.5 e^{i89°}$$

The vector lengths are shown in Fig. IV-39c. If there were a zero of the system near the exciting frequency $\omega = 100$ rad. per sec., then the response would be small; if the zero coincided exactly with the exciting frequency, then the response would be completely eliminated. This case is of great practical engineering importance. It corresponds to the so-called "tuned vibration damper" discussed, for example, by Den Hartog in reference 6. It corresponds physically to adjusting a system so that the exciting force acts at a node of the vibratory system.

The system response to any other input can be computed analogously. Thus, if, for example, it were desired to compute the output $y_0(t)$ for an exponential input $y_i(t) = e^{-\beta t}$, then, since $Y_i(p) = p/(p + \beta)$, we would have

$$Y_0(p) = [p/(p + \beta)] . K_s G_s(p) \qquad \text{(IV-79)}$$

and

$$y_0(t) = B_\beta . e^{-\beta t} + \sum_{r=1}^{n} B_r . e^{p_r t} \qquad \text{(IV-80)}$$

The coefficients B_β and B_r could be written down by the partial fraction rule [Eq. (A-10)] and evaluated graphically in terms of the vector lengths in the p-plane as before.

The error of the response for large values of time t may be determined for a single feedback network for various simple inputs by applying the rule [Eq. (A-16)] that $\lim_{t \to \infty} \epsilon(t) = \lim_{p \to 0} E(p)$. This rule applies if the closed-loop transfer function $G_s(p)$ has no poles on the imaginary axis or in the right half of the p-plane. If the transfer function is of the type

$$G(p) = 1/[p^n(p - p_1)(p - p_2)]$$

we find from Eq. (IV-56)

$$E(p) = Y_i(p)/\{1 + 1/[p^n . (p - p_1)(p - p_2)]\}$$

Consider the following examples.

(a) For a sample step input:

$$y_i(t) = h(t) \qquad Y_i(p) = 1$$

$$\lim_{t \to \infty} \epsilon(t) = \lim_{p \to 0} \frac{1}{1 + \dfrac{K}{p^n (p - p_1)(p - p_2)}} = \begin{cases} \dfrac{1}{1 + (K/p_1 p_2)} & \text{if } n = 0 \\ 0 & \text{if } n \geq 1 \end{cases} \qquad \text{(IV-81)}$$

(b) For a simple velocity input:

$$y_i(t) = V_0 . t \qquad Y_i(p) = V_0/p$$

$$\lim_{t \to \infty} \epsilon(t) = \lim_{p \to 0} \frac{V_0/p}{1 + \dfrac{K}{p^n \cdot (p - p_1)(p - p_2)}} = \begin{cases} \infty & \text{if } n < 1 \\ \dfrac{V_0}{1 + (K/p_1 p_2)} & \text{if } n = 1 \\ 0 & \text{if } n > 1 \end{cases} \qquad \text{(IV-82)}$$

(c) For a simple acceleration input:

$$y_i(t) = (1/2)at^2 \qquad Y_i(p) = (1/2)(a/p^2)$$

$$\lim_{t \to \infty} \epsilon(t) = \lim_{p \to 0} \frac{(1/2)(a/p^2)}{1 + \dfrac{K}{p^n \cdot (p - p_1)(p - p_2)}} = \begin{cases} \infty & \text{if } n < 2 \\ \dfrac{(1/2)a}{1 + (K/p_1 p_2)} & \text{if } n = 2 \\ 0 & \text{if } n > 2 \end{cases} \qquad \text{(IV-83)}$$

(G) *Multiple-Loop Networks*

The autopilot system for an airplane consists of multiple-loop networks, since the six equations of motion of an airplane involve interactions between the pitch, up and down, and fore and aft motion, and also between the roll, yaw, and side motions. If the airplane is in any maneuver except straight flight, the first three longitudinal motions interact with the latter three lateral motions. In addition, the sensing instruments may measure mixed combinations of pitch, yaw, and roll angles when the airplane is undergoing maneuvers.

In order to design such multiple-loop networks, it is usually desirable to consider a single loop at a time using simplified assumptions. After the system parameters are tentatively fixed, it is then instructive to expand the analysis one loop at a time using the root-locus method for each loop. The principles involved are illustrated in Appendix (D) for the case of longitudinal stabilization of an aircraft.

Another method that is recommended by Hänny[13] is as follows: Write down the Laplace transforms of all of the equation and arrange them in determinental form. Then insert a cut in the network, and introduce an input signal $\varphi_e(t)$ at one side of the cut. The condition for closure is that the output signal $\varphi_a(t)$ at the other side of the cut be equal to the input signal. Fig. IV-40 illustrates schematically such a control system for a steam turbine. When an analog computer is

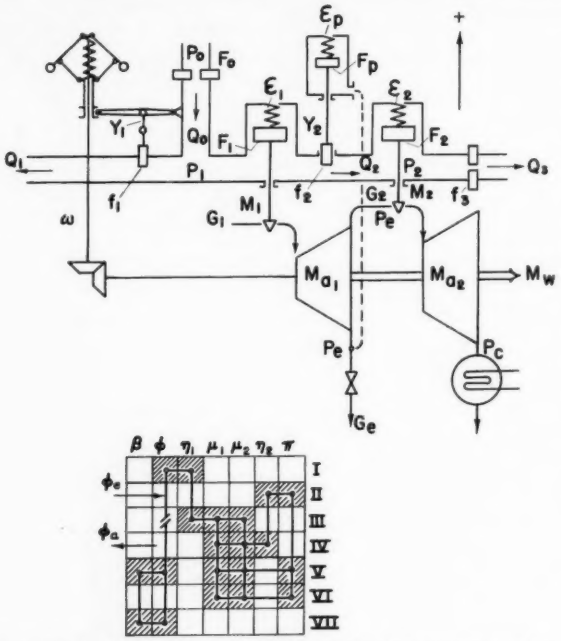

FIG. IV-40. Multiple-loop network representing a steam-turbine regulator.[13]

available, it is ordinarily most convenient to utilize it to study such multiple-loop networks experimentally.

(V) FLIGHT-TESTING TECHNIQUES

Flight tests are an essential step in the development of automatic control systems, both from the standpoint of verifying the performance characteristics of the system as well as the achievement of high reliability under the actual conditions of pressure, temperature, vibration, etc. In the present section, we propose to consider another type of flight test—namely, the determination of the aerodynamic coefficients in order to compare them with the coefficients estimated on the basis of wind-tunnel tests with stationary models.

The basic problem of this flight technique is to determine the aircraft transfer function

$$KG(p) = [\Theta_0(p)]/[\Theta_i(p)]$$

or

$$KG(i\omega) = [\Theta_0(i\omega)]/[\Theta_i(i\omega)]$$

where $\Theta_i(p)$ represents the Laplace transform of a control-surface deflection and $\Theta_0(p)$ represents the resulting motion (linear or angular). This technique was used by Milliken of the Cornell Aeronautical Laboratory in an extensive series of tests on a North American Aviation B-25J airplane to determine the transfer functions for the longitudinal motion of the airplane.[59] The elevator was moved $\pm 1^1/_2°$ sinusoidally at various frequencies from 1 to about 5.5 rad. per sec., and the resulting normal acceleration n and attitude angle θ_0 were measured. These results are shown in Figs. V-1a and V-1b, including a comparison with the theoretically estimated values. This technique of introducing a sinusoidal input deflection δ and measuring the output motion θ_0 is the most straightforward one in principle. Practically, this method has been rather tedious, in that it required about three hours of flight testing to cover the frequency range for one flight condition and required many hours of evaluation to reduce the data. Even so, the phase angles between the motions could not be deduced accurately enough from the separate measurements. There appear to be good potentialities, however, for the development of electrical systems that measure directly the magnification ratio $|[\Theta_0(i\omega)]/[\Theta_i(i\omega)]|$ and the phase angle between output and input. With such equipment, it would then be simple to determine the transfer function for various flight conditions from subsonic through transonic and up to supersonic speeds.

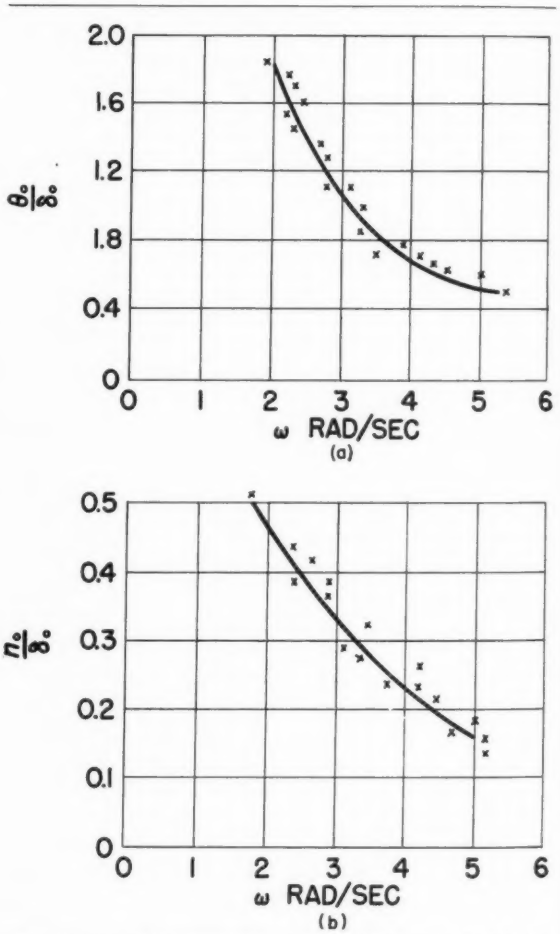

FIG. V-1. Airplane response for a sinusoidal elevator deflection. $\delta = \delta_0 e^{i\omega t}$ = elevator deflection. $\theta = \theta_0 e^{i(\omega t + \epsilon_1)}$ = pitch angle. $n = n_0 e^{i(\omega t + \epsilon_2)}$ = normal acceleration. ××× = experimental; ——— = theoretical. (According to W. F. Milliken, Jr., Cornell Aero Laboratory, B-25J airplane tests.)

In order to proceed from the transfer function to the determination of the principal aerodynamic coefficients, it is necessary to make assumptions about the magnitude of the secondary coefficients. Thus, the flight-test technique provides a check only on the principal aerodynamic coefficients. This is sufficient for verifying the assumptions of the autopilot analysis. Further development of the flight-test techniques is desirable to separate more clearly the effects of aeroelastic deformations and the effects of aerodynamic time lags on the motion of the aircraft.

Other methods for determining the aircraft transfer function for longitudinal motion have been to apply an elevator displacement (a) as a step function and (b) as an impulse (Fig. A-4). Milliken experimented with the step-function input. He found that securing the test data is much simpler; however, the interpretation of the data is more difficult since the control characteristics (particularly the hinge moments) depend not only upon the elevator angle but also upon the rate and acceleration at which the angle is applied. Another difficulty with a step-function input, particularly in roll and yaw, is that the mean flight path may be altered radically, and thus the validity of the linear theory may be exceeded. Furthermore, the step input excites the low-frequency modes of the system much more than the high-frequency modes, and thus important high-frequency modes may be overlooked or located inaccurately.

These last two difficulties are appreciably reduced by the use of a pulse-type input. In this case, a surface deflection is introduced and quickly removed, and the airplane remains near its equilibrium position. In addition, it may be seen that the various modes of oscillation of the aircraft are excited more uniformly. In the limit, as a perfect pulse (infinitely large amplitude and infinitesimal time duration) is approached, all modes are excited equally. Practically, the speed with which the surfaces may be moved and the resulting fidelity of the input pulse determine the range of frequencies over which the pulse spectrum is flat.

Several pulse shapes have been considered, the first resulting from a rapid surface deflection, followed by a period in which the deflection is held constant, and finally, by a rapid restoration of the surface (Fig. V-2a).

Input: $\Theta_i(p) = a(1 - e^{-p\tau})$
Output: $\Theta_0(p)$

The transfer function is given by

$$KG(p) = \frac{\Theta_0(p)}{\Theta_i(p)} = \frac{\Theta_0(p)}{a.(1 - e^{-p\tau})}$$

In the low-frequency range, the process of reducing the data to obtain $KG(p)$ may be simplified by considering the output to be made up of a number of pulses similar in form to the input, as illustrated in Fig. V-2b. With this approximation

$$\theta_0(t) \backsimeq h_0, \qquad 0 < t < \tau$$
$$\theta_0(t) \backsimeq h_1, \qquad \tau < t < 2\tau$$
$$\theta_0(t) \backsimeq h_2, \qquad 2\tau < t < 3\tau$$
$$\vdots$$

and

$$\Theta_0(p) = \sum_{n=1}^{m} h_n.(1 - e^{-p\tau}).e^{-np\tau}$$

Thus,

$$KG(p) = \frac{1}{a} \sum_{n=1}^{m} h_n e^{-np\tau}$$

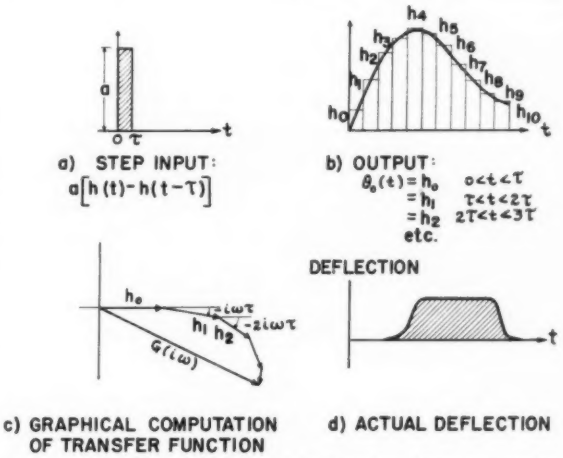

FIG. V-2. Determination of transfer functions from rectangular pulse inputs.

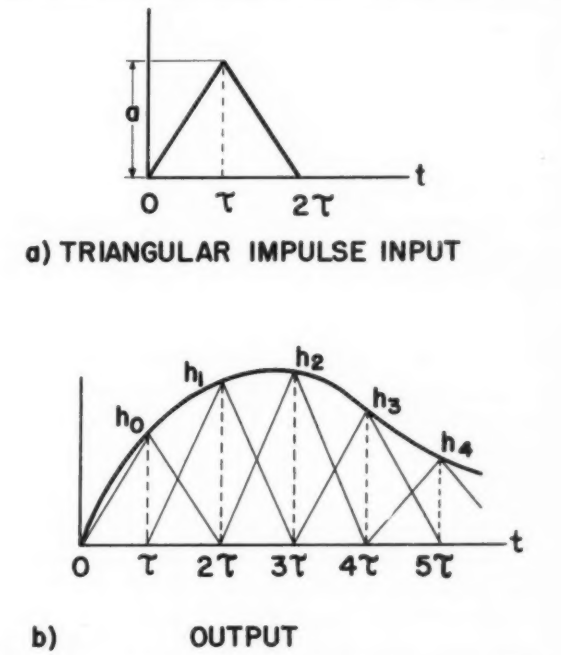

FIG. V-3. Determination of transfer function from triangular pulse inputs.

and

$$KG(i\omega) = \frac{1}{a}\sum_{n=1}^{m} h_n . e^{-in\omega t}$$

Since the factor $e^{-in\omega\tau}$ represents only a phase shift, the transfer function is obtained by adding the h_n with the proper relative phase as shown in Fig. V-2c. The required vector addition may be accomplished simply with either punch-card or elementary analog equipment.

Practically, it is not possible for the surfaces to be deflected instantaneously as indicated; a finite deflection time is required, as shown in Fig. V-2d. Since the frequency spectrum of the input is constant over the largest frequency range when the time interval of the pulse is a minimum, it appears desirable, from the standpoint of uniform mode excitation, to employ a triangular pulse in which the slope of the sides corresponds to the maximum rate of surface deflection. This technique was first applied to the experimental determination of the aircraft transfer function by Seamans, Blasingame, and Clementson of the M.I.T. Instrumentation Laboratory (Dr. C. S. Draper).[75] In this case the input signal of Fig. V-3a has the transform

$$\Theta_i(p) = \frac{a}{\tau}\cdot\frac{1}{p}\cdot(1 - 2e^{-\tau p} + e^{-2\tau p}) = \frac{a}{\tau}\cdot\frac{1}{p}\cdot (1 - e^{-\tau p})^2$$

Again, for low frequencies, the transfer function may be obtained most simply by considering the output to consist of a number of pulses similar in form to the input. Thus

$$\Theta_0(p) = \frac{h_0}{\tau}\cdot\frac{1}{p}\cdot(1 - e^{-\tau p})^2 + \frac{h_1}{\tau}\cdot\frac{1}{p}e^{-\tau p}(1 - e^{-\tau p})^2 + \frac{h_2}{\tau}\cdot\frac{1}{p}e^{-2\tau p}(1 - e^{-\tau p})^2 + \ldots .$$

In this case, the output is approximated by a series of straight-line segments connecting the points at time equal to 0, τ, 2τ, etc., as shown in Fig. V-3b. As in the case already considered,

$$KG(i\omega) = \frac{1}{a}\sum_{n=1}^{m} h_n e^{-in\omega\tau}$$

A transfer function obtained in this manner is satisfactory for low frequencies. For the higher frequencies, it is necessary to consider the fine structure of both the input and the output and to use the exact expression for $G(i\omega)$. This is particularly important when it is desired to determine the influence of factors, such as aerodynamic time lags, which primarily affect the high-frequency response of an aircraft. Before this effort is considered, however, it appears desirable to study the problem of noise in the measuring equipment and its possible effect on the results. The amplitude of the high-frequency response is normally small, and delicate measuring equipment is required to detect it. In this regard, it appears that some improvement might be obtained by averaging the results of a number of tests, thereby reducing the effect of random disturbances.

In general, the pulse method is superior to the steady-state techniques: Simpler equipment and considerably less flight time are required to obtain the results. From the standpoint of accuracy, however, neither method appears to offer substantial advantage. Considerable improvement is required before either method will be suitable for extending our knowledge of aircraft dynamics.

(VI) Future Problems and Potentialities

(A) *Future Problems*

(*1*) *Nonlinear Systems.*—The theory and practice of automatic control systems are still in the early stage of development. Thus far, only linear systems have been thoroughly analyzed. Nonlinear systems have been studied only for especially simple cases. Summaries of the theoretical work in this field are available.[39, 83, 85, 86] The advent of the new computing machines may make it possible to carry out systematic studies of nonlinear elements and thus provide background information that will permit the intuitive synthesis of nonlinear controllers of desired characteristics. An energetic attack of this problem is under way by the Office of Air Research, U.S.A.F., under the direction of Dr. Frank W. Bubb.

(*2*) *Treatment of "Noise."*—The problem of "noise" in electromechanical networks is similar to that of turbulence in a fluid flow. Taylor,[88] in his early studies on the statistical theory of turbulence, introduced the idea of correlation coefficients. Wiener, Kolmogoroff, and others have carried over the use of these concepts to the treatment of noise in electrical filter networks. With the aid of this theory, the communication engineers have learned to design optimum linear filter networks that reduce to a minimum the effect of the noise relative to the signal.[15, 84, 87, 89, 90] Many of the principles for the design of "smoothing networks" which have been developed by the communication engineers are being taken over in the design of automatic control equipment. The application of these techniques to controller design promises to be one of the fertile fields for improvement in the accuracy of response of control systems.

(*3*) *Optimum Controller Design.*—The design of a corrective electrical network for a control circuit which will have prescribed characteristics is one of the means of improving the response of control systems. The general techniques for the design of such networks have been worked out by the communication engineers.[3, 11] These corrective networks are variously called "controllers" or "equalizers." These more complicated networks may have application to aircraft

control systems, although probably only for specialized applications. The reason is that the transfer function of the airplane is not a fixed quantity but varies over wide limits, and thus it is not generally worth while to go to extreme pains to design an optimum controller circuit for any one design point.

There are, however, a number of simple tricks that may well be incorporated in the synthesis of the controller. Moore describes two methods for designing a controller that converts the equations of the unequalized system into the desired form. The first alters the system equations by the addition of certain terms; the second method inverts certain terms. An example of the former occurs in the case of aircraft control where undesirable rolling moments occur as the result of rudder deflection. Here, the controller anticipates the rolling moment associated with rudder deflection and automatically calls for a compensating aileron deflection. Another example occurs in the case of an undesirable yawing moment resulting from rolling angular velocity. Here, the rudder is deflected by an amount necessary to compensate for the calculated yawing moment based on rate gyro measurements of roll rate. The use of the inverting controller is illustrated when there is a necessity for compensating autopilot gain for variations in dynamic pressure. Here, the system gain is increased as the dynamic pressure decreases so that the overall system characteristics are as independent of dynamic pressure variations as is economical.

The methods of direct synthesis involve measurement of functions of dependent variables of the system to compensate for effects of these functions on the outputs. However, since such controllers are inside the system feedback loops, they must be used with caution, because any uncertainty in the form of the system equations may cause overcompensation and actual instability.

Another method for improving the performance of control systems is to use an open-cycle controller to schedule the approximate value of an output and to use a closed-cycle system to supply the vernier control. Such a system, proposed by Moore, is shown in Fig. VI-1. A more extensive discussion of this same topic is given in reference 18. As an example, the yawing motion due to rolling angular velocity can be compensated in open-cycle control by anticipating the rolling rate that will result from application of a given aileron deflection and calling for a proper amount of rudder deflection to eliminate the yawing moment resulting from such a roll rate.

(*B*) *Future Potentialities for Aircraft*

There are many applications of automatic control systems to aircraft beyond the automatic flight and landing systems discussed so far. Among the more important ones are the following.

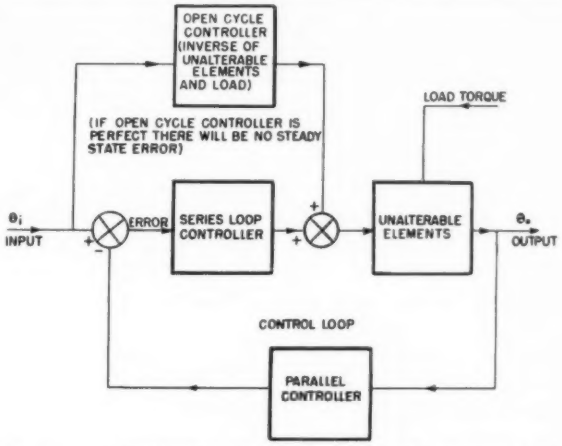

FIG. VI-1. Combination open-cycle closed-cycle system (J. R. Moore).

(*1*) *Automatic Cruise Control of Propulsion System.*—Most propulsion systems have two or more parameters that can be varied to produce a given thrust. During cruise, the important problem is to operate the system at the optimum specific fuel consumption expressed in pounds per mile. An open-cycle, closed-cycle system appears well adapted to schedule the operation at approximately the correct speed and altitude and to depend thereafter upon the direct measurement of fuel flow and distance in order to adjust the parameters for optimum performance. The adjustment of the controls must be carried out consistent with the limitations of the engine and the aircraft. The various adjustable parameters and the limiting factors are shown in Table VI-1. All of these power plants suffer under certain conditions from instabilities. The first four may experience a pulsation associated with the compressor;

TABLE VI-1

Propulsion System	Adjustable Parameters	Principal Operating Limits
Piston engine and propeller	r.p.m.—by propeller pitch Manifold pressure—by fuel flow	(1) Maximum r.p.m. (2) Maximum manifold pressure
Turbojet	r.p.m.—by fuel flow Turbine inlet temperature—by exhaust nozzle area	(1) Maximum r.p.m. (2) Maximum turbine inlet temperature (3) Pulsation limit (4) Combustion blowout limit
Propeller turbine	r.p.m.—by propeller pitch Turbine inlet temperature—by fuel flow	(1) Maximum r.p.m. (2) Maximum turbine inlet temperature (3) Pulsation limit (4) Combustion blowout limit
Ram-jet	Maximum temperature—by fuel flow Pressure recovery—by exhaust nozzle area	(1) Maximum temperature (2) Pulsation limit (3) Blowout limit
Rocket	Fuel flow Fuel ratios	(1) Maximum pressure (2) Combustion instability

the last four may experience instabilities associated with combustion. There is a good possibility that automatic control systems may either prevent operation in these unstable regimes or, under certain conditions, perhaps permit the damping of these oscillations by introducing a feedback link into the system.

(*2*) *Automatic Stabilization of Aircraft Under Stall Conditions.*—An aircraft is ordinarily unstable in roll as it approaches the stall. It tends to fall off on one wing or the other. It should be possible to eliminate this instability by an automatic control system that applies a rudder deflection to counteract the unstable roll.

(*3*) *Automatic Stabilization of Helicopters.*—It was pointed out by von Kármán[80] in 1925 that helicopters are dynamically unstable. This prediction was verified when helicopters were successfully flown in the 1930's in that they had to be continuously controlled. There are aerodynamic methods for stabilizing the helicopter. However, the automatic stabilization by an autopilot may well prove to be the generally most flexible system.

(*4*) *Gust Alleviation.*—Many studies have been carried out on the possibility of reducing the effect of gusts on aircraft both from the standpoint of permitting reduced design load factors and to improve passenger comfort. Most of the previous studies were carried out on a semiempirical basis. With the advent of rapidly responsive servosystems, it may well be possible now to achieve a better measure of success on this problem.

(*5*) *Automatic Stabilization of Seaplanes and Hydroplanes Riding on the Water.*—Seaplanes experience a longitudinal dynamic instability called porpoising. It should be possible to devise an automatic control system that will damp out these oscillations. For example, a hydrofoil surface arranged either ahead or behind the main float could be actuated by an automatic control system.

Hydrofoils have also been repeatedly proposed as a more efficient method of cruising either ships or aircraft in the water at high speeds (by Tietjens and others). One of the problems of hydrofoil systems is again the achievement of longitudinal stability. Automatic control systems should be able to provide stability either with the use of a control surface in front or behind the main lifting hydrofoils.

Conclusions

We have seen that the current high-performance aircraft are flying in the transonic speed regime that is the most difficult from the standpoint of stability and control. In order to overcome the requirements of high stick forces, power controls had to be introduced. In order to increase the precision of maneuvers, automatic control systems were required to supplement the human pilot. The fighter airplane with automatic and power controls therefore represents an intermediate version between the conventional aircraft of World War II and the guided missiles of the near future.

The application of automatic control systems to aircraft promises to bring about the most important new advances in aeronautics in the future. The past 25 years have seen a tremendous development in the fields of propulsion, aerodynamics, and structures. The next 25 years will probably see comparable major developments in the application of automatic control systems to stabilize and control accurately and reliably the aircraft of the future from its initial take-off to its landing. The student of aeronautics would, therefore, be well advised to include in his program a study of the fundamentals of dynamics and of servomechanisms. The practicing aeronautical engineer will find it necessary to gain an understanding of these principles in order to design the optimum aircraft systems.

Appendix (A)

Method of Laplace Transforms

(*A*) *Solution of Linear Differential Equations*

The theory of Laplace transforms represents one of the most useful tools of dynamic analysis. A complete discussion of this theory is given in a number of excellent texts.[28–40] In order to follow the analysis of the present paper, the following condensed summary may be of help. The more important rules are illustrated by some problems whose solution is well known to the aeronautical engineer.

The Laplace transform* of a function $y(t)$ is denoted by $Y(p)$ and is defined as follows:

$$Y(p) = p \int_0^\infty e^{-pt} . y(t) . dt \qquad \text{(A-1)}$$

It is assumed that $y(t) = 0$ for $t < 0$. The variable t ordinarily denotes the time and is a real number. The variable p may, however, be a complex number.

The above integral defines $Y(p)$ as long as the integral converges. For example, if $y(t) = e^{+at}$, then

$$Y(p) = p \int_0^\infty e^{-pt} . e^{+at} . dt = \frac{p}{p - a} \left[-e^{-(p-a)t} \right]_{t=0}^{t=\infty}$$

* In the mathematical literature it is conventional to define the Laplace transform

$$F(s) = \int_0^\infty y(t) . e^{-st} . dt$$

and its inverse

$$y(t) = \frac{1}{2\pi} \int_{a-i\infty}^{a+i\infty} F(s) . e^{st} . ds$$

This form has advantages of greater symmetry in its transformations compared to our $Y(p)/p$. Our form [Eq. (A-1)] has the advantage, however, that the dimensions of $Y(p)$ are the same as those of $y(t)$ since p has the dimensions of (1/time).

At the upper limit, the function $e^{-(p-a)t} \to 0$ as $t \to \infty$ *if* $(p - a)$ is positive—i.e., if $p > +a$. At the lower limit, $e^{-(p-a)t} \to 1$ as $t \to 0$, and thus the integral defines $Y(p) = p/(p - a)$ for $p > +a$. As part of the definition of the Laplace transform of $y(t) = e^{at}$, we *define*

$$Y(p) = p/(p - a) \text{ for } p < a$$

This part of the definition follows by analytic continuation (i.e., by using the same analytic expression of the function) rather than as a consequence of the integral definition, Eq. (A-1).

In a similar manner, it is possible to substitute other simple functions $y(t)$ under the integral sign and to compute the corresponding values of $Y(p)$. A short table of such transforms is given in Appendix (B) (in both the engineer's p and the mathematician's s notation). It is understood that $y(t)$ has the values shown only for $t > 0$ and that $y(t) = 0$ for $t < 0$.

If the function $y(t)$ or its derivatives have a discontinuity at the origin, it is necesary to define more carefully what we mean by $y(0)$—i.e., the value of y at a time $t = 0$, and $y'(0)$—i.e., the value of dy/dt at time $t = 0$, etc. If, for example, an elevator rising at a uniform velocity V_0 picks up a load at position h_0, the position of this load at time t is shown in Fig. A-1c. We shall, as a matter of definition, agree that

$$\begin{aligned} y(0) &= y(t) \text{ at } t = 0 - \epsilon \\ y'(0) &= dy/dt \text{ at } t = 0 - \epsilon \end{aligned}$$

where ϵ is a very small quantity that approaches zero; i.e., we take the values of these functions to the *left* of the origin.* Thus, in the present case $y(0) = h_0$ and $y'(0) = 0$ (*not* $y'(0) = V_0$). Let us now study the Laplace transform of a derivative dy/dt by carrying out an integration by parts:

$$p \int_0^\infty \underbrace{e^{-pt}}_{u} \cdot \underbrace{\frac{dy}{dt}}_{dv} \cdot dt = p \cdot \underbrace{[e^{-pt}}_{u} \cdot \underbrace{y(t)]_0^\infty}_{v} - p \int_0^\infty \underbrace{y(t)}_{v} \cdot \underbrace{(-p) \cdot e^{-pt} \cdot dt}_{du}$$

The value of $e^{-pt} \cdot y(t) \to 0$ as $t \to \infty$ if $y(t)$ either is finite at $t = \infty$ or diverges less strongly than e^{pt}. The value of $e^{-pt} \cdot y(t) \to y(0)$ as $t \to 0$, and, as agreed above, we shall take $y(0) = y(0 - \epsilon)$. Thus, we get

$$p \int_0^\infty e^{-pt} \cdot \frac{dy}{dt} \cdot dt = -p \cdot y(0) + p \cdot Y(p) \quad \text{(A-2)}$$

and similarly,

$$p \int_0^\infty e^{-pt} \cdot \frac{d^2y}{dt^2} \cdot dt = -p \cdot y'(0) - p^2 \cdot y(0) + p^2 \cdot Y(p) \quad \text{(A-3)}$$

With these two rules, we can convert a linear differential equation with constant coefficients into an algebraic equation. For example, the differential equation of a mass-spring system with velocity damping and an input force $f_i(t)$ is

$$m(d^2y/dt^2) + c(dy/dt) + ky = f_i(t) \quad \text{(A-4)}$$

with the boundary conditions

$$\left.\begin{aligned} y &= y(0) \\ dy/dt &= y'(0) \end{aligned}\right\} \text{at } t = 0 - \epsilon$$

We multiply this equation by pe^{-pt} and integrate from $t = 0$ to $t = \infty$

$$mp \int_0^\infty e^{-pt} \cdot \frac{d^2y}{dt^2} \cdot dt + cp \int_0^\infty e^{-pt} \cdot \frac{dy}{dt} \cdot dt + kp \int_0^\infty e^{-pt} \cdot y(t) \cdot dt = p \int_0^\infty e^{-pt} \cdot f_i(t) \cdot dt$$

We define as before

$$Y(p) = p \int_0^\infty e^{-pt} \cdot y(t) \cdot dt \quad \text{(A-5)}$$

and

$$F_i(p) = p \int_0^\infty e^{-pt} \cdot f_i(t) \cdot dt \quad \text{(A-6)}$$

and evaluate the integrals according to our definitions

$$m[-p.y'(0) - p^2.y(0) + p^2.Y(p)] + c[-p.y(0) + pY(p)] + k.Y(p) = F_i(p)$$

or rearranging terms

$$(mp^2 + cp + k).Y(p) = F_i(p) + mpy'(0) + (mp^2 + cp).y(0) \quad \text{(A-7)}$$

and solving for

$$Y(p) = \frac{F_i(p)}{mp^2 + cp + k} + \frac{m.p.y'(0) + (mp^2 + cp).y(0)}{mp^2 + cp + k} \quad \text{(A-8)}$$

In order to find $y(t)$, the inverse transform of $Y(p)$, we first resolve $Y(p)$ into terms of the type $A_r \cdot [p \div (p - p_r)]$, for which we know the inverse transform is $A_r \cdot e^{p_r t}$. We use the following "partial fraction rule":

If $G(p) = N(p)/D(p)$ where $N(p)$ and $D(p)$ are polynomials in p, we have

$$\begin{aligned} N(p) &= a_0 + a_1.p + a_2.p^2 + \ldots + a_m p^m \\ D(p) &= (p - p_1)(p - p_2) \ldots (p - p_n) \end{aligned}$$

and $m \leq n$ and none of the factors $p - p_r$ in $D(p)$ is repeated; then $G(p)$ may be separated into fractions as follows:

* It is also possible to build up a logically correct system with other definitions of $y(0)$ and $y'(0)$. For example, references 5 and 32 use $y(0) = y(0 + \epsilon)$ and $y'(0) = y'(0 + \epsilon)$ and define the Laplace transform of dy/dt as $s.F(s) - y(0 + \epsilon)$.

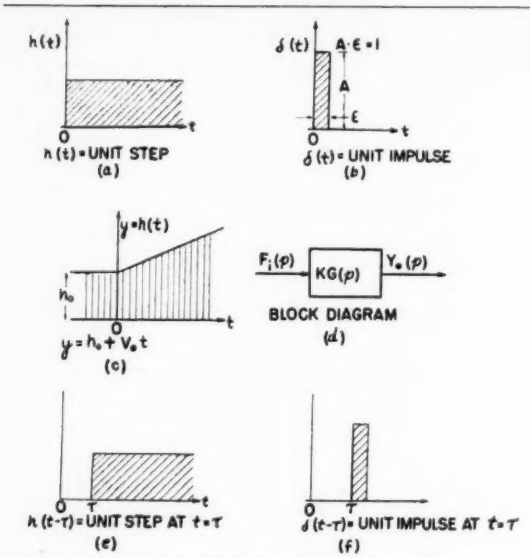

FIG. A-1. Definition of singularities.

$$G(p) = A_0 + A_1 \cdot \frac{p}{p - p_1} + A_2 \cdot \frac{p}{p - p_2} + \ldots + A_n \cdot \frac{p}{p - p_n}$$

where*

$$A_0 = N(0)/D(0) = G(0)$$

and

$$A_1 = N(p_1)/[p_1 . D'(p_1)]$$
$$A_2 = N(p_2)/[p_2 . D'(p_2)]$$
$$\vdots$$
$$A_n = N(p_n)/[p_n . D'(p_n)]$$

or alternately

$$A_1 = \frac{N(p_1)}{p_1 . 1 . (p_1 - p_2)(p_1 - p_3) \ldots (p_1 - p_n)}$$

$$A_2 = \frac{N(p_2)}{p_2 . (p_2 - p_1) . 1 . (p_2 - p_3) \ldots (p_2 - p_n)}$$

$$\vdots$$

$$A_n = \frac{N(p_n)}{p_n . (p_n - p_1)(p_n - p_2) \ldots (p_n - p_{n-1}) . 1}$$

where $D'(p) = dD/dp$. If $G(p)$ is the Laplace transform of $g(t)$, we find

$$g(t) = A_0 + A_1 . e^{p_1 t} + A_2 . e^{p_2 t} + \ldots + A_n e^{p_n t}$$

This expansion theorem may therefore be stated as follows:

If $G(p) = N(p)/D(p)$, this may be expanded into

$$G(p) = G(0) + \sum_{r=1}^{n} \frac{N(p_r)}{p_r . D'(p_r)} \frac{p}{p - p_r} \qquad \text{(A-9)}$$

and its inverse transform is

$$g(t) = G(0) + \sum_{r=1}^{n} \frac{N(p_r)}{p_r . D'(p_r)} e^{p_r t} \qquad \text{(A-10)}$$

where $p_1, p_2, \ldots p_r \ldots p_n$ are the roots of the frequency equation $D(p) = 0$.

Let us consider the application of this rule to Eq. (A-8). We note that $Y(p)$ consists of two parts:

$$Y_0(p) = \frac{F_i(p)}{mp^2 + cp + k} =$$

Laplace transform of output motion due to the input force $f_i(t)$

$$Y_0(p) = \frac{m . p . y'(0) + (mp^2 + cp) . y(0)}{mp^2 + cp + k} =$$

Laplace transform of output motion due to the boundary conditions $y(0)$ and $y'(0)$

In the analysis of automatic control systems we shall be primarily concerned with $Y_0(p)$. We denote the ratio

$$\text{output/input} = Y_0(p)/F_i(p) = KG(p) \qquad \text{(A-11)}$$

where

$$K = Y_0(0)/F_i(0) \qquad \text{(A-12)}$$

is a constant called the "gain"

$$G(p) = \frac{1}{K} \cdot \frac{Y_0(p)}{F_i(p)} = \text{transfer function} \qquad \text{(A-13)}$$

[In the above example $K = 1/k$ and $G(p) = \dfrac{1}{(m/k)p^2 + (c/k)p + 1}$.] We denote this relationship by a block diagram as shown in Fig. A-1d.

The solution of Eq. (A-10) for two important special cases of input force may be written down immediately:

* To find A_1, note that

$$\frac{N(p)}{p . D(p)} = \frac{G(p)}{p} = \frac{A_1}{p - p_1} + \underbrace{\left(\frac{A_0}{p} + \frac{A_2}{p - p_2} + \ldots + \frac{A_n}{p - p_n}\right)}_{\varphi(p)/\Phi(p)} = \frac{A_1 . \Phi(p) - (p - p_1)\varphi(p)}{(p - p_1) . \Phi(p)}$$

and that

$$N(p_1) = A_1 . \Phi(p_1)$$

i.e.,

$$A_1 = N(p_1)/\Phi(p_1)$$

where

$$\Phi(p_1) = p_1 . (p_1 - p_2) \ldots (p_1 - p_n)$$

which could also be written

$$\Phi(p_1) = p_1 . \left[\frac{d}{dp} D(p)\right]_{p = p_1} = p_1 . D'(p_1)$$

The other coefficients are obtained analogously.

(a) If $f_i(t) = F_m . h(t)$ where F_m is a constant and $h(t)$ is the unit step function, then $F_i(p) = F_m$. From Eq. (A-11) we then have

$$Y_0(p) = F_m . K . G(p)$$

and assuming $G(p)$ is given in the form of Eq. (A-9)

$$y_0(t) = F_m . K . \left[G(0) + \sum_{r=1}^{n} \frac{N(p_r)}{p_r . D'(p_r)} e^{p_r t} \right] \quad \text{(A-14)}$$

is the motion due to the input force $f_i(t)$.

(b) If $f_i(t) = F_m . e^{i\omega t}$, then

$$F_i(p) = F_m . p/(p - i\omega)$$

and from Eq. (A-11),

$$Y_0(p) = F_m . [p/(p - i\omega)] . KG(p)$$

This expression is expanded similarly to Eq. (A-9) considering $G_1(p) = [p/(p - i\omega)]G(p)$. The new numerator is $N_1(p) = p . N(p)$. The new denominator is $D_1(p) = (p - i\omega)D(p)$, and thus we find

$$y_0(t) = F_m . K . \Big\{ \underbrace{G(i\omega) . e^{i\omega t}}_{\text{steady-state vibration}} + \underbrace{\sum_{r=1}^{n} \frac{N(p_r)}{(p_r - i\omega) . D'(p_r)} e^{p_r t}}_{\text{transient vibration}} \Big\} \quad \text{(A-15)}$$

Similarly, the motion $y_b(t)$ due to the boundary conditions may be found by expanding $Y_b(p)$ in partial fractions. The motion $y_b(t)$ is independent of the exciting force $f_i(t)$ and must be added to $y_0(t)$ if the resulting motion is desired. In many automatic control problems the initial boundary conditions may be neglected; in these cases $y_b(t) = 0$.

The similarity between the coefficients of Eqs. (A-14) and (A-15) is apparent. If the zeros and poles of $G(p)$ are known, it is possible to construct graphically the function $G(i\omega)$ by the methods outlined in Section (IV).

The second term of Eq. (A-15) represents the transient oscillation as a result of the initial disturbance, and the first term represents the remaining vibration after the transient has damped out.

(B) *Limiting Value of* $y(t)$ *as* $t \to \infty$

Another special case that follows from the above expansion theorem is the limiting value of the function $y(t)$ as $t \to \infty$. We note that

$$Y(p) = p/(p - a)$$

for $y(t) = e^{at}$.

When $a = -b \pm i\omega$ where b is a *positive* real number, then

$$\lim_{t \to \infty} e^{at} = \lim_{t \to \infty} e^{-bt} . e^{\pm i\omega t} \to 0$$

and

$$\lim_{p \to 0} p/(p - a) \to 0$$

When the function $Y(p)$ can be expanded by Eq. (A-9) in terms of

$$Y(p) = A_0 + \sum_{r=1}^{n} A_r \cdot \frac{p}{p - p_r}$$

we therefore find that

$$\lim_{p \to 0} Y(p) = \lim_{p \to 0} \left(A_0 + \sum_{r=1}^{n} A_r \cdot \frac{p}{p - p_r} \right) = A_0$$

This is the same as

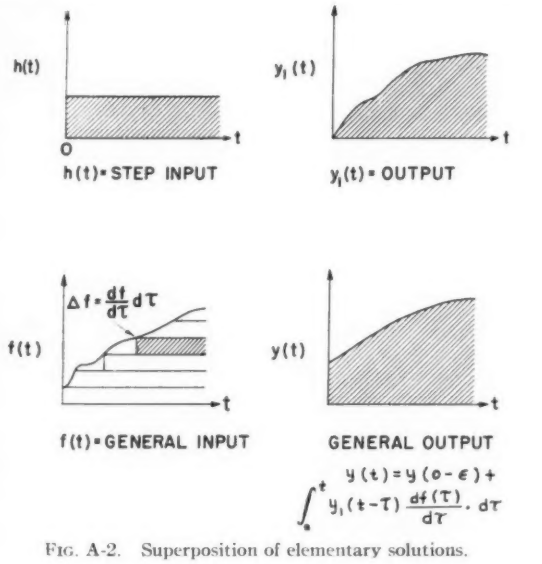

FIG. A-2. Superposition of elementary solutions.

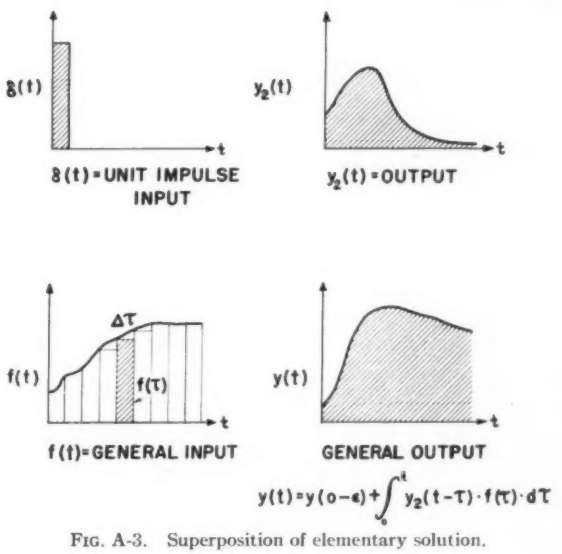

FIG. A-3. Superposition of elementary solution.

TYPE	SHAPE	$y(t)$	$Y(p)$
STEP INPUT AT ORIGIN	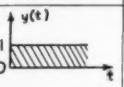	$h(t)$	1
STEP INPUT AT $t = T_1$	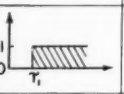	$h(t-T_1)$	e^{-pT_1}
RECTANGULAR PULSE: T_1 TO T_2	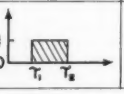	$h(t-T_1)-h(t-T_2)$	$e^{-pT_1}-e^{-pT_2}$

FIG. A-4. Construction of Laplace transforms of a rectangular pulse.

TYPE	SHAPE	$y(t)$	$Y(p)$
LINEAR INPUT STARTING AT $t=0$		$\lambda \cdot t$	$\frac{\lambda}{p}$
LINEAR INPUT STARTING AT $t = T_1$	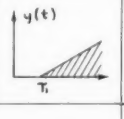	FOR $t < T_1$: $y(t)=0$ FOR $t > T_1$: $y(t)=\lambda(t-T_1)$	$\frac{\lambda}{p}e^{-pT_1}$
	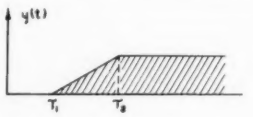	FOR $t < T_1$ $y(t)=0$ FOR $T_1 < t < T_2$ $y(t)=\lambda(t-T_1)$ FOR $t > T_2$ $y(t)=\lambda(T_2-T_1)$	$\frac{\lambda}{p}e^{-pT_1}-\frac{\lambda}{p}e^{-pT_2}$
	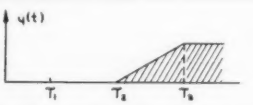	SIMILAR TO ABOVE EXAMPLE	$\frac{\lambda}{p}e^{-pT_2}-\frac{\lambda}{p}e^{-pT_3}$
	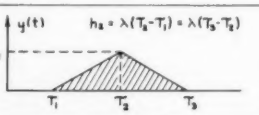		$\frac{\lambda}{p}\left[e^{pT_1}-2e^{-pT_2}+e^{-pT_3}\right]$

FIG. A-5. Construction of Laplace transforms of a triangular pulse.

$$\lim_{t \to 0} y(t) = \lim_{t \to 0} \left(A_0 + \sum_{r=1}^{n} A_r e^{p_r t} \right) = A_0 \quad \text{(A-16)}$$

if and *only if* none of the roots p_r is on the imaginary axis or in the right half plane.

(C) *Singularities*

The method of Laplace transforms presents in a simple manner the response of a system when the input is a unit step function $h(t)$ (Fig. A-1a) or a unit impulse $\delta(t)$ (Fig. A-1b). The latter is the equivalent of a rectangular impulse of amplitude A and duration from $t = 0$ to $t = 0 + \epsilon$ such that the area under the curve is $A.\epsilon = 1$. The width ϵ of the pulse is made shorter, the amplitude larger, such that the product remains constant at 1. The limiting case as $\epsilon \to 0$ represents $\delta(t)$. It will be noted that a step function starting at the time τ will be represented by $h(t - \tau)$ (Fig. A-1c). Similarly, a unit impulse located at time τ will be represented by $\delta(t - \tau)$ (Fig. A-1f).

(D) *Superposition Theorems*

Methods for assembling solutions from these elementary functions are given by the following rules.

(a) A dynamic system has the response $y_1(t)$ as the result of a unit step input $h(t)$ at $t = 0$. If an input $f(t)$ is applied starting at time $t = 0$, then the resulting motion at any time t is

$$y(t) = y(0 - \epsilon) + \int_0^t y_1(t - \tau) \cdot \underbrace{\frac{df(\tau)}{d\tau}}_{\Delta f} d\tau \quad \text{(A-17)}$$

This theorem is obvious by inspection of Fig. A-2. The input force $f(\tau)$ is broken up into a number of horizontal rectangles. Their height is $\Delta f = [df(\tau)/d\tau].\Delta\tau$. The length of time since the initiation of the force increment is $t - \tau$. The resulting motion at time t is the sum of all of the elementary increments.

(b) A dynamic system has the response $y_2(t)$ as the result of a unit impulse $\delta(t)$ at $t = 0$. If an input $f(t)$ is applied starting at time $t = 0$, then the resulting motion at any time t is

$$y(t) = y(0 - \epsilon) + \int_0^t y_2(t - \tau).f(\tau).d\tau \quad \text{(A-18)}$$

This theorem is obvious by inspection of Fig. A-3. The input force is broken up into a number of vertical rectangles of height $f(\tau)$ and width $\Delta\tau$. The effect of each rectangle at time t is $f(\tau)\Delta\tau$ times as much as that of a unit impulse placed at the same point τ. A unit impulse at the point τ corresponds to an "influence function" of unit force at the point τ. The overall effect is the sum of these contributions.

(E) *Construction of Simple Pulse Shapes*

It follows from the definition of the Laplace transform that if

$$p \int_0^\infty y(t).e^{-pt}.dt = Y(p)$$

then

$$p \int^\infty y(t - \tau).e^{-pt}.dt = e^{-\tau p}.Y(p) \quad \text{(A-19)}$$

This relation is useful for finding the transforms of some of the pulse shapes used in the analysis of flight-test data. Figs. A-4 and A-5 illustrate the method of building up response curves in terms of simple singularities.

Appendix (B)

TABLE OF LAPLACE TRANSFORMS

$y(t)$	$Y(p)$	$F(s)$	Equation Reference Number
$e^{\lambda t}$	$p/(p-\lambda)$	$1/(s-\lambda)$	(B-1)
$e^{i\omega t}$	$\frac{p}{p-i\omega} = \frac{p}{p^2+\omega^2}(p+i\omega)$	$\frac{s+i\omega}{s^2+\omega^2}$	(B-2)
$\cos \omega t$	$p^2/(p^2+\omega^2)$	$s/(s^2+\omega^2)$	(B-3)
$\sin \omega t$	$\omega p/(p^2+\omega^2)$	$\omega/(s^2+\omega^2)$	(B-4)
$e^{(-\lambda+i\omega)}$	$\frac{p}{(p+\lambda)-i\omega} = p\frac{(p+\lambda)+i\omega}{(p+\lambda)^2+\omega^2}$	$\frac{(s+\lambda)+i\omega}{(s+\lambda)^2+\omega^2}$	(B-5)
$e^{-\lambda t}\cdot\cos \omega t$	$\frac{p(p+\lambda)}{(p+\lambda)^2+\omega^2}$	$\frac{(s+\lambda)}{(s+\lambda)^2+\omega^2}$	(B-6)
$e^{-\lambda t}\cdot\sin \omega t$	$\frac{p\omega}{(p+\lambda)^2+\omega^2}$	$\frac{\omega}{(s+\lambda)^2+\omega^2}$	(B-7)
$(1-e^{-\lambda t})/\lambda$	$1/(p+\lambda)$	$1/[s(s+\lambda)]$	(B-8)
Unit step: $h(t)$	1	$1/s$	(B-9)
t	$1/p$	$1/s^2$	(B-10)
$t^n/n!$	$1/p^n$	$1/p^{n+1}$	(B-11)
$te^{-\lambda t}$	$\frac{p}{(p+\lambda)^2}$	$\frac{1}{(s+\lambda)^2}$	(B-12)
Unit impulse: $\delta(t)$	p	1	(B-13)

Appendix (C)

THE EQUATIONS OF MOTION OF THE AIRPLANE

The equations of motion of the airplane are

$$\bar{F} = m[(d\bar{V}/dt) + \bar{\omega} \times \bar{V}]$$

and

$$\bar{L} = (d\bar{H}/dt) + \bar{\omega} \times \bar{H}$$

where $\bar{F}$ is the resultant externally applied force due to gravity, the thrust, and the airforces; $\bar{L}$ is the corresponding externally applied torque; $\bar{V}$ is the resultant airplane velocity; $\bar{\omega}$ is its angular velocity; and $\bar{H}$ is its angular momentum.

These equations that were first expressed in moving body axes by Euler (1707–1783) were linearized by Routh[22] with the assumption that the body carries out small perturbations about a mean equilibrium condition. Bryan and Williams (1903)[41] first applied them to study the dynamic stability of an airplane. Bryan expanded this theory in his book (1911) into what is still the classic treatise on the subject.[42] Milliken[59] recently presented an excellent summary of the history of dynamic stability of aircraft, and further review of this topic therefore appears unnecessary at this time.

The resulting equations of the linearized theory are given below—(a) for body axes and (b) for so-called stability axes. The definitions of the terms are given in Figs. C-1 and C-2.

(a) *Body Axes*

(1) Longitudinal equations:

$$m\left[\frac{du}{dt} + U_0\alpha_0\frac{d\theta}{dt} + g\theta\cos\theta_0\right] = \frac{\partial X_B}{\partial\alpha}\alpha + \frac{\partial X_B}{\partial u}u + \frac{\partial X_B}{\partial T}T + \frac{\partial X_B}{\partial\delta_E}\delta_E$$

$$m\left[U_0\left(\frac{d\alpha}{dt} - \frac{d\theta}{dt}\right) + g\theta\sin\theta_0\right] = \frac{\partial Z_B}{\partial\alpha}\alpha + \frac{Z_B}{\partial u}u + \frac{\partial Z_B}{\partial T}T + \frac{\partial Z_B}{\partial\delta_E}\delta_E$$

$$I_Y\frac{d^2\theta}{dt^2} = \frac{\partial M_B}{\partial\alpha}\alpha + \frac{\partial M_B}{\partial(d\theta/dt)}\cdot\frac{d\theta}{dt} + \frac{\partial M_B}{\partial u}u + \frac{\partial M_B}{\partial T}T + \frac{\partial M_B}{\partial\delta_E}\delta_E$$

(2) Lateral equations:

$$m\left[U_0\left(\frac{d\beta}{dt}+\frac{d\psi}{dt}-\alpha_0\frac{d\phi}{dt}\right)-g\,\phi\cos\theta_0\right]=\frac{\partial Y_B}{\partial\beta}\,\beta+\frac{\partial Y_B}{\partial\delta_R}\,\delta_R$$

$$I_x\frac{d^2\phi}{dt^2}=\frac{\partial L_B}{\partial\beta}\,\beta+\frac{\partial L_B}{\partial(d\psi/dt)}\cdot\frac{d\psi}{dt}+\frac{\partial L_B}{\partial(d\phi/dt)}\cdot\frac{d\phi}{dt}+\frac{\partial L_B}{\partial\delta_R}\,\delta_R+\frac{\partial L_B}{\partial\delta_A}\,\delta_A$$

$$I_z\frac{d^2\psi}{dt^2}=\frac{\partial N_B}{\partial\beta}\,\beta+\frac{\partial N_P}{\partial(d\psi/dt)}\cdot\frac{d\psi}{dt}+\frac{\partial N_B}{\partial(d\phi/dt)}\cdot\frac{d\phi}{dt}+\frac{\partial N_B}{\partial\delta_R}\,\delta_R+\frac{\partial N_B}{\partial\delta_A}\,\delta_A$$

(b) Stability Axes

(1) Longitudinal equations:

$$m\left[\frac{du}{dt}+g(\theta-\alpha)\cos(\theta_0-\alpha_0)\right]=\frac{\partial X_s}{\partial\alpha}\,\alpha+\frac{\partial X_s}{\partial u}\,u+\frac{\partial X_s}{\partial T}\,T+\frac{\partial X_s}{\partial\delta_E}\,\delta_E$$

$$m\left[U_0\left(\frac{d\alpha}{dt}-\frac{d\theta}{dt}\right)+g(\theta-\alpha)\sin(\theta_0-\alpha_0)\right]=\frac{\partial Z_s}{\partial\alpha}\,\alpha+\frac{\partial Z_s}{\partial u}\,u+\frac{\partial Z_s}{\partial T}\,T+\frac{\partial Z_s}{\partial\delta_E}\,\delta_E$$

$$I_y\frac{d^2\theta}{dt^2}=\frac{\partial M_s}{\partial\alpha}\,\alpha+\frac{\partial M_s}{\partial u}\,u+\frac{\partial M_s}{\partial T}\,T+\frac{\partial M_s}{\partial\delta_E}\,\delta_E+\frac{\partial M_s}{\partial(d\theta/dt)}\cdot\frac{d\theta}{dt}$$

(2) Lateral equations:

$$m\left[U_0\left(\frac{d\beta}{dt}+\frac{d\psi}{dt}\right)-g\phi\cos(\theta_0-\alpha_0)\right]=\frac{\partial Y_s}{\partial\beta}\,\beta+\frac{\partial Y_s}{\partial\delta_R}\,\delta_R$$

$$I_x\frac{d^2\phi}{dt^2}-I_{xz}\frac{d^2\psi}{dt^2}=\frac{\partial L_s}{\partial\beta}\,\beta+\frac{\partial L_s}{\partial(d\psi/dt)}\cdot\frac{d\psi}{dt}+\frac{\partial L_s}{\partial(d\phi/dt)}\cdot\frac{d\phi}{dt}+\frac{\partial L_s}{\partial\delta_R}\,\delta_R+\frac{\partial L_s}{\partial\delta_A}\,\delta_A$$

$$I_z\frac{d^2\psi}{dt^2}-I_{xz}\frac{d^2\phi}{dt^2}=\frac{\partial N_s}{\partial\beta}\,\beta+\frac{\partial N_s}{\partial(d\psi/dt)}\cdot\frac{d\psi}{dt}+\frac{\partial N_s}{\partial(d\phi/dt)}\cdot\frac{d\phi}{dt}+\frac{\partial N_s}{\partial\delta_R}\,\delta_R+\frac{\partial N_s}{\partial\delta_A}\,\delta_A$$

Since modern aircraft and missiles may take off and climb almost vertically, the previously used assumptions that lift = weight and drag = thrust are no longer generally valid. It is then most convenient to study the dynamic stability at a discrete number of points along the trajectory and to substitute numbers directly into the above equations rather than to transform them in terms of dimensionless coefficients. This method is illustrated in the example, Figs. IV-37 and IV-38.

One of the questions at the present time is still the magnitude of the ratio (nonstationary air force/quasi-steady air force). Studies of this question have been started by Miles[56] and others.[51] For airplanes equipped with autopilots, an exact solution of this problem is not critical, since most of the effective damping is introduced by the autopilot.

A simple similarity analysis of dynamic stability yields some interesting results. Let us consider the simplified pitching equation, writing $\theta = \gamma + \alpha$ where γ = flight-path angle. Then we have

$$I_y\cdot\frac{d^2\theta}{dt^2}+M_q\cdot\frac{d\theta}{dt}+M_\alpha\cdot\theta=M_\alpha\cdot\gamma(t)$$

where

$$I_y=(\rho_m l^3)\cdot l^2$$
$$M_q=C_{M_q}\cdot(1/2)\rho V^2\cdot l^3\cdot l/V$$
$$M_\alpha=C_{M_\alpha}\cdot(1/2)\rho V^2\cdot l^2\cdot l$$

and

ρ_m = mass density of aircraft
ρ = mass density of air
l = a typical length dimension of the airplane

Comparing this equation with the spring-mass-damping system,

$$\frac{d^2\theta}{dt^2}+2\zeta\omega_0\frac{d\theta}{dt}+\omega_0^2\,\theta=f(t)$$

we notice that

$$\omega_0=\sqrt{(1/2)C_{M_\alpha}}\cdot\sqrt{\rho/\rho_m}\cdot\frac{V}{l}$$

and

$$\zeta=C_{M_q}/\sqrt{(1/2)C_{M_\dot{\alpha}}}\,\sqrt{\rho/\rho_m}$$

The dimensionless ratios that we find are the following,

TABLE C-1

Altitude, Ft.	0	10,000	20,000	30,000	40,000	50,000	60,000
$\zeta/\zeta_{sl} = \sqrt{\rho/\rho_{sl}}$	1	0.86	0.73	0.61	0.50	0.39	0.31

(a) Aerodynamic coefficients, C_{M_α} and C_{M_q}, which depend largely upon other dimensionless ratios—angle of attack, Mach Number, Reynolds Number, etc.

(b) Frequency ratio, $F = \omega_0 l/V$.

(c) Damping ratio, $\zeta \approx \sqrt{\rho/\rho_m}$ when the aerodynamic coefficients C_{M_α} and C_{M_q} are constant.

The conclusions that follow are that for dynamic similarity of maneuvers:

(a) $F_0 = \omega_0 l/V =$ constant. This implies that $\omega_0 \approx 1/l$ and $\omega_0 \approx V$.

Thus, a missile 6 in. in diameter flying at 2,000 m.p.h. has a natural frequency approximately 100 times as high as a geometrically similar airplane of 60 in. in diameter flying at 200 m.p.h. Small high-speed missiles represent, therefore, the most difficult autopilot problems. In order to ease the autopilot problems, it is desirable to reduce the static stability coefficient C_{M_α} to as near zero as possible. (See Fig. IV-30, a and b.)

(b) $\zeta \approx \sqrt{\rho/\rho_m}$.

If we compare two identical airplanes, the first at sea level (sl) and the second one at altitude flying at the same dynamic pressure, then the natural frequency ω_0 is the same for both (except for Mach Number effects). The damping coefficient ζ is, however, much less at altitude since $\zeta/\zeta_{sl} \approx \sqrt{\rho/\rho_{sl}}$. This reduction in the damping coefficient with altitude is shown in Table C-1.

Appendix (D)

THE "PIN-BALL METHOD" OF SOLVING HIGH-ORDER ALGEBRAIC EQUATIONS

Evans' root-locus method is essentially a graphical method for solving the frequency equation $D(p) = 0$. This is an algebraic equation, and thus the root-locus method is generally useful for solving high-order algebraic equations. Evans calls the following method the "pin-ball technique" because of its analogy to the well-known game: A new ball (representing a pole) entering upon the scene disturbs all of the other balls (poles) more or less.

Let us illustrate the procedure for simple algebraic equations and follow the previous convention, indicating a root of $D(p) = 0$ by a small circle in the p-plane. A root of $D(p) = 0$ is a pole of the general response $Y(p) = N(p)/D(p)$. The first-order equation

$$D_1(p) = (p + 3) = 0$$

has as its root $p = -3$. This is shown in Fig. D-1a. The second-order equation

$$D_2(p) = p^2 + 3p + \alpha_2 = 0$$

may be written

$$D_2(p) = (p + 3)p + \alpha_2 = 0$$

or

$$[p(p + 3)]/\alpha_2 = -1 = 1e^{i180°}$$

The left-hand side had roots at $p = 0$ and $p = -3$. The root locus is shown in Fig. D-1b for any value of α_2. Suppose $\alpha_2 = 2$; then the magnitude condition is satisfied at $p = -2$ and -1 and

$$D_2(p) = p^2 + 3p + 2$$

The third-order equation

$$D_3(p) = (p^2 + 3p + 2)p + \alpha_3$$

may be written

$$[(p + 2)(p + 1)p]/\alpha_3 = -1$$

The root locus for this case is shown in Fig. D-1c. The values of the parameter α_3 can be easily computed

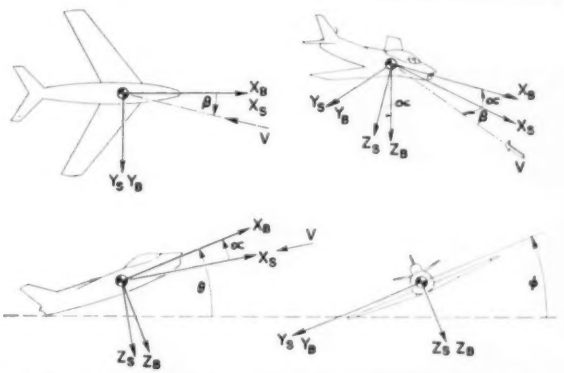

FIG. C-1. Coordinate systems associated with aircraft stability. Subscript B = body axis and subscript S = stability axis.

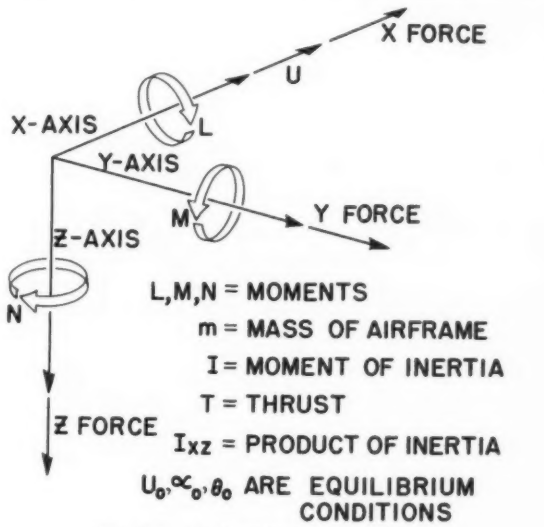

FIG. C-2. Axis system and notation.

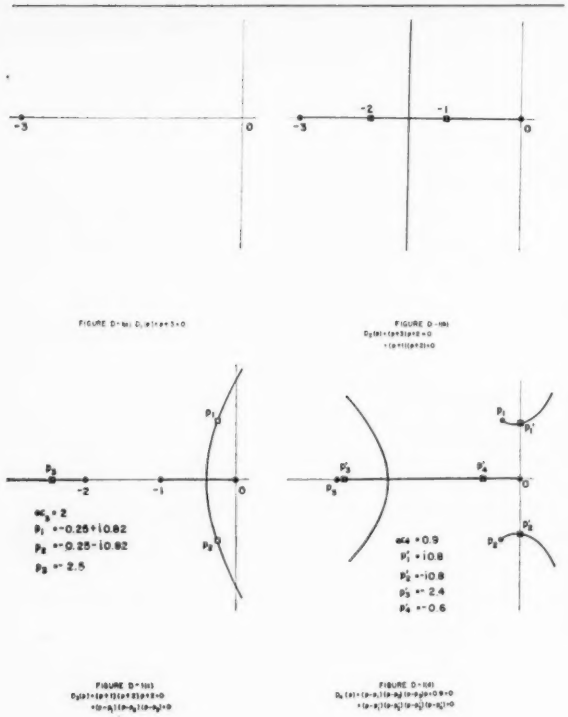

for various points along this locus. At $\alpha_3 = 2$ the roots are $p_1 \cong -0.25 + 0.82i$, $p_2 \cong -0.25 - 0.82i$, $p_3 \cong -2.5$.

This process can be continued. The fourth-order equation

$$D_4(p) = p^4 + 3p^3 + 2p^2 + 2p + \alpha_4 = 0$$

may be written

$$[(p - p_1)(p - p_2)(p - p_3)p]/\alpha_4 = -1$$

The root locus for this case is shown in Fig. D-1d. For $\alpha_4 = 0.9$ the roots are

$$p_1' \cong 0.8i$$
$$p_2' \cong -0.8i$$
$$p_3' = -2.4$$
$$p_4' = -0.6$$

Every time the order of the equation is increased by one, a new pole enters the picture. The effect is to give a displacement to all of the existent poles, the amount of the displacement depending upon the value of the parameter α.

It is convenient to use a similar technique for the study of the motions of coupled systems. Each time a new degree of freedom is introduced, the characteristic determinant has more terms that are combined step-by-step into a single factored term. This procedure is illustrated by the following steps.

(a) The airplane is mounted in a wind tunnel with an axis of rotation permitting a rotation in pitch; the resulting equation of motion is:

$$D_0 = (p^2 + 0.25p + 0.8)\theta = 0$$

The corresponding oscillatory "short period" roots p_{10} and p_{20} are shown in Fig. D-2a.

(b) The airplane is permitted an additional degree of freedom—namely, an up-and-down motion. The resulting equations of motion are:

$$\begin{array}{llll} (p^2 + 0.25p + 0.8)\theta - & & 0.8\gamma & = 0 \\ 0.2 & \theta - (p + 0.2)\gamma & & = 0 \end{array}$$

The expanded form of the characteristic determinant is then:

$$D_1 = -(p^2 + 0.25p + 0.8)(p + 0.2) + (0.2)(0.8) = 0$$

The general procedure is to find the zeros of the sum of two terms by plotting the locus of values of p which make the ratio of the two terms equal to -1. Since the signs of the terms are opposite in this case, the ratio must equal 1, as shown in Fig. D-2b.

One of the roots is at the origin, as can be checked by noting that the constant terms cancel. Denoting the new roots as p_{11} and p_{21}, the determinant can now be expressed as:

$$D_1 = -p(p - p_{11})(p - p_{21})$$

(c) An additional degree of freedom is introduced in that the airplane is permitted to move fore and aft. The new equations of motion are:

$$\begin{array}{llll} (p^2 + 0.25p + 0.8)\theta - & 0.8\gamma + & 0.\ u & = 0 \\ 0.2\ \theta - & (p + 0.2)\gamma + & 0.01\ u & = 0 \\ 0.4\ \theta + & 0.6\gamma + & (p + 0.03)u & = 0 \end{array}$$

This determinant should be expanded by minors about the third column in order that the previous determinant appears as one of the minors.

$$D_2 = (p + 0.03)D_1 - 0.01\underbrace{[(p^2 + 0.25p + 0.8) \times 0.6 + 0.4 \times 0.8]}_{\Delta_2} = 0$$

The second minor Δ_2 is simply a quadratic having zeros s_1 and s_2 and the locus plot for the ratio of the two remaining terms is shown in Fig. D-2c. Note that the phugoid oscillation is introduced by the horizontal degree of freedom but that the short period roots are shifted slightly to p_{12} and p_{22}.

(d) If a rate gyro is introduced to control the elevator and a perfect servo is assumed, the equations of motion are:

$$\begin{array}{llll} (p^2 + 0.25p + 0.8)\theta - & 0.8\gamma + 0.\ u + & C_\delta.\delta & = 0 \\ 0.2\ \theta - & (p + 0.2)\gamma + 0.01u + & 0.\delta & = 0 \\ 0.4\ \theta + & 0.6\gamma + & & \\ & (p + 0.03)u + & 0.\delta & = 0 \\ K_\theta.p\ \theta + & 0.\ \gamma + 0.\ u - & \delta & = 0 \end{array}$$

The expansion of the determinant by minors about the fourth row or column gives:

$$D_3 = (-1)D_2 - C_\delta K_\theta p\underbrace{[-(p + 0.2)(p + 0.03) - (0.6)(0.01)]}_{\Delta_3}$$

Denoting the zeros of the new minor Δ_3 by s_3 and s_4, the root-locus plot versus $K_\theta C_\delta$ as the variable is shown in Fig. D-2d. Selecting $K_\theta C_\delta$ to be 1, the roots are at p_{13}, p_{23}, p_{33}, and p_{43}.

(e) Damping of the phugoid terms can be achieved by introducing elevator control proportional to upward velocity. The resulting equations of motion are then as follows:

$$\begin{aligned}
(p^2 + 0.25p + 0.8)\theta - \quad & 0.8\ \gamma + 0.\ u + C_\delta.\delta = 0 \\
0.2\quad \theta - (p + 0.2)\gamma + \quad & 0.01u + 0.\delta = 0 \\
0.4\quad \theta + \quad & 0.6\ \gamma + \\
& (p + 0.03)u + 0.\delta = 0 \\
K_\theta.p\quad \theta + \quad & K_\gamma\ \gamma + 0.\ u - \delta = 0
\end{aligned}$$

The complete determinant is then:

$$D_4 = D_3 + K_\gamma C_\delta[0.2(p + 0.03) - (0.4)(0.01)]$$

The locus versus K_γ is shown in Fig. D-2e.

The above example, which was worked out for the author by W. R. Evans, shows nicely the effect of various terms upon the roots of the frequency equation and indirectly therefore upon the transient response.

Acknowledgments

I wish to thank my former associates at North American Aviation, Inc., who assisted me in the compilation of this report. Particularly, I wish to thank R. Sohn, J. M. Guthrie, D. D. Myers, D. Gildea, and W. E. Strohmeyer, who provided me with the facts on the aerodynamic control problems during the past decade; W. R. Evans, R. M. Osborn, and J. F. Rentz, who assisted me in the analysis of the servosystems; Dr. N. F. Parker for his help on the flight testing and simulator techniques; and J. R. Moore for his comments on optimum controller design. I also wish to acknowledge helpful discussions with E. J. Horkey and H. A. Storms on some of the aerodynamic problems and with Dr. J. L. Barnes on the theory of "noise."

References

(A) Historical

[1] Lanchester, F. W., *Aerodonetics;* London, Constable and Company, Ltd., 1908.

[2] Turner, C. C., *The Romance of Aeronautics,* pp. 170–171; Seeley, Service and Company, Ltd. (London), 1912.

(B) Automatic Control Systems

[3] Bode, H. W., *Feedback Amplifier Design,* Bell System Tech. Jour., Vol. XIX, p. 42, 1940.

[4] Brown, A. B., British Patent No. 2253, 1871.

[5] Brown, G. S., and Campbell, D. P., *Principles of Servomechanisms;* J. Wiley & Sons, New York, 1948.

[6] Den Hartog, J. P., *Mechanical Vibrations;* McGraw-Hill Book Company, Inc., 1934.

[7] Edlefsen, N. E., *Cybernetics, the Application of a New Science to Problems of Flight Control,* Skyline, Vol. 8, No. 3, August, 1950 (North American Aviation, Inc., magazine).

[8] Engel, F. V. A., and Oldenbourg, R. C., *Mittelbare Regler und Regelanlagen;* VDI Verlag, Berlin, 1944.

[9] Evans, W. R., *Servo Analysis by Locus of Roots Method,* North American Aviation, Inc., Aerophysics Lab. Report 787, November 1, 1948; *Graphical Analysis of Control Systems,* A.I.E.E. Transactions, Vol. 67, pp. 547–551, 1948. (An extensive summary of solutions of control problems by the root locus method is being prepared in book form by Evans and is to be published in 1952.)

[10] Farcot, J., *Le Servo Moteur ou Moteur-Asservi. Gouvernails a vapeur Farcot, Description Theoretique et Pratique;* J. Baudry, Paris, 1873.

[11] Guillemin, E. A., *Communication Networks,* Vols. 1 and 2; John Wiley & Sons, Inc., New York, 1935.

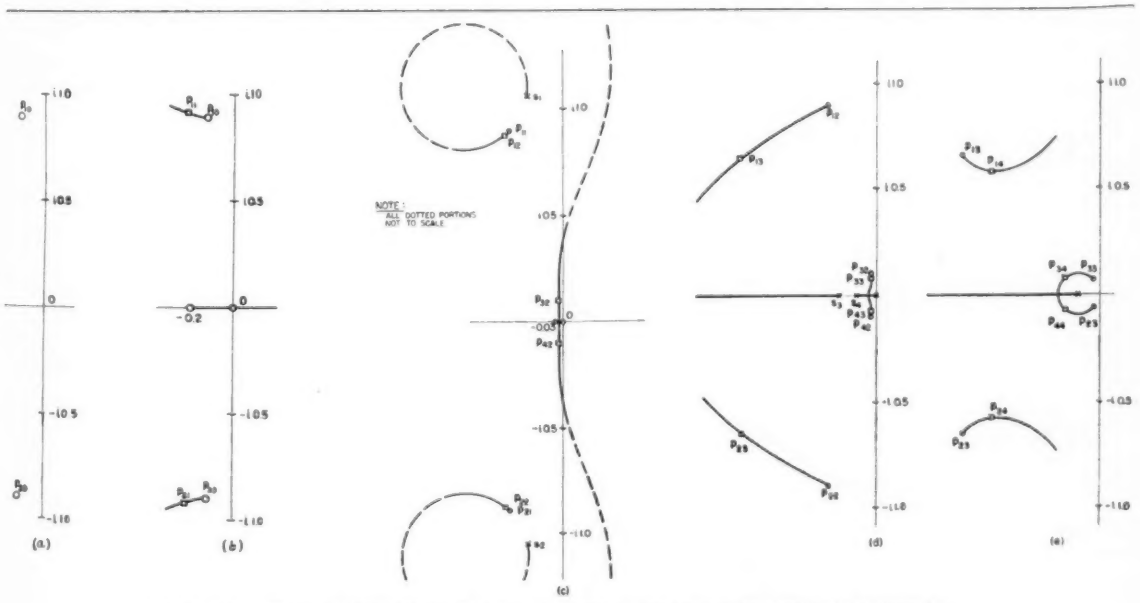

FIG. D-2. Effect of introducing additional degrees of freedom on longitudinal stabilization.

[12] Hall, A. C., *The Analysis and Synthesis of Linear Servomechanisms;* M.I.T. Technology Press, May, 1943.

[13] Hänny, Jost, *Regelung Theorie;* A. G. Gebr. Leemann & Company, Zurich, 1946.

[14] Hazen, H. L., *Theory of Servomechanisms,* J. Franklin Inst., p. 218, 1934.

[15] James, H. M., Nichols, N. B., Phillips, R. S., *Theory of Servomechanisms;* M.I.T. Radiation Laboratory Series, No. 25, McGraw-Hill Book Company, Inc., 1947.

[16] Lincke, F., *Das Mechanische Relais,* Zeitschrift des Vereins Deutscher Ingenieure, pp. 510–524, 578–616, 1879.

[17] Minorsky, N., *Directional Stability of Automatically Steered Bodies,* Jour. Am. Soc. Naval Engineers, pp. 34, 280, 1922.

[18] Moore, J. R., *Combination Open-Cycle Closed-Cycle Systems,* presented at Summer Meeting, Institute of Radio Engineers, San Francisco, August, 1949.

[19] Nyquist, H., *Regeneration Theory,* Bell System Jour., Vol. XI, p. 126, 1932.

[20] Osborne, R. M., *Criteria Relating Steady-State Response to Transient Response of Closed Loop Systems,* presented at Summer Meeting, Institute of Radio Engineers, San Francisco, August, 1949.

[21] Profos, P., *A New Method for the Treatment of Regulation Problems,* Sulzer Technical Review (Winterthur, Switzerland), No. 2, 1945; *Die Behandlung von Regel Problemen vermittels des Frequenzganges des Regelkreises,* Ph.D. Dissertation, Zurich, 1943, A. G. Gebr. Leemann & Company, Zurich, 1943.

[22] Routh, E. J., *Advanced Rigid Mechanics,* 4th Ed.; Macmillan and Company, London, 1884.

[23] Routh, E. J., *Elementary Rigid Mechanics,* 5th Ed.; Macmillan and Company, London, 1891.

[24] Siemens, C. W., *On Uniform Rotation,* Phil. Transactions of Royal Soc. of London, Vol. 156, Chap. 23, pp. 657–670.

[25] Stodola, A., *Die Dampf Turbinen,* 4th Ed., pp. 340–346; Springer, Berlin, 1910.

[26] Tolle, M., *Regelung der Kraftmaschinen,* 3rd Ed.; Springer, Berlin, 1921.

[27] Wünsch, G., *Regler für Druck und Menge;* R. Oldenbourg, Munich, 1930.

(C) Operational Methods

[28] Bush, V., *Operational Circuit Analysis;* John Wiley & Sons, New York, 1929.

[29] Campbell, G. A., and Foster, R. M., *Fourier Integrals for Practical Applications,* Bell System Tech. Jour., B 584, September, 1931.

[30] Carslaw, H. S., and Jaeger, J. C., *Operational Methods in Applied Mathematics;* Oxford, New York, 1941.

[31] Doetsch, G., *Theorie und Anwendung der Laplace Transformation;* Springer, Berlin, 1937.

[32] Gardner, M. F., and Barnes, J. L., *Transients in Linear Systems;* John Wiley & Sons, New York, 1942.

[33] Heaviside, O., *Electromagnetic Theory;* Vol. I, 1893; Vol. II, 1899; Vol. III, 1912; *On Operators in Physical Mathematics,* Proc. Roy. Soc., Series A, Vol. 52, pp. 504–529, 1893; Vol. 54, pp. 105–143, 1894.

[34] Macrobert, T. M., *Functions of a Complex Variable;* Macmillan and Company, 1917.

[35] von Kármán, Theodore, and Biot, M. A., *Mathematical Methods in Engineering;* McGraw-Hill Book Company, Inc., New York, 1940.

[36] Jeffreys, H., *Operational Methods in Mathematical Physics;* Cambridge Univ. Press, 1931.

[37] Pipes, L. A., *Applied Mathematics for Engineers and Physicists;* McGraw-Hill Book Company, Inc., New York, 1946.

[38] Pipes, L. A., *The Operational Calculus,* Journal of Applied Physics, Vol. 10, No. 3, pp. 172–180, March, 1939.

[39] Wagner, K. W., *Einführung in die Lehre von den Schwingungen und Wellen;* Dieterich'sche Verlagsbuchhandlung, Wiesbaden, 1947.

[40] Wagner, K. W., *Operatorenrechnung, nebst Anwendungen in Physik und Technik;* J. A. Barth, Leipzig, 1940.

(D) Applications to Aircraft

[41] Bryan, G. H., and Williams, Proc. Roy. Soc., June, 1903.

[42] Bryan, G. H., *Stability in Aviation;* Macmillan and Company, London, 1911.

[43] Carpenter, P. J., and Paulnock, R. S., *Hovering and Low-Speed Performance and Control Characteristics of an Aerodynamic-Servocontrolled Helicopter Rotor System as Determined on the Langley Helicopter Tower,* N.A.C.A. T.N. No. 2086, 1950.

[44] Cornell Aeronautical Laboratory, *Lectures on Dynamic Stability and Control Evaluation,* November–December, 1947.

[45] Feder, M. S., and Hood, R., *Analysis for Control Applications of Dynamic Characteristics of Turbojet Engine with Tail-Pipe Burning,* N.A.C.A. T.N. No. 2183, September, 1950.

[46] Fossier, M. W., Bratt, R. W., Dill, D. G., *Comparison of Analytical and High-Speed Calculator Solutions of the Lateral Motions of an Airplane Including Product of Inertia Terms,* Journal of the Aeronautical Sciences, Vol. 17, No. 5, pp. 271–277, May, 1950.

[47] Gates, S. B., and Lyon, H. M., *A Continuation of Longitudinal Stability and Control Analysis,* British R & M No. 2027, February, 1944.

[48] Gessow, A., and Amer, K. B., *An Introduction to the Physical Aspects of Helicopter Stability,* N.A.C.A. T.N. No.1982, November 1949.

[49] Hohenemser, K., *A Type of Lifting Rotor with Inherent Stability,* Journal of the Aeronautical Sciences, Vol. 17, No. 9, pp. 555–565, September, 1950.

[50] Imlay, F. H., *A Theoretical Study of Lateral Stability with an Automatic Pilot,* N.A.C.A. Rep. No. 693, 1940.

[51] Jones, R. T., *The Unsteady Lift of a Wing of Finite Aspect Ratio,* N.A.C.A. T.R. No. 681, 1940.

[52] Kuethe, A. M., and Schetzer, J. D., *Foundations of Aerodynamics;* John Wiley & Sons, Inc., 1950.

[53] Kurzweg, *Die Aerodynamische Entwicklung der Flakrakete "Wasserfall,"* A.M.C. Translation Rep. No. F-TS-615-RE, July, 1946.

[54] Lyons, D. J., *Present Thoughts on the Use of Powered Flying Controls in Aircraft,* Jour. Roy. Aero. Soc., Vol. 53, pp. 253–292, 1949.

[55] Meredith, F. W., *The Modern Autopilot,* Jour. Roy. Aero. Soc., Vol. 53, p. 409, 1949.

[56] Miles, J. W., *Quasistationary Thin Airfoil Theory,* Journal of the Aeronautical Sciences, Vol. 14, No. 6, p. 356, June, 1947; Vol. 16, No. 6, pp. 378–379, June, 1949; Vol. 16, No. 8, p. 509, August, 1949; Vol. 16, No. 7, p. 440, July, 1949; Vol. 17, No. 1, p. 62, January, 1950.

[57] Miller, R. H., *A Method for Improving the Inherent Stability and Control Characteristics of Helicopters,* Journal of the Aeronautical Sciences, Vol. 17, No. 6, pp. 363–375, June, 1950.

[58] Millikan, C. B., *Aerodynamics of the Airplane,* p. 153; John Wiley & Sons, New York, 1941.

[59] Milliken, W. F., Jr., *Progress in Dynamic Stability and Control Research,* Journal of the Aeronautical Sciences, Vol. 14, No. 9, pp. 493–520, September, 1947.

[60] Moore, J. R., *Application of Servo Systems to Aircraft,* Aeronautical Engineering Review, pp. 32–43, January, 1949.

[61] Morgan, F. W., *High Speed Aircraft Flying Limitations and Handling Problems,* Jour. Roy. Aero. Soc., pp. 733–738, 1947.

[62] Morgan, M. G., and Thomas, *Control Surface Design in Theory and in Practice,* Jour. Roy. Aero. Soc., 1945.

[63] Mueller, R. K., *An Electrical Device for Solving the Equations of Longitudinal Stability,* Journal of the Aeronautical Sciences, Vol. 3, pp. 158–160, March, 1936.

[64] N.A.C.A., University Conference on Aerodynamics, June 21–23, 1948. (Reprinted by Durand Reprinting Committee, California Institute of Technology, Pasadena 4, Calif.)

[66] Neumark, S., *The Disturbed Longitudinal Motion of an Uncontrolled Aircraft and of an Aircraft with Automatic Control*, R & M No. 2078, January, 1943.

[66] North American Aviation, Inc., *Super Controls of New Sabre, the F-86E, Announced by USAF, North American Skywriter*, Vol. 10, No. 23, November 10, 1950.

[67] Otto, E. W., and Taylor, B. L. III, *Dynamics of a Turbojet Engine, Considered As a Quasi-Static System*, N.A.C.A. T.N. No. 2091, 1950.

[68] Pritchard, H. C., *The Problems of Blind Landing*, Jour. Roy. Aero. Soc., pp. 935–973, 1946.

[69] Rea, J. B., *Dynamic Analysis of Aeroelastic Aircraft by the Transfer Function-Fourier Method*, Journal of the Aeronautical Sciences, Vol. 18, No. 6, pp. 375–397, June, 1951.

[70] Rees, Mina, *The Federal Computing Machine Program*, Science, Vol. 112, No. 2921, December 22, 1950.

[71] Reissner, E., *Effect of Finite Span on the Airload Distributions for Oscillating Wings*, N.A.C.A. T.N. No. 1194, 1947.

[72] Rogallo, F. M., Lowry, J. G., and Fischel, J , *Lateral Control Devices Suitable for Use with Full Span Flaps*, Journal of the Aeronautical Sciences, Vol. 17, No. 10, pp. 629–638, October, 1950.

[73] Schairer, G. S., *Hydrodynamic Longitudinal Stability*, Journal of the Aeronautical Sciences, Vol. 17, No. 8, pp. 513–518, August, 1950.

[74] Seacord, C. L., Jr., *Application of Frequency-Response Analysis to Aircraft Autopilot Stability*, Journal of the Aeronautical Sciences, Vol. 17, No. 8, pp. 481–499, August, 1950.

[75] Seamans, R. C., Blasingame, B. P., and Clementson, G. C., *The Pulse Method for the Determination of Aircraft Dynamic Performance*, Journal of the Aeronautical Sciences, Vol. 17, No. 1, pp. 22–39, January, 1950.

[76] Smilg, B., *The Prevention of Aileron Oscillations at Transonic Airspeeds*, A.A.F. Tech. Rep. No. 5530, December, 1946.

[77] Sponder, E. W., *Investigations of Lateral Stability of a Glide Bomb Using Automatic Control Having No Time Lag*, ZWB Forschungsbericht 1819, May, 1943 (Translated as N.A.C.A. T.M. No. 1248).

[78] Taylor, B. L., III, and Oppenheimer, F. L., *Investigation of Frequency-Response Characteristics of Engine Speed for Typical Turbine Propeller Engine*, N.A.C.A. T.N. No. 2184, 1950.

[79] Vazsonyi, A., *Longitudinal Stability of Autopilot-Controlled Aircraft*, Journal of the Aeronautical Sciences, Vol. 17, No. 7, pp. 399–417, July, 1950.

[80] von Kármán, Theodore, *Seitenwege der Luftfahrt*, Zeitschrift für Motorluftfahrt, 1925.

[81] Walkowicz, T. F., *Dynamic Longitudinal Response of an F-80 Airplane*, Sc.D. Thesis at Massachusetts Institute of Technology.

[82] White, R. J., *Investigation of Lateral Dynamic Stability in the XB-47 Airplane*, Journal of the Aeronautical Sciences, Vol. 17, No. 3, pp. 133–149, March, 1950.

(E) Theory of Noise and Nonlinear Systems

[83] Andronow, A. A., and Chaikin, C. E., *Theory of Oscillations;* (original Russian Edition, 1937), translation by S. Lefschetz, Princeton University Press, 1949.

[84] Lawson, J. L., and Uhlenbeck, G. E., *Threshold Signals;* McGraw-Hill Book Company, Inc., 1950.

[85] Minorsky, N., *Introduction to Nonlinear Mechanics;* J. W. Edwards, Ann Arbor, Mich., 1947.

[86] Kryloff, N. M., and Bogoliuboff, *Introduction to Nonlinear Mechanics;* a free translation by S. Lefschetz, Princeton University Press, 1943.

[87] Shannon, C. E., and Weaver, W., *The Mathematical Theory of Communication;* University of Illinois Press, Urbana, Ill., 1949.

[88] Taylor, G. I., *Diffusion by Continuous Movement*, Proc. London Math. Soc. (2), Vol. 20, pp. 196–212, 1920.

[89] Wiener, N., *On the Representations of Functions by Trigonometric Integrals*, Mathematische Zeitschrift, Bd. 24, H. 3, pp. 575–616, January, 1926.

[90] Wiener, N., *The Extrapolation, Interpolation and Smoothing of Stationary Time Series;* M.I.T. Technology Press, John Wiley & Sons, Inc., 1949.

[91] Wiener, N., *Cybernetics or Control and Communications in the Animal and the Machine;* John Wiley & Sons, Inc., 1949.

Discussions of the Lecture

Preston R. Bassett, President, Sperry Gyroscope Company, Division of The Sperry Corporation: I wish to compliment Dr. Bollay on his most excellent and comprehensive paper. When I say comprehensive, I mean something much greater than what we used to consider the scope of this field. The addition of the two great new zones in aerodynamics—namely, transonic and supersonic—has tremendously increased the complications of stability and control problems. Dr. Bollay's paper is interesting in showing the relationships and the differences of the problems and methods of solution in the three speed fields.

As I have personally been associated with the progress in this field from the time in 1914 when Lawrence Sperry won his first prize for the gyro stabilizer in Paris, I would like to call attention to the changing approaches to this problem which have been made during the 40 years of its history.

When Mr. Sperry was developing the stabilizer from the years 1910 to 1915, his objective was to supply an accessory to the airplane which would make it a more practical device. I mean by this that the stability of the early designs of airplanes had so little margin that it was only the extreme and continuous alertness of the human pilot which kept them in the air. It seemed that some aid was necessary. There were two approaches—Sperry's approach of a gyro accessory and the aerodynamic approach of better stability designed into the airplane itself. During the war years from 1915 to 1920, so much was learned about stability in airplane design that the gyro accessory was found to be nonessential, and inherent stability reached a point where the human pilot could at least relax a little.

But by the late 1920's, airplane performance had improved to the point where the duration of flight and the range of the airplanes were so great that the element of fatigue entered the problem and automatic control again came into the picture—not so much to give improved stability to the craft as to relieve the

pilot from long continuous hours of playing servomotor. I think that Wiley Post's flight around the world alone in 1933 with an automatic pilot first demonstrated the advantages of automatic flight from the fatigue point of view.

Both military and air transport planes have used automatic flight to considerable extent from that time on. But up to World War II, automatic flight consisted of two parts: (1) any design of airplane built for human control and (2) an added accessory called an automatic pilot. During World War II, with the increased performance and speed of the military planes plus the increased demand for accuracy of the flight control, a new concept became necessary, and that was the treatment of the aerodynamic plane, its control system, and the automatic flight controller as a single system. Great progress has been made along this line during the past ten years. I highly endorse the statements that Dr. Bollay has made throughout his paper of the importance of the control designers' and the airplane designers' working more closely together and treating their problem as a single overall system.

When it comes to problems in the transonic and supersonic and those of guided missiles, we have reached the point where automatic controls have become such an integral part of the unit that it would be quite foolish to design one portion without relation to the others, and, in guided missiles, the human element has already dropped out of the picture.

It is interesting to note, therefore, that we have more or less completed a cycle in the field of automatic control and are back to the original objective of increasing the stability and improving the control of the entire aerodynamic unit. This time, however, the function has become vital—it is here to stay.

Dr. Bollay's paper is impressive in pointing out the numerous analytical methods of approach to the complicated problems. I wish to comment on a few specific points that Dr. Bollay mentions in his paper. He predicts that the future interceptor will carry out automatically all the necessary functions in interception, with the pilot's job being that of switching from one phase to the next. We agree with this and would call attention to the fact that in our automatic instrument landing approach this system of having the human pilot switch from phase to phase is already in successful use. The so-called "push button" flight of the Air Force from the United States to England in 1947 was also a demonstration of these possibilities.

Dr. Bollay comments on the importance of aeroelasticity in automatic control. Mention is made of F80. In our experience in controlling the F80 automatically, we have not run into aeroelasticity troubles, but, in larger high-speed planes, the effects may be serious. We might add that although aeroelasticity usually makes the control system problem more difficult, in some cases it does provide an advantage; for example, the twist of wings which varies with speed and altitude and is in a direction to reduce control effectiveness, may be used to minimize the need for gain changes under varying flight conditions of speed and altitude.

On this point it might be mentioned here that the big problem in automatic control at present is the design of a system that will work under all flight conditions with widely changeable parameters. This is analogous to the aerodynamic problem of designing a plane that flies at high speed and is capable of landing at low speed.

Dr. Bollay comments upon the use since 1940 of the techniques devised by electrical engineers for the analysis of automatic control systems, such as the work of Nyquist and Bode. This is important, and it can be pointed out that, although these methods might be somewhat new to the majority of aeronautical engineers, they were first extensively used in the design of fire-control equipment, then later applied to automatic airplane control.

Dr. Bollay gives a description of the use of analog type simulators in the solution of automatic control problems. Examples are given based upon the use of the Reeves type computer. This has been an outstanding improvement in the technique of pretesting control systems. It is interesting to note, however, that prior to electronic analog computers, similar studies were made by a mechanical analog we called a synthetic airplane.

It might be mentioned that a simulator solution is only as good as the data used and is only as informative as the questions asked of it. In the past, the use of simulators has been limited by the knowledge of aerodynamic parameters. Even with the data fully known, it is necessary for the full use of a simulator for the engineer to have such imagination and experience as to be able to anticipate all the conditions that might occur in flight and to be able properly to define them in mathematical form.

Dr. Bollay mentions a method of open-cycle control which improves automatic control. As an example, he states that the yawing motion due to rolling angular velocity can be compensated open cycle by anticipating the rolling rate that will result from application of a given aileron deflection and calling for a proper amount of rudder deflection to eliminate the yawing moment resulting from such a roll rate. This has been used for some time in our own automatic pilots by a simultaneous introduction of aileron and rudder signals to initiate a coordinated turn.

Dr. Bollay mentions among the future problems the automatic control of helicopters. Great progress has been made on this problem during the past year, and I can state that the solution of the problem has proven much easier than anticipated.

Philip Colman, Chief Aerodynamics Engineer, Lockheed Aircraft Corporation: Dr. Bollay is to be complimented on an excellent summary of where we have been and where we are going in the research and application of the science of stability and control. There is little one can criticize or add to such a complete treatment of the subject. I do have a reaction, however, which results from the title of Dr. Bollay's paper, which could be slightly altered to say: "We are gradually abandoning aerodynamic stability and becoming dependent on automatic control."

In the past we have "pulled little tricks" to improve what we could produce in the basic aerodynamic stability and control aspects of our airplanes. These "tricks" included such items as:

(1) Aerodynamic balance and geared balance tabs to tailor aerodynamic hinge moment to a desired variation.

(2) Flying tabs for pilot actuation which could float the major control surfaces to the desired position.

(3) Spring tabs to incorporate the benefits of balance and flying tabs by a mechanical spring relationship for airplanes with increased flight-speed range.

(4) Variable mechanical advantage control systems to utilize the favorable hinge moments in a differential aileron control system or to take advantage of the difference in required elevator or rudder surface angular positions required at low and high speeds.

(5) Surface "bungees" to create a constant mechanical spring hinge moment to be balanced by a variable aerodynamic hinge moment to attain apparent level flight longitudinal stability or proper lateral "feel."

(6) Control system "bob weights" to simulate the favorable mechanical hinge moment of the "bungee" with the added apparent stability in accelerated maneuvers.

Our schemes have expanded with the incorporation of boosted control systems. These presently incorporate proportional control "feel" in the majority of systems, but the trend toward irreversible systems with "synthetic feel" is clearly discernible. Thus, it is only one more step to the fully automatic control system in which the pilot only monitors the mechanical brain.

The dynamic stability problems became manageable several years ago when we perfected the aircraft designed to fly at half the speed of sound. These aircraft encouraged the establishment of dynamic stability criteria, which we are presently finding increasingly difficult to meet on the newer "improved" airplanes. Our troubles stem from: (1) increased flight-speed range; (2) increased flight-altitude range; (3) smaller wings—higher wing loading; (4) revised wing shapes, changing the relationships of the fundamental aerodynamic parameters; (5) reduced effective aspect ratios and redistribution of airplane weight components increasing the importance of inertia factors; (6) variations in aerodynamic parameters in the transonic range; and (7) markedly increased flexibility of airplane structural components.

Thus, aerodynamic stability is deteriorating and automatic control is becoming increasingly necessary. We must now learn to pull "big tricks" with automatic control to attain the ability to fly at higher speeds and under more adverse conditions than we have presently been forced to operate under.

Harry J. Goett, National Advisory Committee for Aeronautics: The Institute is to be commended both for its timely choice of subject for the Fourteenth Wright Brothers Lecture and for the selection of a man uniquely qualified to discuss the subject. Dr. Bollay's coherent synthesis of the concepts and methods from at least three fields—aerodynamics, servomechanics, and electrical engineering—will be most useful to the aeronautical engineer in his attempt to understand the problems of the expanding field of automatic control of aircraft.

In his introduction, Dr. Bollay remarked that the airplane is going through a period of transition because of its increase in speed and the resort to powered and automatic controls. It also became evident, as the talk progressed, that the aeronautical engineer engaged in the field of stability and control is going through a transition. He is being called upon not only to master more complex mathematical tools, but also to take for his own the techniques and methods of the servo designer and the electrical engineer. In this process, there is the danger of losing a grasp of the manner in which the various parameters influence the physical behavior of the final airplane-autopilot combination. This situation promises to get worse rather than better as the added complexities of nonlinearities or added degrees of control are introduced. It is interesting to note that one of the factors of importance in Dr. Bollay's evaluation of the various methods of analysis and synthesis is the degree of insight they give as to the importance of the parameters involved. Incidentally, in this regard, an aerodynamicist finds some consolation in Dr. Bollay's comment that there appears little reason to introduce a concept of decibel per octave into the aeronautical dynamics literature.

Dr. Bollay's remark that in the use of Routh's criterion one loses insight into the physical behavior as the various parameters are changed deserves comment. Somewhat of an extension of this method is the construction of stability boundary charts that, in the past, proved useful in the analysis of unregulated aircraft and which are proving equally useful at the present time in the analysis of automatically controlled aircraft. The advantage of using these charts is that, in addition to having the stability boundaries defined in two of the important system parameters, such as control gearing and static margin, it is possible with

little extra computation to superimpose grid lines of constant damping and constant period. The presentation of all this information in the form of one compact plot is advantageous in many ways, and to produce this information using the root-locus or any of the frequency-response methods would require much more time and effort. The necessity of "translating" the meaning of points on the p-plane to points on the t-plane is also eliminated. Of course, the other methods have their own peculiar advantages, as pointed out by Dr. Bollay, and the relative merit of the various methods depends on whether they are being used to analyze or synthesize a system.

Possibly an even more basic question than the foregoing is that relating to just what physical behavior is desired of the airplane-servo combination beyond the obvious requirement of stability. The phrase "optimum airplane-autopilot combination" is frequently used, but I personally have never encountered any quantitative definition of this "optimum." The analysis techniques permit assessment of various performance criteria of which the following four appear to be the most significant: (a) speed of response, (b) steady-state error, (c) time to damp, and (d) amount of initial overshoot. Any numbers that have been assigned in regard to these characteristics have come from functional requirements in fields other than that of aircraft control and, therefore, are deserving of renewed scrutiny. The situation we find ourselves in reminds me somewhat of that which existed around 1935 in regard to static stability requirements. We knew then that we wanted a stable slope of C_M vs. C_L, but, beyond that, the aeronautical engineer had to select his own requirements as to the magnitude of such quantities as stick force per g or stick force variation with speed. This vagueness was finally resolved by the development of "flying qualities requirements" pioneered by the work of Soulé and Gilruth of the N.A.C.A. and eventually adopted by the Services.

The parallel to our present situation in the airplane servo field is obvious. We need a more explicit appreciation of the relation of the several oscillation characteristics previously mentioned to the ultimate function of the servo-controlled airplane. In asking for this, I realize that the human pilot, whom we previously considered the somewhat variable and temperamental quantity to be satisfied, is relatively uniform when compared to the wide variety of functions that the servo-controlled aircraft will be asked to perform. The question is, therefore, how long do we have to remain in this stage of somewhat intuitively adjusting the rates of response, overshoot, or time to damp of our airplane-servo combination, after which we wait for the final judgment on the basis of such things as miss distance or compatibility with associated radar or automatic computer equipment as determined by actual flight tests.

W. F. Milliken, Jr., Manager, Flight Research Department, Cornell Aeronautical Laboratory, Inc.: The subject of this year's Wright Brothers Lecture is obviously one of considerable scope. The speaker has chosen to focus primarily upon the analytical aspects of dynamic analysis or what is commonly referred to as servomechanism theory. It is important that this material become a part of the tools of the stability and control designer, for many of his problems are no longer completely solvable by aerodynamic means alone. The paper serves to point this up in a timely manner, and Dr. Bollay is highly deserving of congratulations.

It is indeed fortunate, as the speaker points out, that these mathematical methods have been available to us from the electrical engineering field and that we have been saved from a large part of their development. There are, however, unique areas for research which the aeronautical profession itself must pursue if it is to be able to wisely and economically avail itself of what the servomechanist has to offer. These areas evolve around two items: (1) the rational determination of the extent to which servomechanisms are desirable and necessary for a given operational situation and (2) the determination of the aerodynamic transfer functions.

Present applications of servomechanisms to aircraft divide into those whose primary function is to improve the handling qualities of the manually flown aircraft and those in which fully automatic control is provided. While it is easy to envision completely automatic control from take-off through landing, it should be noted that such "push button" operations are seriously lacking in tactical flexibility. For many problems, the partial use of servomechanisms in the form of artificial stability and control will be the better solution. The full implications of artificial stability, of which the rate damper on the yaw axis is but one example, are yet to be realized. By such means, it appears practical to eliminate the Dutch roll, the spiral instability, and the phugoid modes of the conventional airplane and replace them with highly damped subsidences. Such an aircraft—in no wise programmed or in any way confined in its operational use—may greatly influence our philosophy in the combining of servomechanisms with air frames.

With regard to the aerodynamic transfer functions, they are vitally important, since our ultimate objective is the control or stabilization of aerodynamic devices through the characteristics and limitations of aerodynamic flight controls. The still incomplete knowledge of these aerodynamic quantities remains as a stumbling block in systems analyses. It may be in order to supplement the author's excellent introduction to these matters by a statement of "where we stand" in this country in relation to the determination of aerodynamic transfer functions.

Response methods have been devised which determine in flight the aerodynamic transfer functions, and appropriate analysis schemes are available for extracting the derivatives. Rather complete measurements have been made on several moderately rigid aircraft and have shown the practical equivalence of transient and steady-state oscillation testing. A variety of types of transient inputs have been tried, and the optimum—if such exists for a given situation—is yet to be determined. The measurements have now extended on manned aircraft to high subsonic Mach Numbers, with a small amount in the trans- and supersonic regime, some information here being available from missiles. Some work is under way on large flexible aircraft.

The full-scale flight methods now yield repeatable data, and, while a considerable degree of reliance may be placed upon them, they are not simple to obtain. Neither can the methods be said to have reached routine use. Theory and experiment by no means exactly agree, even in the subsonic range, and the evidence is that the theory may not adequately take into account all of the physical facts. At any rate, much solid research remains to tie up the loose ends.

The question of the importance of nonstationary flow effects is still under much discussion and some investigation. The best experimental evidence indicates that these effects may not be nearly so great as the two-dimensional theory earlier indicated. The only comprehensive three-dimensional theoretical treatment agrees well with experiment in showing the minor effects of nonstationary flow to high subsonic Mach Numbers. By all means, let us hope that these effects are negligible in normal stability and control problems.

Some evidence exists that the dynamic downwash effects for both rigid and flexible airplanes need much more investigation. Experimental measurements are required on the amplitude and phase of the downwash.

The necessity for more research on the responses of aeroelastic aircraft, which the author mentions, needs greater emphasis. This experimental work should go far in orienting theoretical effort and, at the same time, should have immediate usefulness in connection with servomechanism applications.

All of the transfer functions referred to above are for control surface inputs, and only recently has any appreciable work been undertaken in the response due to gust inputs. A method for determining in flight the frequency response in phase and amplitude to a gust input is required. Certainly continued research on the application of statistical methods to this problem is in order.

Groundwork, leading to the stabilization of helicopters, which the author mentions as a future automatic control application, is in fact well under way. An appreciable number of full-scale dynamic responses to impulsive inputs has been determined and is now available. These should be usable for some purposes immediately, though they may well defy detailed analysis to the derivatives.

For at least one research airplane, a sizable body of transfer data is available from stalled flight, and an automatic control is being devised to fly in the stalled regime.

There is a great need at the present time for the development and general adoption of new wind-tunnel techniques for the determination of transfer functions and derivatives using ordinary nondynamically similar models of good size. The flight methods should be used as a basis of development of dynamic wind-tunnel balances, so that more complete dynamic data can be made available in the design stages.

Little aerodynamic information is available for missiles at large displacements relative to the air stream. Here, nonlinearities will doubtless be encountered, and, as the author points out, we may well expect that nonlinear mechanics will come in for much research in the future.

Allen E. Puckett, Head, Missile Aerodynamics Section, Hughes Aircraft Company: The paper presented by Dr. Bollay has pointed out most clearly that the science of controlling and stabilizing aircraft is in a transition phase—the transition from manual control using human intelligence and muscles to various degrees of automatic control using electrical and mechanical brains and muscles. This comprehensive and detailed survey of the subject will demonstrate to the engineer the nature of this transition and will form an excellent basic catalog of the types of new problems which are now being encountered. Moreover, it provides a description of most of the new tools and techniques that are being used in the solution of these problems, with particular emphasis on the vocabulary of the communications and servo engineers. This is a timely and forceful reminder that the aeronautical engineer must apply these methods in conjunction with his aerodynamic analyses.

The most important reason for this transition can be described in terms of time constants. The important time constants in the dynamic performance of an airplane are various natural periods and damping times. As Dr. Bollay has shown, these vary inversely with velocity. The pilot, manually controlling an aircraft, can be regarded as a servomechanism with rather long time constants and also limited ranges of gain factors. At high velocities, the aerodynamic time constants may become short compared to the pilot time constants; moreover, the required range of control system gains may vary by factors larger than the pilot can accommodate. An automatic control system, for at least some functions, then becomes inevitable.

It appears, incidentally, that an important possibility in the study of dynamic stability of manually con-

trolled aircraft may have been largely neglected. Dr. Bollay observed that the study of dynamic stability in the past has occupied a relatively academic position because of the artificial character of the boundary conditions imposed—controls fixed, controls free, or various other conditions. Stated another way, the real artificiality is in the omission of the pilot as an essential feedback element in the closed-loop system; the real "dynamic stability" of the aircraft depended upon the pilot's ability, or lack of ability, to react. For example, one of the classical modes of oscillatory longitudinal motion is the slow "phugoid" oscillation, which is usually highly undamped. The pilot, as a servosystem, eliminates this oscillation so easily that he is hardly aware of it. Several other types of "instabilities," such as the "Dutch roll," or the spiral mode, may exist without appreciably affecting the "flying qualities" of an airplane if the time constants are sufficiently long. The definition of satisfactory dynamic stability, or "flying qualities" of an airplane, has, in the past, depended upon a highly empirical correlation of pilot reaction or opinion with the "open loop" dynamics of the aircraft.

There appears to be no reason why a complete closed-loop stability analysis of the manually controlled airplane could not be made for at least some of the simple modes of motion. The pilot would be represented by a servosystem with particular reactions and time constants to signals such as changes in air speed, normal and lateral acceleration, etc. By making a reasonable representation of an "average" pilot, the actually dynamic characteristics of a particular plane could be investigated, or, for a particular airplane, the necessary pilot gains and time constants required to achieve certain specified dynamic behaviors could be calculated and used to describe the "flying qualities" of the airplane. This is only one step beyond the specification of some of the steady-state pilot responses, such as stick force or stick motion per g.

The introduction of the automatic control system, particularly in pilotless aircraft, points up another basic change in our philosophy of aircraft control. The pilot was not only an essential part of the control system but also of the guidance system. Having rather clearly understood, but never too formally defined, capabilities, he could respond to certain types of information. Even modest departures from a conventional presentation and processing of this information, as, for example, in the question of the I.L.S. versus the G.C.A. type of landing systems, can cause badly nonlinear reactions at first. With the automatic control system, the whole question of what guidance information is presented and how it is processed becomes completely open and, moreover, becomes an integral part of the control and stability problem. Therefore, the aerodynamicist must consider the guidance system together with the control system in making a complete dynamic analysis.

We must indeed express our congratulations and appreciation to Dr. Bollay for this comprehensive presentation of topics and techniques with which the aeronautical engineer must now rapidly become familiar.

George S. Schairer, Staff Engineer, Aerodynamics and Power Plant, Boeing Airplane Company: Dr. Bollay, in this Wright Brothers Lecture, has completely and concisely summarized the basic facts related to the servo-loop problem in aeronautics. This is timely and important, and I would like to suggest that this lecture marks the official point at which the fundamental understanding of this knowledge becomes a necessary tool of the aeronautical engineer and the aerodynamicist in particular.

As one who has worked in this field over 8 years, I am glad to be able to tell the uninitiated that after an initial struggle with the subject, a fairly good understanding of the problem can be reached which requires little further reference to the more complicated equations. The fundamental conceptions are of vital importance and must be learned.

This subject is still new, and many years will be required before a mature view of its relationship to aeronautics can be evolved. Since much of the background material originated with the electrical engineer, we find the literature filled with electrical terminology and mathematics. We also find a strong tendency to solve all servo-loop problems with electrical gadgets. The next step is towards hydraulic servomechanisms. The step after this appears to be a return to aerodynamic servos. With time, we will find simple solutions to most of the problems that we now solve with complicated mechanisms. The understanding of these solutions will not be simple, but the devices almost certainly will be simple. It is doubtful whether we can count on any of the complicated mechanisms to accomplish any large percentage of our first-order vitally important tasks. Complicated devices are not that reliable yet.

After digesting the straightforward linear theory, we will most always find that the actual solution of a problem is only started when we have solved those problems that the simple linear theory treats. Nearly every problem involves a number of important nonlinearities. The most common ones are aerodynamic dead spots, static friction, and slop in our mechanisms. There are ways to get around or minimize many of these problems, and theoretical treatments are useful. However, we will spend a great deal of time on practical cut-and-try solutions of these problems.

Much effort in automatic stability has been directed toward the directional stability problem. The paper by R. J. White published in the March, 1950, issue of the JOURNAL OF THE AERONAUTICAL SCIENCES,

"Investigation of Lateral Dynamic Stability in the XB-47 Airplane," presents the problem and an electromechanical solution to the problem. The effort along this line has been continued with studies of other solutions to the same problem. A number of years ago aerodynamicists became aware of the large amount of directional stability which was being lost with trailing rudders. This resulted in the use of rudders with small trailing tendencies or even leading tendencies. This was followed by a bad epidemic of directional oscillations. A large percentage of these cases was caused by rudder movement of leading rudders. A recent attempt has been made to solve the directional damping problem by the use of a strongly trailing rudder, wherein the rudder moves to reduce the static stability but increases the damping of the directional oscillation. Such a rudder was tried on a Boeing 377 stratocruiser. The rudder was made to trail strongly through neutral and to thereby wash out about half the basic directional stability of the vertical tail. This trailing action was sufficiently damped by aerodynamic forces to give a phase shift to the rudder motion and thus an increase in damping. The response of the airplane to gusts appears to have been materially reduced by the reduction in directional stability, and the damping of the ensuing oscillation was greatly increased. The period of the motion was also increased. This is an example of how the basic servo-loop theory can be used to solve a problem by simple means. Before leaving this, it would be well to mention that this solution does not appear to be a general solution to the directional oscillation problem and will not work in many cases. The theory given by Dr. Bollay can be used to separate the workable cases from the unworkable ones.

I hope that the aerodynamic educators of this country will take note that this subject has been added to the required list. This will not make their task any easier but is necessary just the same. Many of us were students of Prof. Stark Draper at M.I.T. during the period when he was first adding the fundamentals of this subject to his courses. We all feel that his leadership in this field has been outstanding and should be recognized.

R. C. Seamans, Jr., Professor, Department of Aeronautical Engineering, Massachusetts Institute of Technology: In the late thirties, Dr. Bollay was at Harvard University, and I was fortunate to be one of his students. Therefore I am not in the least surprised to find that his discussion of aerodynamic stability and automatic control is up to date, interesting, and especially thorough. I feel that this lecture will serve as a standard reference for aeronautical engineers in the field of stability and control. I would like to take this opportunity to congratulate Dr. Bollay and to make several observations that occurred to me while listening to his address.

In this paper, the transformation into the complex domain is carried out by use of equation $Y(p) = p\int_0^\infty e^{-pt}\, Y(t)\, dt$. This transformation is equal to p times the conventional Laplace transform used in standard textbooks. Dr. Bollay includes the p so that the transformed quantity will have the same dimensions as the original quantity in the time domain. I feel that this argument hardly justifies the added complication of the extra term and the confusion that will arise out of the lack of uniformity between the transforms listed in this paper and those found in most textbooks.

It is stated in this paper that control engineers prefer an airplane that is approximately neutrally stable. The advantage of such an airplane is that it can be made maneuverable even with a low elevator effectiveness, since its static stability is low. However, if a small elevator displacement gives a large angle of attack, it is impossible to limit a maneuver with stops on the elevator servo drive. Automatic limiting is required as a function of either angle of attack or normal acceleration. It is felt that this problem is sufficiently important to warrant thorough study by some research agency.

By means of dimensional analysis, Dr. Bollay develops a relationship between the natural frequency of a missile and an airplane. He concludes that the missile has 100 times as large a natural frequency in the longitudinal mode. This figure, although possible, is not representative. When comparing the longitudinal responses, the important linear dimension is the length, not the diameter. In addition, the speed ratio is larger than is ordinarily encountered. For this reason it is felt that a natural frequency ratio of between 10 and 20 is more likely to be experienced.

Dr. Bollay outlined the four steps required when developing a control system for an airplane. These four steps are: (1) theoretical design, (2) simulation, (3) flight test, and (4) refinements based on fundamental noise studies.

These four phases overlap one another on a chronological basis. For example, as a result of flight test, the dynamic performance of an airplane may be found different from that predicted by theoretical and wind-tunnel considerations. When this is the case, the theoretical design of the control system must be modified, and consequently step (1) may depend on step (3).

Also, when the automatic control equipment is undergoing flight test, it is highly desirable to check the flight results against simulator results so that valuable flight time is not wasted. One highly satisfactory procedure involves the use of a high-speed electronic simulator. This simulator is a combination of the straightforward type and the electronic integrating type mentioned in Dr. Bollay's paper. It

(*Continued on page 640*)

A Limiting Case for Missile Rolling Moments

ERNEST W. GRAHAM*

Douglas Aircraft Company, Inc.

SUMMARY

Missile rolling moments are studied by linearized theory for the limiting case in which infinitely many wings are symmetrically arranged around a circular cylinder.

This case is physically interesting when interference effects prevent the rolling moments from getting too far out of the range of those practically obtainable with a finite number of wings. Mathematically, the limiting case is convenient because it can be analyzed through knowledge of the rate at which angular momentum is being added to the air, the rolling moment being proportional to this quantity.

The analysis is independent of Mach Number, and, since there are few restrictions on the geometry of the system, it should furnish an upper limit for rolling moments for a variety of configurations and flight speeds. Many cases with a finite number of wings are difficult to analyze, and knowledge of a limiting value may help in checking intermediate cases.

For a delta wing system with leading edges on the Mach lines, body of zero radius, and each wing acting as an aileron, the rolling moment coefficient for an infinite number of wings is π times that for the planar wing and 1.85 times that for the cruciform wing. For *narrow* delta systems, the above values apply exactly for the planar case and approximately for the cruciform.

Wing-tail interference effects on aileron rolling moments may also be studied for the limiting case. Here, all angular momentum is removed from the disc corresponding to the maximum cross section of the tail (unless opposite surfaces of the tail are designed to "float" relative to each other and are controlled only through the sum of their displacements). If the tail disc is as large as the wing disc, then no resultant rolling moment is produced by wing ailerons in the limiting case. This assumes the discs to be concentric. For a lifting wing, the effective displacement of the disc centers might introduce important nonlinear effects.

Damping in roll can be studied by assuming the wing angle of attack proportional to the radius. Equating the damping moment to the aileron moment gives an equilibrium rate of roll which may be expressed as the ratio of tip helix angle to aileron displacement angle. For the delta wing system previously considered (with sonic leading edges), this ratio decreases as the number of wings increases. For an infinite number of wings, the ratio is two-thirds of the planar value or 0.73 times the cruciform value. For a given aileron displacement, the equilibrium rate of roll is therefore *decreased* by increasing the number of wings. Physically, this corresponds to the fact that interference effects on damping in roll are less than on aileron rolling moments. The above figures are *approximately* correct for *narrow* delta systems.

INTRODUCTION

IN MISSILE DESIGN, the wing surfaces do not necessarily lie in a single plane but may, for example, be given a cruciform arrangement. The analysis of such systems is more difficult than the analysis of planar systems, and for this reason it is desirable to consider a limiting case in which infinitely many wings are symmetrically arranged around the body axis. This case is of physical interest because interference effects may limit the rolling moments to values not too greatly exceeding those for the cruciform narrow delta wings.

DEVELOPMENT*

Procedure

The rolling moment acting on a wing is ordinarily determined by finding the spanwise lift distribution and integrating the rolling moment contributions of all the differential elements of span. Alternatively, the rolling moment acting on the wing may be obtained from a knowledge of the rate at which angular momentum is being added to the air, as shown in Eq. (1).

$$M_R = \int_0^\infty \int_0^{2\pi} \rho u V_\theta r^2 \, d\theta \, dr \qquad (1)$$

where

M_R = rolling moment
ρ = mass density of the air
u = axial velocity of the air
V_θ = tangential velocity of the air about the rolling axis
r = radius out from the rolling axis
θ = angular displacement about the rolling axis

The integral is taken in a plane behind the wing and normal to the flow direction. Fig. 1 shows the coordinate system and type of problem being considered.

Eq. (1) can be obtained by applying a general momentum theorem[1] stating that in a steady flow the moment exerted on the surfaces bounding a region fixed in space is equal to the net rate of flow of angular momentum out of the region. If the region is chosen to be that between two planes normal to the flow direction, one ahead of and one behind the wing, then Eq. (1) is obtained, since no net angular momentum flows through the upstream plane and the only moments acting on the bounding surfaces are those contributed by the wing itself.

Eq. (1) may be written as

$$M_R = \int_0^\infty \int_0^{2\pi} (\rho_0 + \Delta\rho)(u_0 + \Delta u) V_\theta r^2 \, d\theta \, dr \qquad (2)$$

Presented at the Supersonic Aerodynamics Session, Nineteenth Annual Meeting, I.A.S., New York, January 29–February 1, 1951.

* Aerodynamics Consultant, Santa Monica Plant.

* Valuable contributions have been made by Drs. P. A. Lagerstrom and Z. O. Bleviss, of the California Institute of Technology, and by Harold Luskin, Aerodynamics Research Engineer, Douglas Aircraft Company, Inc., Santa Monica Plant.

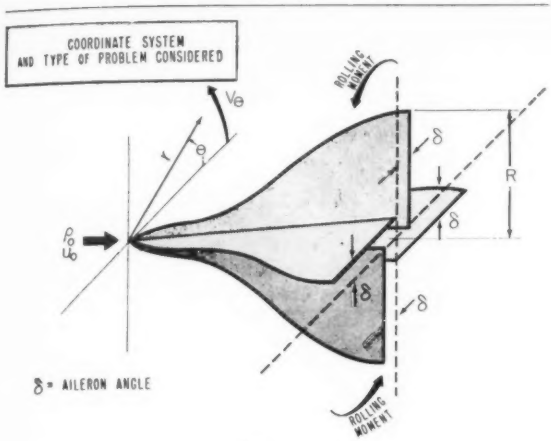

FIG. 1.

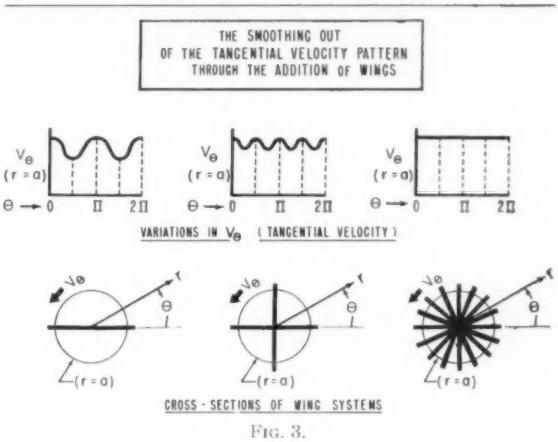

FIG. 3.

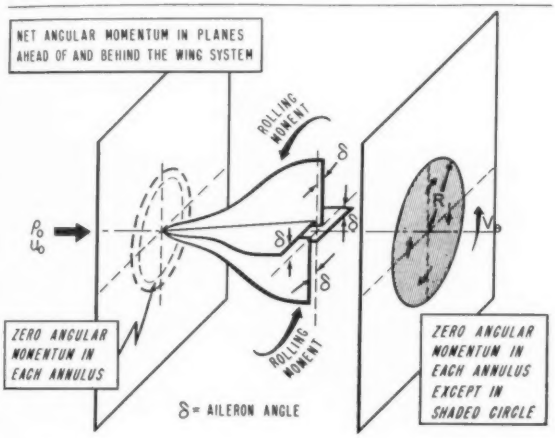

FIG. 2.

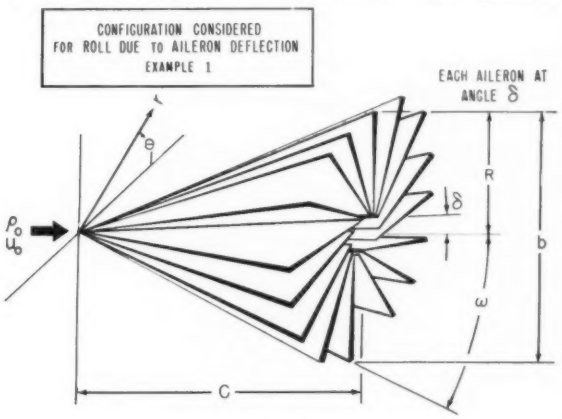

FIG. 4.

where $\rho = \rho_0 + \Delta\rho$, $u = u_0 + \Delta u$, and the subscript 0 indicates free-stream conditions.

Effect of Linearization

For a flow in which the velocity perturbations are small, the equation may be linearized to give

$$M_R = \rho_0 u_0 \int_0^\infty \int_0^{2\pi} V_\theta r^2 \, d\theta \, dr \qquad (3)$$

This can be further simplified, since $r \int_0^{2\pi} V_\theta \, d\theta$ taken outside the wing tip circle is the circulation around a closed curve in the fluid. This circulation is zero, since the flow was originally irrotational and no viscous effects have been encountered. If R = wing tip radius, then (as indicated in Fig. 2) Eq. (3) can be rewritten as

$$M_R = \rho_0 u_0 \int_0^R \int_0^{2\pi} V^0 r^2 \, d\theta \, dr \qquad (4)$$

Introduction of an Infinite Number of Wings

If a planar wing with deflected ailerons is considered, then the value of tangential velocity (V_θ) is known at the wing surfaces within linearized theory, since $V_\theta = \alpha u_0$, where α is the local angle of incidence. However, this determines V_θ only at $\theta = 0$, π, and 2π as shown in Fig. 3, and, presumably, V_θ is less at intermediate angles as shown. For a cruciform wing with four ailerons deflected, V_θ is known at $\theta = 0, \pi/2, \pi, 3\pi/2$, and 2π, and, if the same chordwise dimensions are retained as on the planar system, the fluctuations in V_θ should be decreased between the wings. Since this still does not provide sufficient information to permit solving Eq. (4) for the rolling moment, it is necessary to consider the limiting case in which infinitely many wings are arranged about the axis so that adjacent wings are separated by an infinitesimal distance. Here, the fluctuation in tangential velocity between two wings is negligible (assuming finite chordwise dimensions), and therefore the tangential velocity distribution is known everywhere inside the wing tip circle. Only the tangential velocities at the trailing edges of the wing system are important. Behind the trailing edges

$$\int_0^{2\pi} V_\theta r \, d\theta$$

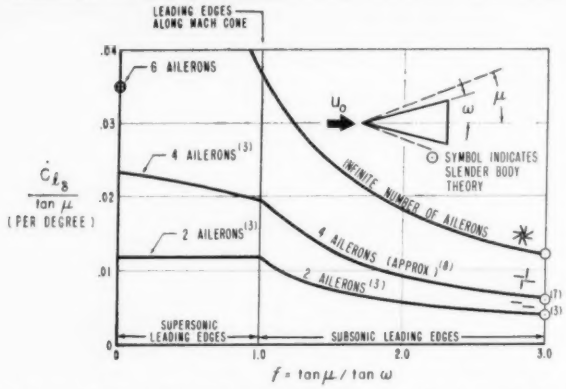

FIG. 5. Rolling moment coefficient vs. sweepback angle for delta ailerons (Example 1).

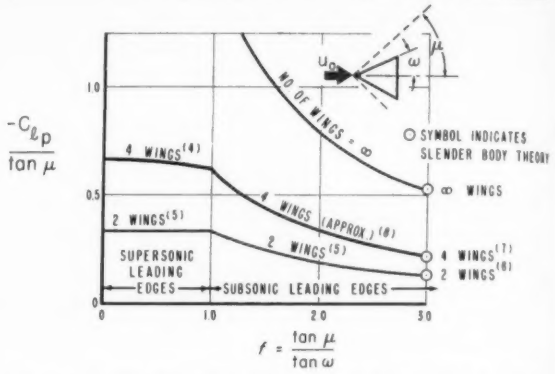

FIG. 7. Rolling moment coefficient due to damping in roll vs. sweepback for delta wings.

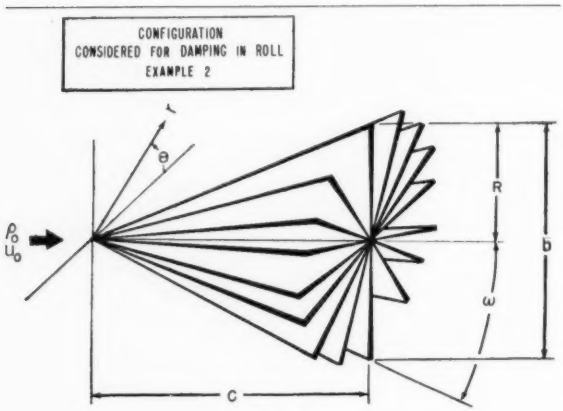

FIG. 6.

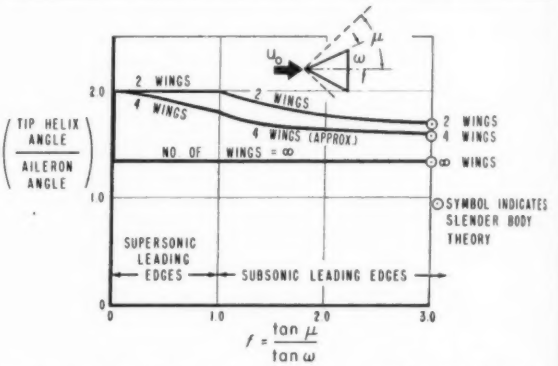

FIG. 8. Equilibrium rate of roll vs. sweepback for delta wings.

remains constant for a given radius, since the circulation is constant for that radius. Therefore, the rolling moment (M_R) can be evaluated from Eq. (4) using the trailing-edge values of V_θ. The trailing edges are defined as all edges that are the last encountered by air leaving the wing system.

The above method of analysis is related to methods used in propeller theory.[2]

DISCUSSION

Limitations

The preceding analysis of the limiting case is independent of Mach Number and independent of the longitudinal shape of the wing system. It is only necessary that, for a given finite Mach Number, the ratio of the distance between adjacent wing tips to chordwise and spanwise dimensions of the wing system approach zero. For a system with a finite number of wings, such dimensionless ratios give a crude qualitative indication of how closely the limiting conditions are approached.

Modifications and Extensions

The presence of a circular cylinder in the system is accounted for by modifying the inner limit of integration. Other bodies of revolution produce a radial displacement of the stream lines, which should be considered.

Damping moments in roll can be calculated by assuming the wing angle of attack proportional to the radius, and equilibrium rates of roll are then obtained by equating damping moments to aileron moments. When the equilibrium rate of roll is attained, the net angular momentum left behind the wing system is zero.

It is also possible to determine rolling moment interference effects between wing and tail if one assumes that the tail also has an infinite number of symmetrically arranged surfaces. This is actually a special case of a wing system having an irregular longitudinal shape. In general, the tail (assumed to be in the rear) merely removes all angular momentum from the disc that it covers, and, if it is as large as the aileron disc and concentric with it, no resultant rolling moment is produced by wing ailerons. However, the tail does not affect the

damping moment in roll* (unless its diameter is greater than the wing disc diameter). This follows because the air flowing through the tail system has already been given an angular velocity by the rolling of the wing and, hence, has no angle of attack relative to the tail surfaces.

Nonlinear Effects

If a lifting wing is considered so that the wing wake is displaced relative to the fuselage axis, then, in effect, the tail and wing discs are not concentric and some of the angular momentum of the wing wake may not be removed by the tail even though the discs have the same diameter. This is a nonlinear effect that may be important* and tends to reduce the unfavorable rolling moment produced on the tail for the case where the wing and tail discs are of equal diameter. For the case where the tail disc is of smaller diameter than the wing disc, it is not necessarily true that the nonlinear effects on rolling moment are favorable. The effective displacement of the disc centers may also introduce nonlinear yawing moments.

* Suggested by Dr. Lagerstrom.

Results and Comparison

Table 1 shows some comparative values of C_{l_δ} and C_{l_p} and equilibrium rate of roll for delta wing systems having two wings, four wings, and an infinite number of wings. The values are obtained from Examples (1) and (2) of this paper and from the references listed.

Example (1). The Limiting Case of Infinitely Many Ailerons Deflected in the Same Direction

Assume that each surface in Fig. 4 is an aileron deflected through an angle δ. Then, the tangential velocity $(V_\theta) = \delta u_0$ and, from Eq. (4),

$$M_R = \rho_0 u_0 \int_0^R \int_0^{2\pi} \delta u_0 r^2 \, d\theta \, dr$$

or

$$M_R = \rho_0 u_0^2 \delta \, (2\pi R^3/3)$$

letting

$$q = (1/2)\rho_0 u_0^2, \quad M_R = \delta q (4/3)\pi R^3$$

The rolling moment coefficient (C_{l_δ}) defined as

Table 1. Rolling moment coefficients and equilibrium rates of roll for delta wing systems.

TYPE OF WING SYSTEM →		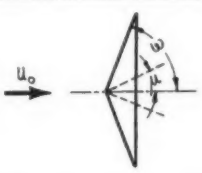	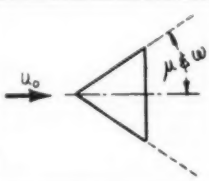	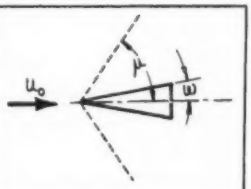
$\frac{\tan\mu}{\tan\omega} = f$ →		0	1.0	∞
$\left[C_{l_\delta}/\tan\mu\right]$ AILERON EFFECT	2 WINGS	$0.667^{(3)}$	$0.667^{(3)}$	$0.667/f^{(3)}$
	4 WINGS	$1.333^{(3)}$	$1.132^{(3)}$	$1.016/f^{(7)}$
	∞ WINGS	∞	2.094	$2.094/f$
$\left[-C_{l_p}/\tan\mu\right]$ DAMPING IN ROLL	2 WINGS	$0.333^{(5)}$	$0.333^{(5)}$	$0.393/f^{(6)}$
	4 WINGS	$0.667^{(4)}$	$0.623^{(4)}$	$0.637/f^{(7)}$
	∞ WINGS	∞	1.571	$1.571/f$
$\left[\frac{\text{TIP HELIX ANGLE}}{\text{AILERON ANGLE}}\right]$ EQUIL. ROLL	2 WINGS	2.000	2.000	1.697
	4 WINGS	2.000	1.817	1.595
	∞ WINGS	$2.000 \rightarrow 1.333^{*}$	1.333	1.333

* (INDETERMINATE)

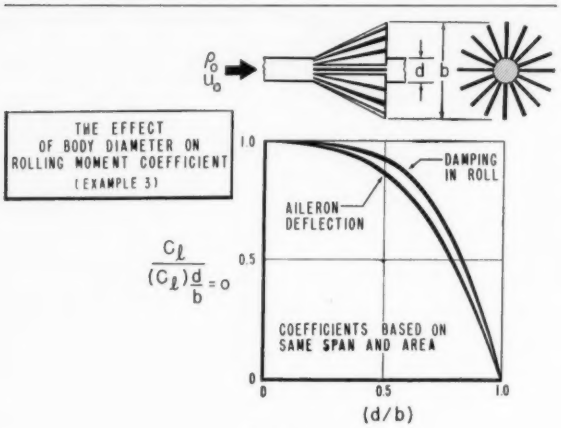

FIG. 9.

$$C_{l_\delta} = M_R/q(cR)b\delta$$

becomes

$$C_{l_\delta} = (2\pi/3) \tan \omega$$

This is plotted in Fig. 5 to compare with values for plane delta and cruciform delta ailerons determined by Bleviss.[3] The cruciform configuration considered by Bleviss has a fixed vertical fin and horizontal ailerons. However, by rotation and superposition, it is easily shown that C_{l_δ} values for horizontal ailerons in the presence of a fixed vertical fin are doubled by deflecting the vertical surfaces through the same angle.

EXAMPLE (2). DAMPING IN ROLL FOR THE LIMITING CASE OF INFINITELY MANY WINGS

Assume that the angle of attack of each wing in Fig. 6 varies linearly from zero at the axis to $-pr/u_0$ at the tip, with p = rolling velocity in radians per second. Then, $V_\theta = -pr$ and, from Eq. (4),

$$M_R = -\rho_0 u_0 \int_0^R \int_0^{2\pi} prr^2 \, d\theta \, dr$$

or

$$M_R = -(qp/u_0)\pi R^4$$

and

$$C_l = -(pb/2u_0)\,(\pi/2) \tan \omega$$

or

$$C_{l_p} = -(\pi/2) \tan \omega$$

This is the rolling moment coefficient due to damping. If the equilibrium rate of roll resulting from a given aileron deflection is desired (assuming that the complete wings act as ailerons), the sum of the rolling moments due to aileron deflection and damping is set equal to zero, giving

$$(pb/2u_0) = (4/3)\delta$$

Figs. 7 and 8 show the effect of number of wings on damping in roll and equilibrium rate of roll. In Fig. 8 it is seen that a singular point occurs at $f = 0$ for an infinite number of wings. If f is set equal to zero and the singularity is approached by starting with a finite number of wings and increasing the number without limit, then the value of 2.0 results for the ratio of tip helix angle to aileron angle. If, alternatively, the singularity is approached by starting with an infinite number of wings and letting f approach zero, then a value of 4/3 results.

EXAMPLE (3). THE EFFECT OF A CENTRAL CIRCULAR CYLINDER

If in Example (1) the inner limit of integration is $d/2$, corresponding to the presence of a central circular cylinder of diameter d (as shown in Fig. 9), then the rolling moment coefficient produced by an aileron deflection δ becomes

$$C_l = (2\pi/3)\delta \tan \omega[1 - (d/b)^3]$$

Similarly, in Example (2), if the inner limit of integration is $d/2$, then the rolling moment coefficient produced by damping in roll becomes

$$C_l = \left(\frac{pb}{2u_0}\right)\frac{\pi \tan \omega}{2}\left[1 - \left(\frac{d}{b}\right)^4\right]$$

Plots of the ratio of C_l to $(C_l)_{d/b=0}$ are shown in Fig. 9. The coefficients are based on the span and area corresponding to $(d/b) = 0$.

REFERENCES

[1] Prandtl, L., and Tietjens, O. G., *Fundamentals of Hydro- and Aeromechanics*, p. 238; McGraw-Hill Book Company, Inc., New York, 1934.

[2] Glauert, H., *Airfoil and Airscrew Theory*, p. 208; Cambridge University Press, 1942.

[3] Bleviss, Zegmund O., *Some Roll Characteristics of Plane and Cruciform Delta Ailerons and Wings in Supersonic Flow*, Douglas Report SM-13431, p. 73, June, 1949.

[4] Bleviss, Zegmund O., *Some Roll Characteristics of Cruciform Delta Wings at Supersonic Speeds*, Journal of the Aeronautical Sciences, Vol. 18, No. 5, pp. 289–297, May, 1951.

[5] Brown, Clinton E., and Adams, Mac C., *Damping in Pitch and Roll of Triangular Wings at Supersonic Speeds*, N.A.C.A. T.R. No. 892, 1948.

[6] Ribner, Herbert S., *The Stability Derivatives of Low-Aspect-Ratio Triangular Wings at Subsonic and Supersonic Speeds*, N.A.C.A. T.N. No. 1423, 1947.

[7] Adams, Gaynor J., *Theoretical Damping in Roll and Rolling Effectiveness of Slender Cruciform Wings*, N.A.C.A. T.N. No. 2270, January, 1951.

[8] Bleviss, Zegmund O., *Interference Effects in Supersonic Flow*, California Institute of Technology (Thesis) Pasadena, Calif., 1951.

Interference Between Wing and Body at Supersonic Speeds—Theoretical and Experimental Determination of Pressures on the Body

R. H. CRAMER†

Cornell Aeronautical Laboratory, Inc.

ABSTRACT

Experimental data are adduced to show the pressure distribution on an axially symmetric body, aft of a lifting wing, in supersonic flow. The axial distribution of integrated lifts, as well as the peripheral pressure plots, is shown to be predicted, to engineering accuracy, by use of the linearized theory propounded by Ferrari, even when only a few terms are used in the Fourier development required by the theory. The theoretical curves were obtained by means of a new simplified solution to Ferrari's differential equation; it is expressed in terms of the hyperbolic functions of successive integral multiples of an argument, so that the work of numerical computation progresses rapidly with the aid of standard tables.

INTRODUCTION

THE THEORY OF WING-BODY INTERFERENCE, propounded by Professor Ferrari in reference 1, presents a method based on the familiar linearization of the equation of motion for calculation of the aerodynamic action of the body upon the wing and also that of the wing upon the body. Experimental pressure distributions are now available to compare the results of theory and experiment for the induced pressures on the body (the results for the body induced effects on the wing have already been noted in reference 2). These data were obtained on a wing-body combination that closely reproduced in the wind tunnel the features of the mathematical model treated by Professor Ferrari in the numerical application of his theory.

DISTRIBUTION OF INCREMENT OF LIFT ALONG BODY

It was demonstrated in reference 1 that the distribution of the incremental lift along the body which arises from the *normal* component of the induced velocity (which must be negated at the body surface by the new distribution of doublets along the body axis) has, for the configuration shown in Fig. 1, a form and magnitude such as given in Fig. 2. To this distribution must be added the effects of the longitudinal components of the induced flow from the wing (a uniform, two-dimensional velocity distribution over a rectangular wing at an angle of attack, β_2, is being assumed at this first stage of the iteration process; the process is described in detail in reference 2). The way these two distributions are related and summed is shown in Fig. 3.

A comparison of this total increment in lift along the body with the experimental result is given in Fig. 4 for 8° angle of attack. Even though the distribution of lift along the body is predicted to good accuracy, one still has no assurance that the actual pressure distribution around the periphery of the body is represented as closely by the theory as is the lift.

LOCAL PRESSURE DISTRIBUTIONS AROUND BODY BEHIND WING

A representative comparison of theory and experiment is presented here as Fig. 5 for the pressures that exist around the periphery of the body at an axial station denoted by $\xi^* = 1.15$. A section through the body at the leading edge of the wing has an axial location given by $\xi^* = 1.0$, where, in general, $\xi^* = x/\lambda$—i.e., the nose length depicted in Fig. 1 is denoted by λ. Thus this particular section selected for illustration of a typical peripheral pressure distribution is located slightly behind the trailing edge of the wing whose axial coordinate is $\xi^* = 1.14$. The physical conditions of the airflow in the wind tunnel have been previously listed in the above-cited paper[2] by Ferrari. The reason for illustrating these results by selection of data for a cross section lying aft of, but near, the wing is merely in order to obtain large values of the increments

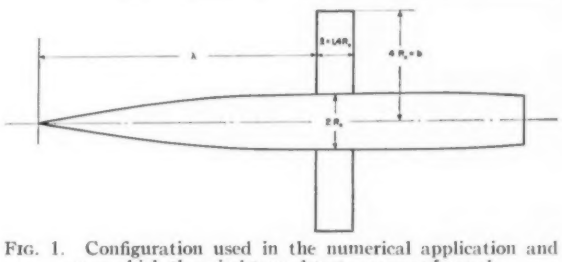

FIG. 1. Configuration used in the numerical application and upon which the wind-tunnel tests were performed.

Received December 29, 1950. This investigation, both experimental and theoretical, was carried out under Navy BuOrd sponsorship.

† Principal Research Engineer.

in pressure due to interference; in this way the contribution to the pressures that arise from the flow about the body alone are rendered relatively inconsequential (although they are actually accounted for in the theoretical distribution plotted in Fig. 5).

Corresponding Theory for the Pressures

The determination of the theoretical results requires some note of explanation. Although the formulas given by Ferrari in reference 1 are valid for calculation of the lift distribution as given by Fig. 2, a modification must be made to the formulas in order to obtain the correct values for the individual pressures. It was noted over a year ago by Lagerstrom and Van Dyke, in a footnote to reference 3, that an operator had been applied incorrectly in obtaining the formulas for the individual pressures according to reference 1. Recently, Bolz[4] has worked out the details of the first two terms; it will require several more terms, however, in order to attain a practical description of the pressures around the body. Therefore, the continuation of the suggested method is apt to become unwieldly.

Simplification of Ferrari's Formulas for Body Pressures

Fortunately, the whole problem can be obviated by noting that the operator procedure is not actually necessary; an identical solution can be obtained by use of hyperbolic functions as follows:

The differential equation to be solved [see Eq. (4) of Professor Ferrari's original paper] is

$$\frac{\partial^2 \phi_m^{(3)}}{\partial r^2} + \frac{2m+1}{r}\frac{\partial \phi_m^{(3)}}{\partial r} = \alpha^2 \frac{\partial^2 \phi_m^{(3)}}{\partial x^2} \tag{1}$$

The required solution of this equation can be shown by direct substitution to be

$$\phi_m^{(3)} = \frac{(-1)^m \alpha^m}{r^m} \int_{\operatorname{arcosh} x/\alpha r}^{0} f_m\,(x - \alpha r \cosh u) \cosh mu\, du \tag{2}$$

This basic result appears to have escaped the attention of Lamb[5] and later researchers.

Ward,[6] however, has presented another simple solution, but the subsequent evaluation of the arbitrary function in terms of the body coordinates would involve the Laplace transform, which may be inconvenient to evaluate.

It follows immediately from Eq. (2) that

$$\left[\frac{\partial (r^m \phi_m^{(3)})}{\partial r}\right]_{r=R} = (-1)^{m+1}\alpha^{m+1} \int_{\operatorname{arcosh} x/\alpha R}^{0} \dot{f}_m(x - \alpha R \cosh u) \cosh mu \cosh u\, du = -F_m\left(\frac{x}{R}\right) \tag{3}$$

Then, by employing the same technique of division of the interval of integration in small subintervals, throughout which the individual $\dot{f}_m$ are assumed constant (as was illustrated in Ferrari's original paper), it follows that

$$\frac{(-1)^m \alpha^{m+1}}{m^2 - 1} K_m^{(1)} \left[\sqrt{\frac{x_1^2}{\alpha^2 R_1^2} - 1} \cosh m \operatorname{arcosh} \frac{x_1}{\alpha R_1} - \frac{m x_1}{\alpha R_1} \sinh m \operatorname{arcosh} \frac{x_1}{\alpha R_1}\right] = F_m\left(\frac{x_1}{R_1}\right) \tag{4}$$

for $m \neq 1$, while the formula previously given by Ferrari in the case of $m = 1$ is still valid. The $K_m^{(1)}$ employed in Eq. (4) are, of course, the constant values of the $\dot{f}_m$ in the *first* small interval; while, in general, if x_{i-1}' and x_i' are the abscissas of the left and right ends of the ith interval, respectively, and $K_m^{(i)}$ is the constant value of $\dot{f}_m$ in that interval, then one has, at the point $P^{(n)}$, with coordinates (x_n, R_n), that

$$\frac{(-1)^m \alpha^{m+1}}{m^2 - 1} \sum_{i-1}^{n} K_m^{(i)} \left[\sqrt{\left(\frac{x_n - x_{i-1}'}{\alpha R_n}\right)^2 - 1} \cosh m \operatorname{arcosh} \frac{x_n - x_{i-1}'}{\alpha R_n} - \sqrt{\left(\frac{x_n - x_i'}{\alpha R_n}\right)^2 - 1} \cosh m \operatorname{arcosh} \frac{x_n - x_i'}{\alpha R_n} - \frac{m(x_n - x_{i-1}')}{\alpha R_n} \sinh m \operatorname{arcosh} \frac{x_n - x_{i-1}'}{\alpha R_n} + \frac{m(x_n - x_i')}{\alpha R_n} \sinh m \operatorname{arcosh} \frac{x_n - x_i'}{\alpha R_n}\right] = F_m\left(\frac{x_n}{R_n}\right) \tag{5}$$

for $m \neq 1$, while the formula previously given by Ferrari in the case of $m = 1$ is still valid.

Confrontation of Experimental and Theoretical Results

Calculations based on Eq. (5) have been carried out in order to obtain the theoretical values for the pressure coefficients pertaining to the wing-body configuration depicted in Fig. 1 and more fully described in reference 1.

The correspondence between theory and experiment shown in Fig. 5 is considered to be good, especially in view of the fact that only an $m = 7$ representation (actually only four nonzero terms computed) is employed in the determination of the effect of the normal components of the induced velocities in producing the graphed pressures; in addition, these four terms are the opening sequence of only the first step in the iteration process mentioned previously.[2]

Further steps in the iteration process would be necessary to give a more precise determination of the flow along the side of the body behind the leading edge of the wing, since the second stage of the iteration process for the distribution[2] of velocities over the wing shows marked changes from the two-dimensional distribution being assumed to exist over the wing when carrying out this first stage of the iteration process for the *body*. Nevertheless, it is highly significant that close correspondence is obtained with the experimental results even without recourse to such further mathematical refinements provided by Ferrari's theory; the more complicated formulas required for carrying out the second and higher numbered steps of the iteration process are available in reference 7. Note, however, that the sequence of steps in the iteration process advocated in reference 2 is reversed in reference 7; the sanction for this change is found in the smallness of the subsequently computed second-order effects. The explanation of why, in the first step of treating the body upwash effect on the wing, a nil amount of upwash is assumed to exist in the region of the wing actually covered by the body acquires an acceptable logical foundation on the basis of the more extensive arguments advanced in this latter reference.

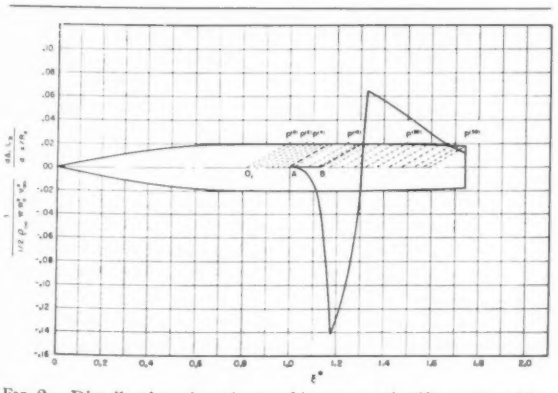

Fig. 2. Distribution along body of increment in lift produced by velocities normal to the body induced by the wing.

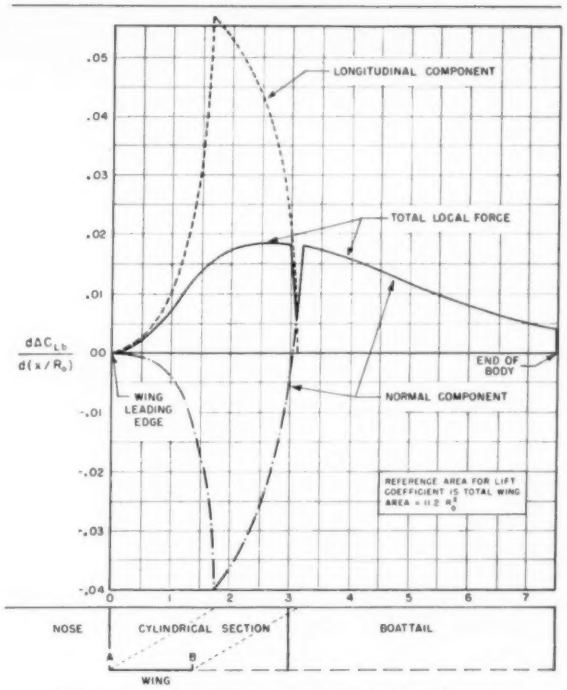

Fig. 3. Lift increment on body due to interference.

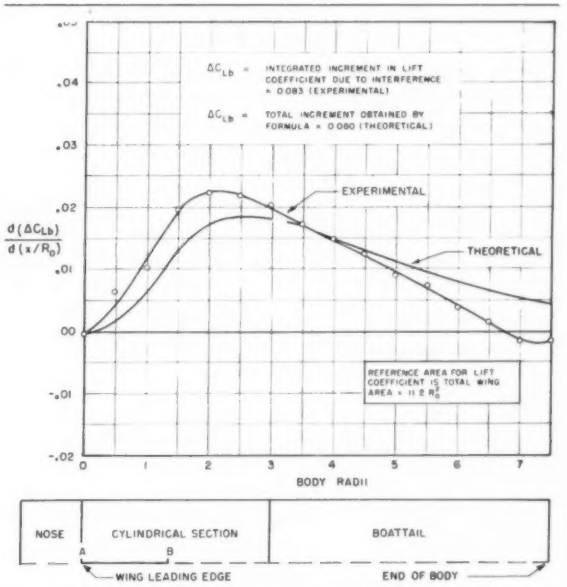
ΔC_{Lb} = INTEGRATED INCREMENT IN LIFT COEFFICIENT DUE TO INTERFERENCE = 0.083 (EXPERIMENTAL)
ΔC_{Lb} = TOTAL INCREMENT OBTAINED BY FORMULA = 0.080 (THEORETICAL)
EXPERIMENTAL
THEORETICAL
REFERENCE AREA FOR LIFT COEFFICIENT IS TOTAL WING AREA = 11.2 R_0^2
BODY RADII
NOSE
CYLINDRICAL SECTION
BOATTAIL
WING LEADING EDGE
END OF BODY

Fig. 4. Lift increment on body due to interference for 8° angle of attack (Mach Number = 2.0).

Pressure "Jumps" Demarcating Shock Surfaces from Wing Leading and Trailing Edges

There will, of course, always tend to be some discrepancy between the experimental distribution and the theory in the neighborhood of the jumps in the distribution which occur at the edges of the region

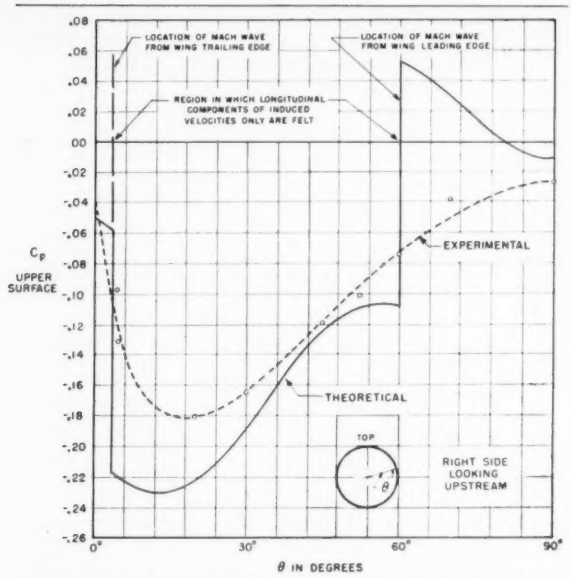

FIG. 5. Final determination of pressure coefficient obtained by adding to distribution resulting from the normal components of the induced velocities that part of the local pressure contributed by the body alone, plus increment to pressures arising from longitudinal components of induced velocity at Station P^6 where $\xi^* = 1.15$ (2.25 in. behind wing leading edge on model). Mach Number = 2.0; 8° angle of attack.

influenced by the longitudinal components of the induced velocities. Because of the ameliorating influence of the boundary layer it can be expected that such sharp discontinuities will not, however, be experienced in physical reality. An experimental value of the pressure at such a jump point which turns out to be approximately the average of the values for the superior and inferior limits of the theoretical curve on either side of the jump can be considered as proper confirmation of the predicted pressure in such a location.

Availability of Additional Data, Including Wing Pressures

These data are but a small part of the results obtained in the wind-tunnel tests on this configuration. It is believed, however, that they are sufficient to show the essential confirmation of Ferrari's theory as it relates to pressures on the body. Confirmation of the theory with regard to pressures on the wing was presented in reference 2. Additional wing data over and above those presented there are also available, although there is little need to further substantiate the evident relationships by means of similar plots. These data include pressure measurements on the aft region of the wings, close to the body, where the lack of information has been deplored by Morikawa.[8] The complete set[9] of experimental data and correlations with theory may be obtained on request from The Johns Hopkins University, Applied Physics Laboratory.

References

[1] Ferrari, C., *Interference Between Wing and Body at Supersonic Speeds—Theory and Numerical Application*, Journal of the Aeronautical Sciences, Vol. 15, No. 6, p. 317, June, 1948.

[2] Ferrari, C., *Interference Between Wing and Body at Supersonic Speeds—Note on Wind Tunnel Results and Addendum to Calculations*, Journal of the Aeronautical Sciences, Vol. 16, No. 9, p. 542, September, 1949.

[3] Lagerstrom, P. A., and Van Dyke, M. D., *General Considerations About Planar and Non-Planar Lifting Systems*, Douglas Aircraft Company, Inc., Report No. SM-13432, p. 63, June, 1949.

[4] Bolz, R. E., *Note on "Interference Between Wing and Body at Supersonic Speeds,"* Readers' Forum, Journal of the Aeronautical Sciences, Vol. 17, No. 7, p. 453, July, 1950.

[5] Lamb, H. L., *Hydrodynamics*, 6th Ed., p. 527; Cambridge University Press, London, 1932.

[6] Ward, G. N., *A Note on Compressible Flow in a Tube of Slightly Varying Cross-Section*, Aeronautical Research Council Technical Report, R. & M. No. 2183 (9205), December, 1945.

[7] Ferrari, C., *Interference Between Wing and Body at Supersonic Speeds, Part III, Numerical Application of the Linear Theory*, Cornell Aeronautical Laboratory Report under Section T Contract with APL/JHU, Report CAL/CM-463, April, 1951.

[8] Morikawa, G. K., *On Wing-Body Interference at Supersonic Speeds*, Readers' Forum, Journal of the Aeronautical Sciences, Vol. 17, No. 5, p. 315, May, 1950.

[9] Cramer, R. H., *Interference Between Wing and Body at Supersonic Speeds. Part V—Phase One Wind Tunnel Tests Correlated with Linear Theory*, Cornell Aeronautical Laboratory Report under Section T Contract with APL/JHU, Report CAL/CM-597, December, 1950.

Readers' Forum

BRIEF REPORTS of investigations in the aeronautical sciences and discussions of papers published in the JOURNAL are presented in this special department. The publication will be completed approximately 8 to 10 weeks after receipt of the material. The Editorial Committee does not hold itself responsible for the opinions expressed by the correspondents. Contributions should not exceed 800 words in length.

Lateral Elastic Instability of Hat-Section Stringers

C. M. Tyler, Jr., and T. J. Walker
Department of Mechanical Engineering, Carnegie Institute of Technology, Pittsburgh
June 11, 1951

STRINGER AND SHEET COMBINATIONS under longitudinal compression loading may fail in several ways. The stringers can fail as columns by buckling perpendicular to the plane of the sheet; they can fail due to local crushing or crippling; or they can fail by the edge of stringer, which is not attached to sheet buckling parallel to the sheet. This last mode of failure is known as lateral instability and commonly occurs with open section stringers.

It is generally believed that closed stringers such as hat sections are unlikely to fail due to lateral instability. As a result of some tests in which this type of failure apparently occurred, Goodman[1] has developed two energy methods for calculating the lowest critical strain corresponding to this mode of failure. The simpler method involves two arbitrary constants and assumes that the legs of the hat are fixed at the sheet. The second inherently more accurate and more complicated method involves five arbitrary constants and assumes that the legs are hinged at the sheet. The second method gives appreciably lower numerical values.

The writers felt that the difference in the numerical results of the two methods was caused primarily by changing from fixed-leg to hinged-leg conditions. Consequently, they adapted Goodman's two-constant method to hinged legs and have found that numerically it checks closely the five-constant method. Thus, it may be concluded that the accuracy of this simpler method is essentially the same as the five-constant method.

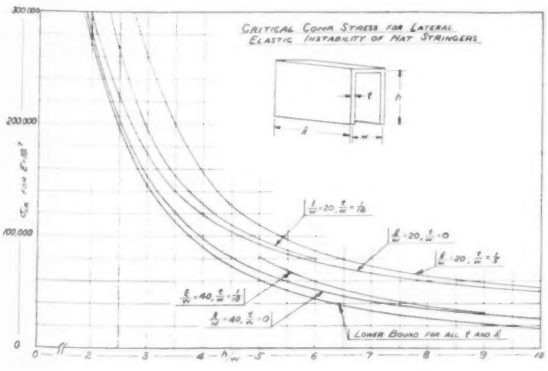

FIG. 1.

This two-constant hinged-leg method has been put into dimensionless form and used to calculate Fig. 1. These curves indicate that lateral elastic instability is not likely to occur unless the height-width ratio is above 5; they also indicate that the critical stress can be rather low for large values of this ratio.

For height-width ratios above 5, Fig. 1 shows that the critical stress is rather insensitive to thickness. Neglecting thickness, a simplified conservative critical strain formula can then be used.

$$\frac{\sigma_{cr}}{E} = \frac{1}{2D+1}\left\{\frac{1}{2.6} - \frac{1}{6.76\left[\frac{\pi^2}{12S^2}(1+2R) + \frac{1}{5.2}\left(\frac{1}{R}+2\right)\right]}\right\} \tag{1}$$

where

$$D = \frac{8}{105}\left(\frac{C^2}{R^3}\right) + \frac{4}{35}CR^2 + \frac{1}{7}R$$
$$C = (1/R) + [1/(1+2R)]$$
$$R = h/w, \text{ height-width ratio}$$
$$S = l/w, \text{ length-width ratio}$$

Eq. (1) is applicable to hat sections with parallel legs and is based on the two-constant hinged-leg method. A lower bound expression can be found by taking the length as infinite.

The possibility of lateral elastic instability being the indicated mode of failure can be checked with the aid of Fig. 1, and, if need be, the critical stress can be conservatively calculated by Eq. (1).

REFERENCE

[1] Goodman, Stanley, *Lateral Elastic Instability of Hat-Section Stringers Under Compressive Load*, N.A.C.A. T.N. No. 2272, January, 1951.

Reflection of Strong Shock at Nearly Glancing Incidence*

Donald R. White
Charles A. Coffin Fellow, Palmer Physical Laboratory, Princeton University
June 7, 1951

TING AND LUDLOFF[1] HAVE OBTAINED a solution for the density and pressure fields in the reflection of shock waves from a wedge of small angle (nearly glancing incidence) and have computed explicit results for a shock of strength $\xi = P_1/P_2 = 0.137$ which sets up a flow of Mach Number 1.21. During the past year the shock reflection problem[2] has been the subject of an experimental survey at this laboratory utilizing a Mach-Zehnder interferometer in conjunction with the shock tube[3] to determine the entire density field for a range of shock strengths and wedge angles. In the course of this program results have been obtained which may be compared with their predictions as presented in Fig. 1 of reference 1. Features of their results to be noted are the region of uniform flow near the leading edge of the wedge, the singular point on the reflected shock where the contours of constant density converge, and the separation of the density and pressure contours in the region where a slipstream† would appear if the reflected shock were not of zero strength at the point where it meets the incident shock. This separation is also implied by the previous result of Lighthill[1] that the Mach stem for strong shocks has a sharp maximum in curvature near the triple point, resulting in different entropies for adjacent streamlines.

* This research was supported by the Office of Naval Research of the Navy Department.

† The term "slipstream" as used here refers to the density and velocity discontinuity surface necessarily resulting from the intersection of three shocks, all of nonzero strength.

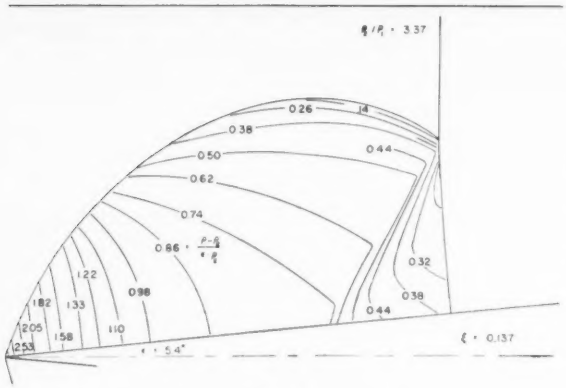

FIG. 1.

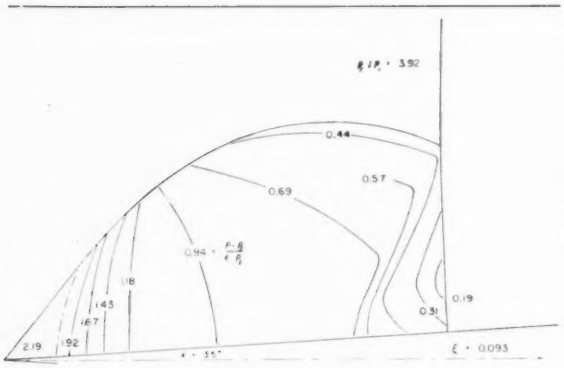

FIG. 2.

Our experimental results for a shock of this strength and a wedge half-angle $\epsilon = 5.4°$ are shown in Fig. 1. This angle is such that the shock is not quite attached, so that one does not observe a region of uniform flow near the leading edge. The density contours do seem to converge toward a point just beyond the reflected shock, and their behavior near the expected position of the slipstream is similar. Fig. 2 represents an attempt to obtain a picture qualitatively similar near the leading edge. To do this it was necessary to use a stronger shock and a smaller angle, but the same general features again appear.

This convergence of the density contours appears to be characteristic of the pattern found when a weak shock is intercepted by a rarefaction and has been observed in several otherwise unrelated experiments, such as the regular reflection of a weak shock and the diffraction of a weak shock over a corner. In the present case the shock is the attached bow wave and the rarefaction is the signal sent out from that portion of the fluid which was at the corner when the shock first hit the wedge. It is observed, in general, that for a shock of small but finite strength the apparent point of convergence lies just beyond the shock, approaching it as the shock strength decreases. Thus, the singularity appears only in the limit of an infinitely weak shock, where the magnitude of the disturbance vanishes.

The similarity of the density contours near the slipstream is striking, but too much significance should not be attached to this point, since the duration of the spark used in taking the interferograms tends to smooth out fringe discontinuities so that the physically sharp slipstream that we would expect for a finite angle wedge would appear as a region of continuous but rapid density change. The maximum shift of the fringes in the interferogram from the undisturbed flow is about one fringe, so the error in the numbers attached to the contours is of the order of the change from one contour to the next, but the shape of the contours is relatively accurate.

REFERENCES

[1] Ting, L., and Ludloff, J. F., *Aerodynamics of Blasts*, Readers' Forum, Journal of the Aeronautical Sciences, Vol. 18, No. 2, pp. 143–144, February, 1951.

[2] Bleakney, Walker, and Taub, A. H., *Interaction of Shock Waves*, Rev. Mod. Phys., Vol. 21, No. 4, pp. 584–605, October, 1949.

[3] Bleakney, Walker, Weimer, D. K., and Fletcher, C. H., *The Shock Tube: A Facility for Investigations in Fluid Dynamics*, Rev. Sci. Inst., Vol. 20, No. 11, pp. 807–815, November, 1949.

[4] Lighthill, M. J., *On the Diffraction of Blast I*, Proc. Roy. Soc., Vol. 198A, No. 1055, pp. 454–470, September, 1949.

Ring Shape Source Distribution in Axially Symmetrical Supersonic Flow

S. I. Pai
Institute for Fluid Dynamics and Applied Mathematics, University of Maryland, College Park, Md.
June 14, 1951

THE LINEARIZED THEORY of axially symmetric supersonic flow can be used to study the supersonic flow past a tube of nearly constant radius for both the external and the internal flow conditions. For simplicity we consider here the case without angle of attack. The fundamental equation is

$$(M^2 - 1)\frac{\partial^2\phi}{\partial x^2} = \frac{\partial^2\phi}{\partial r^2} + \frac{1}{r}\frac{\partial\phi}{\partial r} \tag{1}$$

where M is the Mach Number of the basic supersonic flow, ϕ is the velocity potential of the disturbance, x is the coordinate along the axis of the tube, and r is the radial distance from the axis of the tube.

The most general solution of Eq. (1) is[1]

$$\phi = \int_0^\infty f(x - \beta r \cosh u)\, du + \int_0^\infty F(x + \beta r \cosh u)\, du \tag{2}$$

where $\beta^2 = M^2 - 1$ and both f and F are arbitrary functions to be determined for a given problem so that certain boundary values are satisfied.

In case of external flow past a tube, the condition of no incoming disturbance gives

$$\phi = \int^\infty f(x - \beta r \cosh u)\, du \tag{3}$$

The solution of the problem is to find the source distribution $f(x)$ on the x-axis ($r = 0$) such that the boundary condition on the average radius of the tube is satisfied.

In case of internal flow, it is often erroneously assumed that the solution of the problem is

$$\phi = \int_0^\infty F(x + \beta r \cosh u)\, du \tag{4}$$

Because the Mach lines of Eq. (4) are $x + \beta r =$ constant, it looks like an incoming wave. However, if one investigates Eq. (4) a little in detail, it is easily seen that Eq. (4) does not represent the incoming wave at all. The proof is as follows:

If one uses the transformation

$$x + \beta r \cosh u = \xi \tag{5}$$

Eq. (4) becomes

$$\phi = \int_{x+\beta r}^\infty \frac{F(\xi)\, d\xi}{\sqrt{(\xi - x)^2 - \beta^2 r^2}} \tag{6}$$

where $F(\xi)$ represents a source distribution on the x-axis. For simplicity of illustration, we consider only a simple source situated

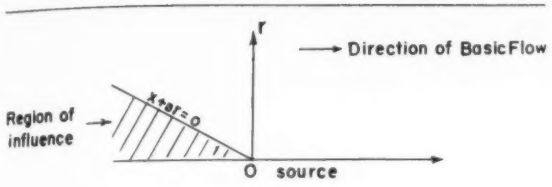

Fig. 1 Region of Influence of a simple Source represented by Eq. (6)

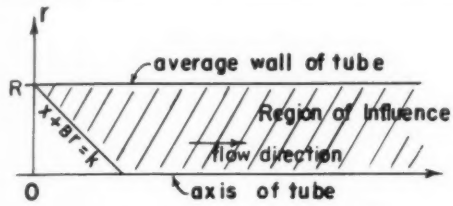

Fig. 2 Flow condition inside the tube

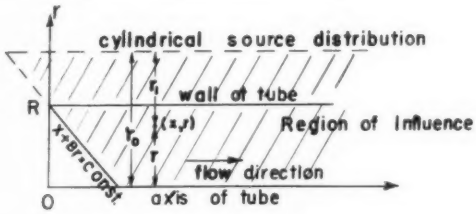

Fig. 3 Cylindrical Source Distribution

at the origin—i.e., only at $x = 0$, $F(\xi) \neq 0$. It is easily seen that the integral (6) is different from zero for all the points on the left of the surface $x + \beta r = 0$ and equal to zero for all the points on the right of the surface. The region of influence is *upstream!* (See Fig. 1.) It contradicts the behavior of supersonic flow. Hence, Eq. (4) or (6) cannot be used to represent the flow inside the tube. Furthermore, it artificially introduces source distribution on the x-axis inside the tube (in the region investigated); that is why some authors found that the solution breaks down behind the leading Mach line from the edge of the tube.

The proper physical picture of this problem is shown in Fig. 2. The present author would suggest that a cylindrical source distribution would correctly represent the actual flow. The cylindrical source distribution is made up of ring shape source distribution. The source strength is constant on each ring whose radius is r_0 and whose center is on the x-axis. Each source on the ring will have the velocity potential,

$$\phi = \int_0^\infty f[x - \beta(r_0 - r)\cosh u]\,du = \int_0^\infty f[x + (\beta r - \beta r_0)\cosh u]\,du \quad (7)$$

It is evident that the Mach line is $x + \beta r =$ constant and the region of influence is downstream (Fig. 3). Furthermore, if one chooses $r_0 > R$, where R is the average radius of the tube, no artificial sources are introduced in the region where the flow is investigated.

The application of this method of ring shape source distribution to axially symmetrical supersonic flow will be reported later.

A similar attempt of this method was given in reference 2, but our formulation of the formula is different. We use a method that is a modification of Weinstein's method of ring shape source in potential flow.[3]

References

[1] Lamb, H., *Hydrodynamics*, 6th Ed., p. 298; Dover Publications, 1945.

[2] Ludloff, H. F., and Reiche, F., *Linearized Treatment of Supersonic Flow Through Ducts*, Journal of the Aeronautical Sciences, Vol. 16, No. 1, pp. 5–21, January, 1949.

[3] Weinstein, A., *On Axially Symmetrical Flows*, Quart. Appl. Math., Vol. 5, No. 4, pp. 429–444, January, 1948.

The Effect of Surface Cooling on Laminar Boundary-Layer Stability

Martin Bloom
Research Associate, Polytechnic Institute of Brooklyn Aeronautical Laboratory, Brooklyn, N. Y.
May 10, 1951

THE STATEMENT IS MADE in reference 1 that the minimum critical Reynolds Number for laminar boundary-layer stability is increased in a pronounced manner by surface cooling, especially at supersonic speeds. This is based on results of reference 2, which state that, at a free-stream Mach Number (M) of 4, complete stability in an isobaric flow can be achieved by cooling the surface to 0.86 of its equilibrium temperature (T_e). On this basis, it is estimated in reference 1, that the results derived therein for adiabatic flow are conservative.

An investigation, carried out at the Polytechnic Institute of Brooklyn under the sponsorship of the N.A.C.A., indicates otherwise. Results of this study (Figs. 1 and 2) show that surface cooling has little stabilizing effect on an isobaric flow in the supersonic range, so that the calculations of reference 1 are less conservative than it is believed. The accompanying figures show that complete stability can be achieved by surface cooling for $1 < M < 5.7$ only. Moreover, whereas surface cooling is effective for stabilization at $M < 1.5$, its effect at higher Mach Numbers is small, since the amount of required cooling increases sharply with increasing M in the supersonic range. In particular, at $M = 4$, the surface temperature required for any practical amount of stabilization is close to that required for complete stabilization—namely, $0.25T_e$. These results seem reasonable in view of the known destabilizing effect of high Mach Numbers on adiabatic flows. Comparable results of reference 2 appear to be in error in this respect; this is probably due to the assumption of a small value for a parameter

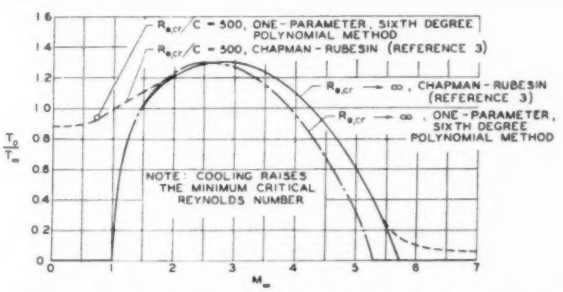
$R_{e,cr}/C$ = 500, ONE-PARAMETER, SIXTH DEGREE POLYNOMIAL METHOD
$R_{e,cr}/C$ = 500, CHAPMAN-RUBESIN (REFERENCE 3)
$R_{e,cr} \to \infty$, CHAPMAN-RUBESIN (REFERENCE 3)
$R_{e,cr} \to \infty$, ONE-PARAMETER, SIXTH DEGREE POLYNOMIAL METHOD
NOTE: COOLING RAISES THE MINIMUM CRITICAL REYNOLDS NUMBER
$\frac{T_0}{T_\infty}$
M_∞

FIG. 1. Surface temperature required to stabilize the laminar boundary layer by cooling at various free-stream Mach Numbers and $N_{PR} = 1$.

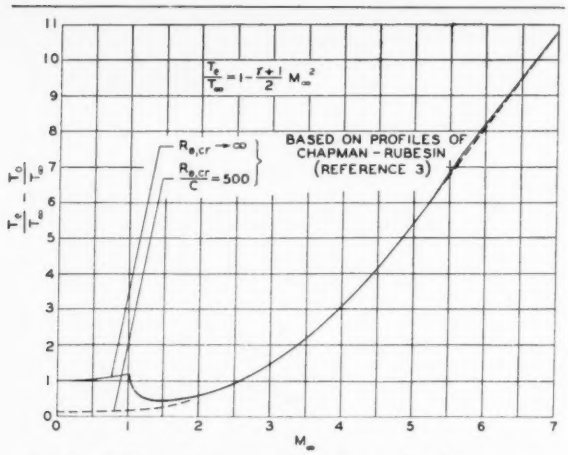

FIG. 2. Difference between equilibrium and surface temperature required to stabilize the laminar boundary layer by cooling at various free-stream Mach Numbers and $N_{PR} = 1$.

[Eq. (15), reference 2], which in these cases may be large, as well as to numerical errors.

The stability calculations represented in Figs. 1 and 2 were carried out according to the theory developed in reference 2, modified somewhat for these applications. For purposes of comparison, mean-flow properties were calculated by two alternative methods—the sixth degree polynomial integral method (also used in reference 1) and the mathematically exact type of analysis of reference 3. The surface temperatures required to stabilize the flow completely and to stabilize the flow only a small amount ($R_{\theta,cr}/C = 500$) were plotted. The symbol θ denotes momentum thickness, and C denotes a constant, of the order of one, which is used to approximate linearly the Sutherland temperature-viscosity relation.[3]

REFERENCES

[1] Weil, H., *Effects of Pressure Gradient on Stability and Skin Friction in Laminar Boundary Layers in Compressible Fluids*, Journal of the Aeronautical Sciences, Vol. 18, No. 5, p. 312, May, 1951.

[2] Lees, L., *The Stability of the Laminar Boundary Layer in a Compressible Fluid*, N.A.C.A. Report No. 876, 1947.

[3] Chapman, D. R., and Rubesin, M. W., *Temperature and Velocity Profiles in the Compressible Laminar Boundary Layer with Arbitrary Distribution of Surface Temperature*, Journal of the Aeronautical Sciences, Vol. 16, No. 9, pp. 547–565, September, 1949.

Astroballistic Heat Transfer*

R. N. Thomas and F. L. Whipple
University of Utah and Harvard College Observatory
June 1, 1951

ABSTRACT

Some current work on heat transfer to rapidly moving objects is summarized. The work embodies free-flight study of ablation.

INTRODUCTION

WE PRESENT HERE A BRIEF RÉSUMÉ of some recent work on heat transfer in the astroballistic régime. We use heat transfer in the conventional aerodynamic sense of energy received by the body from the original translational plus internal energy of the gas. The measures reported, however, relate to an inference of heat transfer from ablation measures. We have introduced the term "astroballistics" to define that region where the heat transfer to a rapidly moving object is so great as to cause appreciable ablation from the surface of the body. The results on the heat transfer may probably also be taken over directly to some cases of nonablation; at the least, the results suggest the desirability of reassessing current methods used in calculating such heat transfer. The following is a summary of results presented from the engineering-aerodynamic-ballistic aspect. The complete details of the work, presented from the standpoint of the application to the theory of meteors, will appear partly in a forthcoming article in the *Astrophysical Journal* and partly in a later paper.

SUMMARY OF RESULTS

The customary aerodynamic-ballistic representation of heat-transfer calculations (per unit area) is based upon the expressions[1]

$$\text{heat transfer} = h(t_g - t_b) \tag{1}$$

$$\frac{hx}{k} = \text{constant } P_r^{\alpha} R_e^{\beta} \tag{2}$$

where h is the heat-transfer coefficient, k is the thermal conductivity, x is the distance of the surface element from the tip of the body, t_g is the air temperature outside the thermal boundary layer, t_b is the body temperature, and P_r and R_e are the Prandtl and Reynolds Numbers. In the present note, the significant quantity is β, which is usually taken to have the value 0.5 for laminar, and 0.8 for the turbulent flow.[1] On the other hand, the heat transfer in the case of meteors and other phenomena occurring in rarefied gases is generally taken as[2]

$$\text{heat transfer} = \Lambda \rho(v^3/2) \tag{3}$$

where Λ is a dimensionless heat-transfer efficiency coefficient, ρ is the air density, and v is the velocity. If Λ is a sufficiently slowly varying function, Eq. (3) is obviously greatly to be preferred to Eq. (1), since no knowledge of body or gas temperature is required. Both of these temperatures are usually difficult to determine and/or predict, particularly in free-flight experiments.

It is, of course, clear that the Eqs. (1) and (3) are similar under certain conditions at very high velocity, as may be seen by rewriting Eq. (3) as

$$\text{heat transfer} = \frac{\Lambda\gamma}{2c_p}\frac{k}{x}\left(\frac{\mu c_p}{k}\right)\left(\frac{\rho_1 v x}{\mu}\right)\left(\frac{\rho}{\rho_1}\frac{v^2}{a^2}\right)\frac{p}{\rho} \sim \left(\frac{\Lambda}{c_p}\frac{\gamma+1}{4}\frac{k_B}{M}\right)\left(\frac{k}{x}P_r R_e\right) t_g \tag{4}$$

where we have used the standard formula for the pressure rise across a shock wave normal to the flow (for high velocity)

$$p_1/p \sim [2\gamma/(\gamma+1)](v^2/a^2) \tag{5}$$

where k_B is the Boltzman constant and M is the molecular weight of the gas. Thus, in the case that $t_g \gg t_b$ and

$$c_p \alpha P_r^{1-\alpha} R_e^{1-\beta}$$

Eqs. (1) and (3) are seen to be identical. There is, however, no reason to assume such a law of variation for c_p. The fundamental experimental difference between Eqs. (2) and (3) lies then in the variation of heat transfer with air density.

We have performed experiments on free-flight heat transfer, using the controlled-pressure free-flight range of the Naval Ordnance Laboratory through the kind cooperation of the Aeroballistics Department, under R. J. Seeger, with the Harvard Observatory Meteor program. We denote these results by the letters HMP-NOL. We have also a few results on some CO_2 model wind-tunnel experiments, made available to the Meteor Program through the N.O.L. Aeroballistics Department through H. H. Kurzweg and J. M. Kendall. Some experiments on very high velocity pellets have been performed by J. S. Rinehart and his group at the Naval Ordnance Test Station at Inyokern to pro-

* An investigation supported in part by Naval Ordnance Contract No. 10449 Task I, of the U.S. Naval Bureau of Ordnance and in part by the Armament Branch, Office of Naval Research.

TABLE 1

Experimental Results on the Heat-Transfer Efficiency Factor

	$\log_{10}\sigma$ (Minimum) Ergs Gm.$^{-1}$	Λ	Range of v (Km. Sec^{-1})	Range of $\log_{10}\rho$ (Gm. Cm.$^{-3}$)
Free-flight—HMP-NOL	...	0.012	0.76 to 1.8	−3.92 to −2.62
Free-flight—N.O.T.S.	...	0.012 < Λ < 0.024	2.0 to 2.5	−2.92
Free-flight—N.O.T.S.	...	Λ < 0.04	v < 5.0	−2.92
Wind-tunnel	...	0.014	0.48 to 0.67	−3.48 to −4.57
Meteor	−12.2	Λ > 0.05	8 to 65	−5.5 to −9.3

vide a third direct measure of Λ. Rinehart and the Mechanics Branch of N.O.T.S. have kindly permitted us to publish an abstract of these results here to complement our own measures and as part of some cooperative research between N.O.T.S. and the University of Utah currently under way. We denote these results by N.O.T.S. All these experiments refer to direct observations of mass loss by heat transfer resulting in ablation. Finally, we have analyzed the considerable material now available from the Meteor Program being conducted by the Harvard Observatory under a contract with the Naval Bureau of Ordnance. From the free-flight and wind-tunnel experiments we obtain directly the quantity Λ. The meteor observations provide only values of

$$\sigma = \Lambda/2\Gamma\zeta \tag{6}$$

where ζ is the heat of vaporization or fusion according to which process gives the mass loss and where Γ is defined by

$$\text{drag force} = -\Gamma\rho v^2 A \tag{7}$$

with A the projected area perpendicular to the velocity. (Γ and Λ are thus directly efficiency factors expressed relative to the Newtonian putty ball. We regret the introduction of two new coefficients into an already confused ballistic-aerodynamic literature, but these coefficients have been in standard meteoric use.) We conclude that the best value of ζ and Γ for the meteor case are 7.10^{10} ergs Gm.$^{-1}$ (representing vaporization from iron meteoroids) and 0.5, respectively. There is considerable dispersion in the σ value obtained from meteors, but no obvious correlation with velocity or air density.

We tabulate the mean values of Λ for the free-flight and wind-tunnel experiments and σ and Λ from the meteor experiments, in Table 1. We give also the range of v and ρ covered by the experiments.

A combination of HMP-NOL and N.O.T.S. values may provide one more bit of evidence on the internal consistency of the results under certain assumptions. In the HMP-NOL experiments—carried out on woodsmetal projectiles—melting was observed at velocities around 3,500 ft. per sec. and not observed at velocities around 2,500 ft. per sec. It can be shown theoretically, and has been demonstrated experimentally in lined shaped charge experiments, that luminosity produced by rapidly moving bodies comes mainly from the interaction of the ablated material with the atmosphere and not from the solid body itself. At velocities high enough to melt iron, the iron oxide formation should, at least, be visible. If then we use Eq. (1), we have

$$\text{mass loss/unit area} = (\Lambda/\zeta)(\rho v^3/2)$$

Thus, *assuming* that iron should become luminous when it begins to melt and taking $\zeta = 0.5 \times 10^9$ ergs per Gm. for woodsmetal and 1.10^{10} for iron, we predict that an iron missile should become luminous at velocities about $(20)^{1/3}$ those at which woodsmetal began to melt or between 6,800 and 9,500 ft. per sec. (We have assumed Λ constant so the estimate is a lower bound.) Luminosity is observed to begin at about 8,000 ft. per sec.

If we attempt to represent the free-flight data by formulas of the type of Eqs. (1) and (2), using computed temperature behind the shock wave for t_g and room temperature for t_b, we obtain (HMP-NOL free-flight results alone)

$$\beta = 1.06 \pm 0.15 \text{ (std. dev.)}$$

From the wind-tunnel results (only two measures were available), $\beta = 0.97$. From a combination of wind-tunnel and free-flight results, $\beta = 0.95$.

We conclude, therefore, that the data strongly suggest that Eq. (3) provides a satisfactory representation of the heat transfer over a sufficiently wide range of velocity and air density to be generally adopted for current work in high-speed aerodynamics and ballistics, as well as meteorics and astroballistics. We wish, however, to emphasize the desirability of further free-flight experimentation on this heat transfer, for our data are far from complete. With 95 per cent of current research in aerodynamics and ballistics confined to wind tunnels, we cannot overemphasize this need for free-flight experimentation, particularly in the astroballistic régime, since wind-tunnel measures cannot induce mass loss from materials of engineering interest.

REFERENCES

[1] Eckert, E. R. G., *Introduction to the Transfer of Heat and Mass;* McGraw-Hill Book Company, Inc., New York, 1950.

[2] Whipple, Rev. Mod. Phys., Vol. 15, p. 246, 1943. Tsien, H. S., Journal of the Aeronautical Sciences, Vol. 13, P. 653, 1946. Stalder, J. R., and Jukoff, D., N.A.C.A. T.N. No. 1682, 1948.

On an Extension of Glauert's Theory of Thin Airfoils to Profiles in Cascade

N. Scholz

Dr.-Ing., Institute of Fluid Mechanics, Technical University, Braunschweig, Germany

May 12, 1951

IN A FORMER NOTE[1] we have shown how the two-dimensional potential flow through a cascade of airfoils can be calculated by replacing the airfoils by a distribution of vorticity and sources and sinks (method of singularities). We dealt mainly with the "Indirect Problem," where the distribution of vorticity (and sources and sinks) is given and the shape of the profile in cascade is asked for. More important but also mathematically more difficult is the "Direct Problem," where the shape of the airfoil in cascade is given and the distribution of velocity over the surface of the profile is asked for. In this note we want to contribute to this "Direct Problem."

For the very thin single airfoil there exists the well-known solution of the "Direct Problem," due to Glauert,[2] who replaces the airfoil by a vorticity distribution that is expanded into a Fourier series. This method has been further extended by Allen[3] and Riegels[4] for the single airfoil. We want to show that the method of Glauert can also be applied to a cascade of airfoils.

Each airfoil of the cascade in the complex plane $z = x + iy$ is replaced by a vorticity distribution along its chord (see Fig. 1). Then the induced complex velocity distribution $w = u - iv$ on the chord of the profile (x-axis) is, according to reference 1,

$$w(x) = \frac{e^{i\lambda}}{2t}\int_{x'=-c/2}^{+c/2} \gamma(x') \coth\left(\pi e^{i\lambda}\frac{x-x'}{t}\right) dx' \tag{1}$$

Here, $\gamma(x)$ is the vorticity distribution along the chord c, t/c means the solidity, and λ is the angle of stagger. In the limit, $t \to \infty$, one obtains from Eq. (1) the well-known equation for the induced downwash of a single airfoil. The shape of the profile

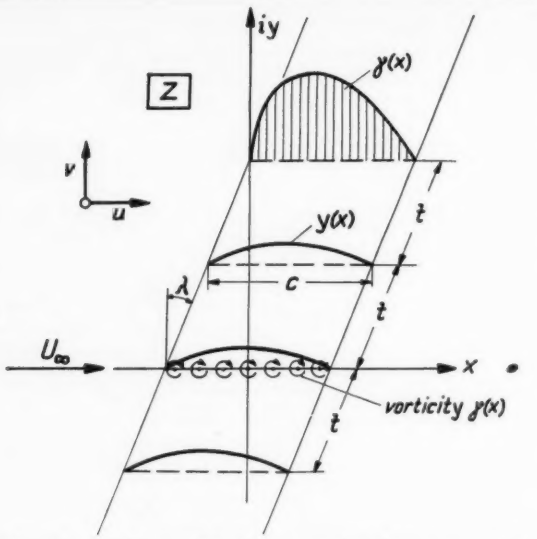

FIG. 1. A cascade of airfoils in the complex plane $z = x + iy$.

$y(x)$ being known, the induced velocity $w(x)$ is also known, so that Eq. (1) is an integral equation for the unknown vorticity distribution $\gamma(x)$. In the same manner as in Glauert's theory of the single airfoil, the solution of the integral Eq. (1) can be given in the form of a Fourier series for $\gamma(x)$. Replacing x, which is running from $-c/2 < x < +c/2$, by a complex angular coordinate φ,

$$-\cos\varphi = \tanh[(\pi x/t)e^{i\lambda}]/\tanh[(\pi c/2t)e^{i\lambda}] \tag{2}$$

yields a real part of φ running from 0 to π, whereas the imaginary part of φ is zero for $x = -c/2$ and $x = +c/2$. With this coordinate, φ, the Fourier expansion of $\gamma(x)$ can be given by just the same series as for a single airfoil, due to Pistolesi,[5]

$$\gamma(\varphi) = U_\infty\left[a_0\cot\frac{\varphi}{2} + \sum_{n=1}^{\infty} a_n \sin(n\varphi)\right] \tag{3}$$

Here, the Fourier coefficients $a_0, a_1, \ldots$, and also $\gamma(\varphi)$ are complex quantities, but only the real part of $\gamma(\varphi)$ has a physical meaning. Introducing Eq. (3) into Eq. (1) and integrating by terms yields for the complex velocity,

$$w(x) = iU_\infty\left[\frac{a_0}{2}\cosh\left(\frac{\pi c}{2t}e^{i\lambda}\right) - \sum_{n=1}^{\infty}\frac{a_n}{2}\cos(n\varphi) + \sum_{n=2}^{\infty}{}^{*}\frac{a_n}{2}\tanh^n\left(\frac{\pi c}{4t}e^{i\lambda}\right)\right] \tag{4}$$

(Here Σ^* means that only the even terms have to be summed up.) By the aid of the series expansion of the hyperbolic functions, it can easily be shown that, in the limit $t \to \infty$ (single airfoil), Eq. (4) becomes purely imaginary and results in the well-known Glauert downwash equation

$$v(x) = U_\infty\left[-\frac{a_0}{2} + \sum_{n=1}^{\infty}\frac{a_n}{2}\cos(n\varphi)\right] \tag{5}$$

As in Glauert's equation [Eq. (5)], as well as in our Eq. (4), the first term yields an induced velocity that is constant along the chord. It means the induced velocity due to the vorticity distribution of a flat plate in cascade; but, furthermore, in Eq. (4) the even sin terms of Eq. (3) by the terms $\tanh^n(e^{i\lambda}\pi c/4t)$ also give a contribution to the constant part of the downwash. The physical meaning of this is that, for a cambered airfoil in cascade, the "ideal angle of attack"† depends on the solidity.

In order to calculate the unknown coefficient $a_0, a_1, \ldots$, we use the kinematic flow condition that the direction of the resulting velocity is tangential to the profile. Since in our linear theory the induced velocity in the x-direction can be neglected, the kinematic flow condition in complex velocities is

$$U_\infty - iU_\infty(dy/dx) = U_\infty + w(x) \tag{6}$$

This is equivalent to $(dy/dx) = v(x)/U_\infty$. Introducing $w(x)$ from Eq. (4) into Eq. (6) yields the coefficients a_n in the same manner as in Glauert's theory by simple quadrature

$$a_n = \frac{4}{\pi}\int_0^\pi\left(\frac{dy}{dx}\right)\cos(n\varphi)\,d\varphi, \quad n = 1,2,\ldots \tag{7}$$

Because of the last sum in Eq. (4) the coefficient a_0 depends on the coefficients a_n, $n > 2$. Therefore it is necessary to calculate a_0 last:

$$a_0 = -\frac{1}{\cosh[(\pi c/2t)e^{i\lambda}]}\cdot\left[\frac{2}{\pi}\int_0^\pi\left(\frac{dy}{dx}\right)d\varphi + \sum{}^{*}a_n\tanh^n\left(\frac{\pi c}{4t}e^{i\lambda}\right)\right] \tag{8}$$

In the limit $t \to \infty$, Eqs. (7) and (8) result in the well-known formulas of a single airfoil due to Glauert. As in the case of a cascade, Eqs. (7) and (8) are complex; they have to be split up into two real equations for numerical evaluation. To each value of the coordinate x there correspond a real and an imaginary part of the complex angle φ, which can be calculated universally from Eq. (2), not depending on the shape of the airfoil but only on the solidity t/c and the stagger λ. After having evaluated the real and imaginary parts of $a_0, \ldots, a_n$ from Eqs. (7) and (8), the vorticity distribution can be calculated as the real part of Eq. (3). The final result is the velocity distribution on the chord of the cascade airfoil

$$W_c(x) = U_\infty + u(x) \pm [\gamma(x)/2] \tag{9}$$

with + for the upper and − for the lower side of the airfoil. For the cascade airfoil there is, in the general case, an induced velocity in the x-direction on the profile, $u(x)$, which has to be determined as the real part from Eq. (4).

The total circulation of one cascade airfoil is obtained from Eq. (3) on integrating in the complex form

$$\Gamma = U_\infty t\left[a_0 e^{-i\lambda}\sinh\left(\frac{\pi c}{2t}e^{i\lambda}\right) + e^{-i\lambda}\sum_{n=2}^{\infty}{}^{*}a_n\tanh^n\left(\frac{\pi c}{4t}e^{i\lambda}\right)\right] \tag{10}$$

where, again, only the real part has a physical meaning. In the limit $t \to \infty$, Eq. (10) also results in the well-known Glauert equation

$$\Gamma = U_\infty c(\pi/2)[a_0 + (1/2)a_1] \tag{11}$$

For staggered cascades with highly cambered profiles it may be necessary that, in the kinematic flow condition, Eq. (7), the induced velocity in the x-direction, $u(x)$, is retained. This leads to a nonlinear relation between the profile shape $y(x)$ and the vorticity distribution $\gamma(x)$.

† This being defined as the angle of attack at which the flow enters the leading edge smoothly.

REFERENCES

[1] Scholz, N., *On the Calculation of the Potential Flow Around Airfoils in Cascade*, Readers' Forum, Journal of the Aeronautical Sciences, Vol. 18, No. 1, p. 65, January, 1951.

[2] Glauert, H., *The Elements of Airfoil and Airscrew Theory*, 2nd Ed.: Cambridge University Press, 1948.

[3] Allen, H. J., *General Theory of Airfoil Sections*, N.A.C.A. Report No. 833, 1945.

[4] Riegels, F., *Das Umströmungsproblem bei inkompressiblen Potentialströmungen*, Ing. Arch., Bd. 16, p. 373, 1948, und Bd. 17, p. 94, 1949. I und II Mitteilung.

[5] Pistolesi, E., *On the Calculation of Flow Past an Infinite Row of Thin Airfoils*, N.A.C.A. T.M. No. 968, 1941.

The Flow Around a Rotating Disc in a Uniform Stream

H. Schlichting and E. Truckenbrodt
Prof. Dr. and Dr.-Ing., Respectively, Institute of Fluid Mechanics, Technical University, Braunschweig, Germany

May 12, 1951

FOR LAMINAR FLOW the solutions of the following two problems are known:

(1) The flow in the vicinity of an infinite plane rotating in a fluid that is at rest far from the plane (von Kármán[1] and Cochran[2]).

(2) The flow with axial symmetry normal to an infinite plane—flow at a stagnation point—(Homann[3]).

The solutions given in references 2 and 3 are exact solutions of the Navier-Stokes equations.

We have solved the more general problem of the laminar flow with axial symmetry normal to an infinite plane that is rotating with constant angular velocity about an axis normal to the plane. This case contains both problems (1) and (2) in the limit. If r, φ, and z are cylindrical polar coordinates, the plane is taken to be $z = 0$; it is rotating with constant angular velocity ω about the axis $r = 0$. From the solutions of (1) and (2), it is known that there is a boundary layer in the vicinity of the plane. If u, v, and w are the components of the velocity in the boundary layer and U, V, and W are the corresponding velocity components of the potential flow outside the boundary layer in the directions of r, φ, and z, respectively, the potential flow is given by

$$U = ar, \quad V = 0, \quad W = -2az \tag{1}$$

with a as a constant, which gives the intensity of the potential flow.

According to the solution of (1), the thickness of the boundary layer is $\delta_1 \sim \sqrt{\nu/\omega}$; whereas, according to (2), $\delta_2 \sim \sqrt{\nu/a}$. In our general case the thickness of the boundary layer δ depends on ν/a and a/ω. We have calculated the velocity distribution in the boundary layer from the momentum theorem, which for the r and φ direction yields the following two equations:

$$\frac{d}{dr}\left[r\int_0^\infty u(U-u)\,dz\right] + r\frac{dU}{dr}\int_0^\infty (U-u)\,dz + \int_0^\infty v^2\,dz = r\frac{\tau_r}{\rho} \tag{2}$$

$$\frac{d}{dr}\left[r^2\int_0^\infty (uv)\,dz\right] = -r^2\frac{\tau_\varphi}{\rho} \tag{3}$$

Here, τ_r and τ_φ are the components of the shearing stress at the disc, $z = 0$, in the direction of r and φ, respectively. Eqs. (2) and (3) have been solved by taking, for u and v, polynomials of the dimensionless distance from the wall, z/δ, which fulfill the most important boundary conditions at the wall and at the edge of the boundary layer. We have taken a polynomial of fourth degree for v and of fifth degree for u. The polynomial for u contains an arbitrary constant that, together with the boundary-layer thickness δ, is left to be calculated from Eqs. (2) and (3). From

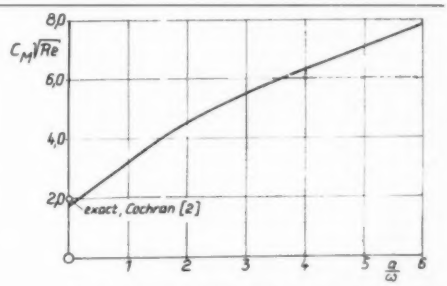

Fig. 1: Moment Coefficient of a rotating disc as a function of a/ω.

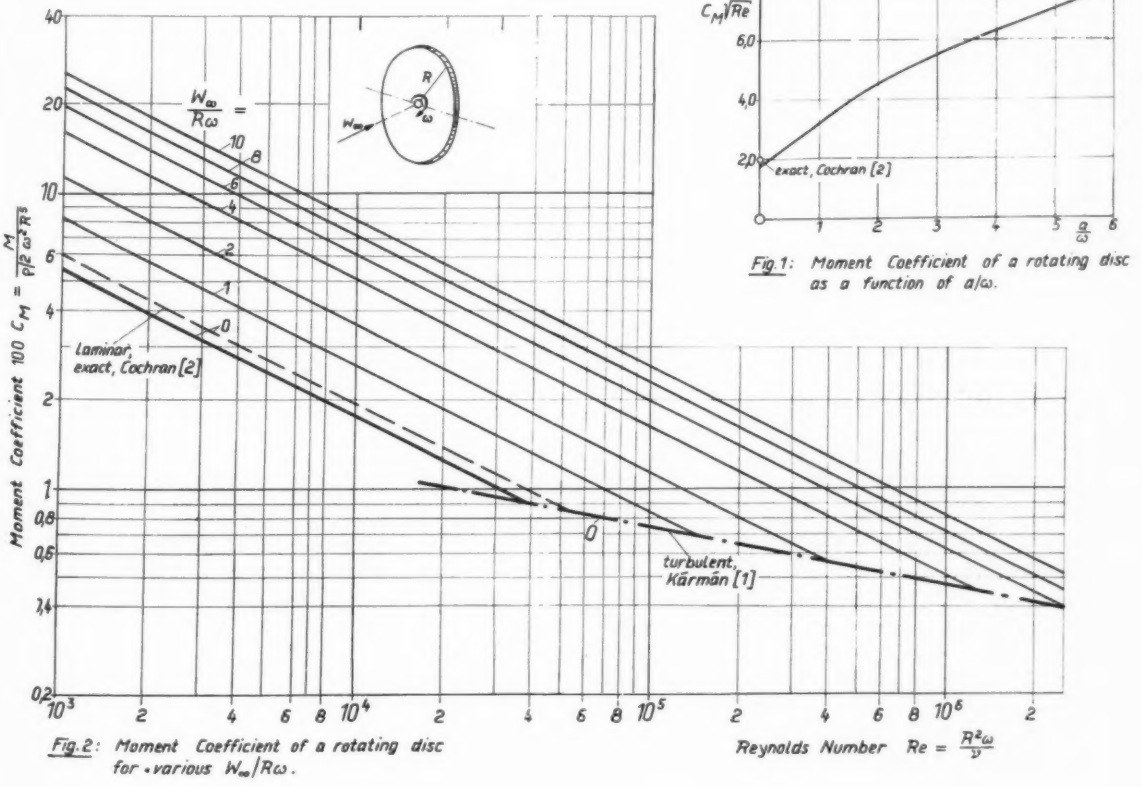

Fig. 2: Moment Coefficient of a rotating disc for various $W_\infty/R\omega$.

these calculations one obtains the boundary-layer thickness δ, the velocity distribution in the boundary layer, and the components of the shearing stress τ_r and τ_φ, all as functions of the dimensionless quantity a/ω, reducing to the known solutions of (1) for $a/\omega \to 0$, and of (2) for $a/\omega \to \infty$.

From τ_φ the total moment M for one side of a disc of radius R can be calculated. Defining the moment coefficient by

$$C_M = M/(\rho/2)\,\omega^2 R^5 \tag{4}$$

yields $C_M\sqrt{Re}$ as a function of a/ω as given in Fig. 1, with $Re = R^2\omega/\nu$ as the Reynolds Number. The dimensionless quantity a/ω of the infinite rotating plane can be related to $W_\infty/V_0 = W_\infty/R\omega$ of a disc with radius R, where W_∞ is the velocity normal to the disc and $V_0 = R\omega$ the velocity of the edge of the disc due to rotation. One gets, from the condition of similarity of both flows in the vicinity of the stagnation point,

$$a/\omega = (2/\pi)\,(W_\infty/R\omega) \tag{5}$$

Therefore, the moment coefficient can also be given as a function of Re and $W_\infty/R\omega$ (see Fig. 2). For $W_\infty/V_0 > 1$, the results can be interpolated by

$$C_M = (2.53/\sqrt{Re})\,\sqrt{W_\infty/V_0} \tag{6}$$

For constant angular velocity the moment increases considerably with increasing W_∞.

More details of our calculations will be published shortly.[4]

References

[1] von Kármán, Theodore, *Laminare und turbulente Reibung*, Z.A.M.M., Vol. 1, p. 235, 1921.

[2] Cochran, W. G., *The Flow Due to a Rotating Disc*, Proc. Cambr. Phil. Soc., Vol. 30, p. 365, 1934.

[3] Homann, F., *Der Einfluss grosser Zähigkeit bei der Strömung um den Zylinder und die Kugel*, Z.A.M.M., Vol. 16, p. 153, 1936.

[4] Schlichting, H., and Truckenbrodt, E., *Die Strömung an einer angeblasenen rotierenden Scheibe.* To be published.

Erratum

T. H. H. Pian

Aero-Elastic and Structures Research Laboratory, Massachusetts Institute of Technology, Cambridge, Mass.

May 28, 1951

THE FOLLOWING ERRORS appeared in the paper "Analytical and Experimental Studies on Dynamic Loads in Airplane Structures During Landing" (JOURNAL OF THE AERONAUTICAL SCIENCES, Vol. 17, No. 12, pp. 765–775, December, 1950) by H. I. Flomenhoft and myself.

The expressions for B_0's in Eqs. (25), (26), and (27) should be as follows:

Equation (25):

$$B_0 = n_{max}\cdot g \int_x^{b/2} \left\{ m + \frac{eM}{I_x}\,[S - m(a-e)] \right\} dx, \quad x > x_F$$

$$B_0 = n_{max}\cdot g \left(\int_x^{b/2} \left\{ m + \frac{eM}{I_x}\,[S - m\,(a-e)] \right\} dx - \frac{1}{2}M \right), \quad x < x_F$$

Equation (26):

$$B_0 = n_{max}\cdot g \int_{b/2}^{x}\int_{b/2}^{x} \left\{ m + \frac{eM}{I_x}\,[S - m(a-e)] \right\} dx\,dx, \quad x > x_F$$

$$B_0 = n_{max}\cdot g \left(\int_{b/2}^{x}\int_{b/2}^{x} \left\{ m + \frac{eM}{I_x}\,[S - m(a-e)] \right\} dx\,dx - \frac{1}{2}M(x_F - x) \right), \quad x < x_F$$

Equation (27):

$$B_0 = n_{max}\cdot g \int_x^{b/2} \left\{ \frac{eM}{I_x}\,[I - S(a-e)] + S \right\} dx, \quad x > x_F$$

$$B_0 = n_{max}\cdot g \left(\int_x^{b/2} \left\{ \frac{eM}{I_x}\,[I - S(a-e)] + S \right\} dx - \frac{1}{2}M\bar{a} \right), \quad x < x_F$$

Discussion of Wright Brothers Lecture

(*Continued from page 623*)

represents a small enough investment so that it can be assigned to a single program; yet it is sufficiently flexible so that it can accommodate changes in aerodynamic and control parameters and can include certain types of nonlinearities.

Frequently the noise problem is so severe that it must be properly taken into account even before the control system can be made to operate. In such cases, a noise study does not lead to a refinement; rather, it dictates the control system that will give satisfactory performance. Hence, the noise study becomes part of the theoretical design.

In conclusion, I want to commend Dr. Bollay for his statement that much closer teamwork is required between the aerodynamicist and the autopilot designer. The aerodynamicist should not expect too much of the autopilot designer, otherwise resulting control system complexity will involve increased costs and decreased reliability. Going back to Wilbur Wright's address in 1901, we find that he was concerned with the problems of power and "steering." Enough power is currently available to fly a barn door. However, let us not expect the autopilot designer to make it maneuverable.